

2016

# Biosynthesis of Cadmium Chalcogenide Quantum Dots and Enhancement of their Functional Properties via Surface Modification

Zhou Yang  
*Lehigh University*

Follow this and additional works at: <http://preserve.lehigh.edu/etd>

 Part of the [Chemical Engineering Commons](#)

---

## Recommended Citation

Yang, Zhou, "Biosynthesis of Cadmium Chalcogenide Quantum Dots and Enhancement of their Functional Properties via Surface Modification" (2016). *Theses and Dissertations*. 2894.  
<http://preserve.lehigh.edu/etd/2894>

This Dissertation is brought to you for free and open access by Lehigh Preserve. It has been accepted for inclusion in Theses and Dissertations by an authorized administrator of Lehigh Preserve. For more information, please contact [preserve@lehigh.edu](mailto:preserve@lehigh.edu).

**Biosynthesis of Cadmium Chalcogenide Quantum  
Dots and Enhancement of their Functional  
Properties via Surface Modification**

By

Zhou Yang

A Dissertation  
Presented to the Graduate and Research Committee  
of Lehigh University  
in Candidacy for the Degree of  
Doctor of Philosophy

In

Chemical Engineering

Lehigh University

September 2016

Copyright by Zhou Yang

2016

# The certificate of approval

Approved and recommended for acceptance as a dissertation in partial fulfillment of the requirements for the degree of Doctor of Philosophy.

---

Date

---

Professor Steven McIntosh  
Dissertation Advisor

---

Accepted Date

Committee Members:

---

Professor Bryan W. Berger

---

Professor Christopher J. Kiely

---

Professor Hugo S. Caram

---

Professor Ivan V. Korendovych

# Acknowledgements

I would like to express my sincere thanks and appreciations to my advisors, Professor Steven McIntosh and Bryan Berger, for their continuous guidance and patience throughout the entire course of my Ph.D. study and research. Without your support and help, I wouldn't be able to accomplish this.

I would also like to thank Professor Christopher Kiely for his guidance on understanding nanocrystal materials, especially electron microscopy characterizations, which is one of the most important parts in this work.

I am very thankful to Professor Hugo Caram and Ivan Korendovych for serving as my committee members, and their advice on my research work.

I want to thank everyone in the group for making the lab a fun place to work. Special thanks go to Leah, Chris, Li, Robert, Roxanne and Tori.

Finally, and most importantly, I thank my parents, my daughter, especially my wife, Yuanyuan Wang, for their unconditional love and support.

# Content

<b>Acknowledgements</b> .....	iv
<b>Content</b> .....	v
<b>List of Tables</b> .....	vii
<b>List of Figures</b> .....	viii
<b>Notations</b> .....	xi
<b>Abstract</b> .....	1
<b>1. Introduction</b> .....	3
1.1 Overview of quantum dots .....	3
1.2 Biomineralization/biosynthesis of quantum dots .....	8
1.3 Objectives and outline of the thesis.....	12
<b>2. Biomineralization of CdS Quantum Dot from <i>Stenotrophomonas Maltophilia</i></b> .....	14
2.1 Introduction .....	14
2.2 Biosynthesis of CdS quantum dots.....	16
2.3 Electron microscopy characterizations of CdS QDs .....	21
2.4 Particle size control of CdS quantum dots .....	30
2.4.1 Particle size control by varying the growth time .....	30
2.4.2 Particle size selection by gel filtration chromatography.....	31
2.5 Conclusions .....	33
<b>3. Optimizing Synthesis Conditions and Improving Functional Properties by Surface Modification of CdS Quantum Dots</b> .....	35
3.1 Introduction .....	35
3.2 Influence of synthesis conditions on CdS QDs growth.....	37
3.2.1 Growth dependency on the concentration of cadmium acetate .....	37
3.2.2 Growth dependency on the concentration of L-cysteine .....	38
3.2.3 Growth dependency on the pH of the buffer .....	41
3.2.4 Growth dependency on the temperature .....	44
3.2.5 Discussions .....	45
3.3 Surface modification of biosynthesized CdS quantum dots.....	46
3.3.1 Phase transfer and capping exchange of the biosynthesized CdS QDs .....	46

3.3.2	ZnS shell growth on CdS via chemical route.....	51
3.4	CdS QDs sensitized solar cell .....	55
3.5	CdS and reduced graphene oxide composite.....	56
3.6	Conclusions .....	58
<b>4.</b>	<b>Biom mineralization of CdSe and Core/shell CdSe/CdS Quantum Dot from Cystathionine <math>\gamma</math>-lyase .....</b>	<b>60</b>
4.1	Introduction .....	60
4.2	Biosynthesis of CdSe quantum dots.....	62
4.3	Photoluminescence enhancement of CdSe quantum dots .....	68
4.3.1	Core/shell CdSe/CdS growth via biosynthesis route .....	68
4.3.2	Photoenhancement of luminescence by UV illumination.....	78
4.4	Conclusions .....	79
<b>5.</b>	<b>Proposed Biosynthesis Mechanism of CdS and CdSe Quantum Dots .....</b>	<b>81</b>
5.1	Introduction .....	81
5.2	Identification of cystathionine $\gamma$ -lyase .....	83
5.3	The QD formation mechanism by cystathionine $\gamma$ -lyase .....	87
5.4	Preliminary results for other types of quantum dots .....	91
5.5	Conclusions .....	94
<b>6.</b>	<b>Summary.....</b>	<b>95</b>
	<b>Reference .....</b>	<b>98</b>
	<b>Appendix: Experimental Section.....</b>	<b>108</b>
A1.	Apparatus and characterizations.....	108
A2.	<i>Stenotrophomonas maltophilia</i> and cystathionine $\gamma$ -lyase production.....	109
A3.	CdS quantum dot biosynthesis. ....	110
A4.	CdSe quantum dot biosynthesis. ....	110
A5.	Phase transfer and capping exchange of quantum dots.....	111
A6.	Core/shell structure synthesis.....	112
A7.	Quantum dot sensitized solar cell assembly.....	113
A8.	Quantum dot/reduced graphene oxide composite. ....	114
	<b>Curriculum Vitae .....</b>	<b>115</b>

## List of Tables

<b>Table 1.1.</b> Biosynthesis of quantum dots from different microorganisms or peptides. ...	11
<b>Table 2.1.</b> Comparison of different growth conditions for CdS QDs synthesis.....	17
<b>Table 2.2.</b> Lattice fitting of nanocrystals in Figures 2.6.c to zinc-blende type CdS. ....	29
<b>Table 2.3.</b> Lattice fitting of nanocrystals in Figures 2.6.d to wurtzite type CdS. ....	29
<b>Table 4.1.</b> Lattice fitting of nanocrystals in Figures 4.3.d to wurtzite type CdSe.....	67



# List of Figures

<b>Figure 1.1.</b> Photoluminescence of quantum dots and electron microscopy characterizations. ....	4
<b>Figure 2.1.</b> Absorption and emission spectra of the as-grown cultures. ....	18
<b>Figure 2.2.</b> Optical properties of the as-grown CdS QDs with different growth times. ..	19
<b>Figure 2.3.</b> Quantum yields of CdS QDs as a function of growth time ranging from 30 min to 180 min. ....	20
<b>Figure 2.4.</b> X-ray powder diffraction pattern of the precipitated CdS quantum dot powder after 360 min of growth. ....	21
<b>Figure 2.5.</b> Electron microscopy characterization of SMCD1 cells and CdS QDs at different purification stage. ....	25
<b>Figure 2.6.</b> Beam damage evidence of CdS QDs at high magnification imaging. ....	26
<b>Figure 2.7.</b> Electron microscopy characterization of purified CdS QDs after 60 min growth. ....	27
<b>Figure. 2.8.</b> TEM images and particle size distributions of CdS QDs as a function of growth time. ....	30
<b>Figure. 2.9.</b> Size selection of CdS quantum dots by gel filtration chromatography. ....	33
<b>Figure 3.1.</b> Aqueous phase optical properties of harvested CdS nanocrystal solutions grown with different concentrations of cadmium acetate ( $\text{Cd}(\text{Ac})_2$ ) ranging from 0.25 mM to 4 mM. ....	39
<b>Figure 3.2.</b> Aqueous phase optical properties of CdS QDs harvested after 30 min incubation time with varying initial concentration of L-cysteine varying between 1 mM and 32 mM. ....	40
<b>Figure 3.3.</b> Aqueous phase optical properties of harvested CdS nanocrystal solutions after 30 min incubation time with varying initial pH. ....	42
<b>Figure 3.4.</b> Aqueous phase optical properties of purified CdS nanocrystal solutions after 30 min incubation time with varying pH of the purified solution. ....	43
<b>Figure 3.5.</b> Aqueous phase optical properties of CdS nanocrystal solutions after 30 min incubation time with varying temperature. ....	45

<b>Figure 3.6.</b> Optical properties of CdS QDs in aqueous phase and 1-octadecene after phase transfer..	47
<b>Figure 3.7.</b> Optical properties of CdS QDs in aqueous phase and organic phase after phase transfer with different capping agent, oleylamine, dodecylamine, octylamine and oleic acid..	48
<b>Figure 3.8.</b> Optical properties of CdS QDs after phase transfer at different pH.....	49
<b>Figure 3.9.</b> Characterizations of CdS QDs before and after phase transfer with 1-dodecanethiol.....	50
<b>Figure 3.10.</b> Normalized optical characteristics of the core CdS QDs capped with oleic acid and resultant core-shell CdS/ZnS QDs..	51
<b>Figure 3.11.</b> Electron microscopy characterizations of CdS and CdS/ZnS quantum dots..	53
<b>Figure 3.12.</b> More characterizations of CdS/ZnS quantum dots.....	54
<b>Figure 3.13.</b> <i>J-V</i> characteristics of the CdS quantum dot based cells measured under one-sun illumination (AM 1.5 G, 100 mW/cm <sup>2</sup> ).....	56
<b>Figure 3.14.</b> Electron microscopy characterizations of CdS and reduced graphene oxide (rGO) composite..	57
<b>Figure 4.1.</b> Optical properties of the as-grown CdSe QDs with increasing growth time..	62
<b>Figure 4.2.</b> Quantum yield of CdSe QDs with increasing growth time from 20 to 100 min..	63
<b>Figure 4.3.</b> Optical properties of the as-grown CdSe QDs with increasing growth time with addition of 3-mercaptopropionic acid.....	64
<b>Figure 4.4.</b> Electron microscopy characterizations of the large core (24 h growth) CdSe QDs.....	66
<b>Figure 4.5.</b> Optical properties of CdSe and CdSe/CdS QDs.....	70
<b>Figure 4.6</b> Electron microscopy characterizations of the large size (24 h core growth) core/shell CdSe/CdS QDs.....	71
<b>Figure 4.7.</b> Electron microscopy characterizations of the large size (24 h core growth) core/shell CdSe/CdS QDs.....	72

<b>Figure 4.8.</b> Electron microscopy characterizations of the small size core CdSe and core/shell CdSe/CdS QDs.....	74
<b>Figure 4.9.</b> Electron microscopy characterizations of the small size (20 min core growth) core/shell CdSe/CdS QDs.....	75
<b>Figure 4.10.</b> Absorbance spectra of core/shell CdSe/CdS growth under inert and in-air conditions.....	77
<b>Figure 4.11.</b> Optical properties of the core CdSe QDs under UV illuminations..	78
<b>Figure 5.1.</b> Optical properties of the as-grown CdS QDs as a function of growth time in the supernatant following removal of cells via centrifugation at 30 minutes..	84
<b>Figure 5.2.</b> SDS-PAGE results of the CdS QDs culture comparing to pure cystathionine $\gamma$ -lyase protein.....	85
<b>Figure 5.3.</b> Sequence of the protein associated with the QDs.....	86
<b>Figure 5.4.</b> Optical properties of CdS QDs by cystathionine $\gamma$ -lyase: absorbance spectrum (black solid line) and emission spectrum (red dash line). .....	87
<b>Figure 5.5.</b> Absorbance of CdS synthesis by cystathionine $\gamma$ -lyase using L-cystine as the sulfur source.....	88
<b>Figure 5.6.</b> A proposed mechanism for selenocystine cleavage by cystathionine $\gamma$ -lyase. ....	88
<b>Figure 5.7.</b> Cystathionine $\gamma$ -lyase forms CdS nanocrystals using Na <sub>2</sub> S as the sulfur source..	90
<b>Figure 5.8.</b> Preliminary result for ZnS QDs synthesis..	92
<b>Figure 5.9.</b> Electron microscopy characterizations of the PbSe nanocrystals. ....	93
<b>Figure 5.10.</b> Preliminary result for ZnSe QDs synthesis with increasing incubation time. ....	93

# Notations

<b><i>E. coli</i></b>	<i>Escherichia coli</i>
<b>HAADF</b>	High angle annular dark field
<b>HRTEM</b>	High resolution transmission electron microscopy
<b>MWCO</b>	Molecular weight cut-off
<b>MPA</b>	3-Mercaptopropionic acid
<b>QD</b>	Quantum dot
<b>QY</b>	Quantum yield
<b>OD<sub>600</sub></b>	Optical density measured at a wavelength of 600 nm
<b>rGO</b>	Reduced graphene oxide
<b>SAED</b>	Selected area electron diffraction
<b>SMCD1</b>	<i>Stenotrophomonas maltophilia</i>
<b>smCSE</b>	Cystathionine $\gamma$ -lyase
<b>STEM</b>	Scanning transmission electron microscopy
<b>TCEP</b>	Tris(2-carboxyethyl)phosphine hydrochloride
<b>TEM</b>	Transmission electron microscopy
<b>Tris</b>	Tris(hydroxymethyl)aminomethane
<b>XEDS</b>	X-ray energy dispersive spectroscopy
<b>XRD</b>	X-ray powder diffraction

# Abstract

This work provides a cell-based process using an engineered strain of *Stenotrophomonas maltophilia* (SMCD1) or cystathionine  $\gamma$ -lyase (smCSE) enzyme that produces high yields of extracellular, water-soluble semiconductor nanocrystals, also known as quantum dots (QDs) from low-cost precursors in aqueous media. SMCD1 enables controlled growth of cadmium sulfide (CdS) QDs over a period of several hours in culture, allowing precise, extrinsic control of QD size and optical properties with photoluminescence emission spanning the visible spectrum. The as-grown CdS QDs show both zinc-blende and wurtzite type crystal structures with a quantum yield of up to 2.08 %. Cadmium selenide (CdSe) QDs was also successfully synthesized by introducing smCSE enzyme instead of SMCD1 cells. This enzyme was produced and identified from the culture of SMCD1 cells and further overexpressed by engineered *Escherichia coli*. The optical properties of CdSe QDs were studied and particle size control was also achieved by varying the growth time. Further characterizations confirmed the formation of CdSe nanocrystals with mainly wurtzite type crystal structure.

Post-treatments, such as core/shell growth, phase transfer, and photoenhancement were utilized to modify the surface chemistry of these nanocrystals to improve their properties for potential applications. Core/shell structures on both CdS and CdSe cores with different shell structure (ZnS for CdS, CdS for CdSe) were achieved. This significantly improved their optical properties, for example, core/shell CdSe/CdS exhibits a quantum yield up to

12 %. A facile phase transfer protocol was proposed to efficiently transfer the QDs from aqueous phase to organic phase. In addition, photoenhancement via UV illumination was also introduced for CdSe QDs and their photoluminescence was highly improved. Owing to the post-treatments, the qualities of these cell-based QDs are comparable to that from chemical synthesis routes. Our biosynthetic approach to cadmium chalcogenide QDs production provides a viable pathway to realize the promise of green biomanufacturing of these materials for optoelectronic, energy, medicine and other emerging technological applications.

# Chapter 1

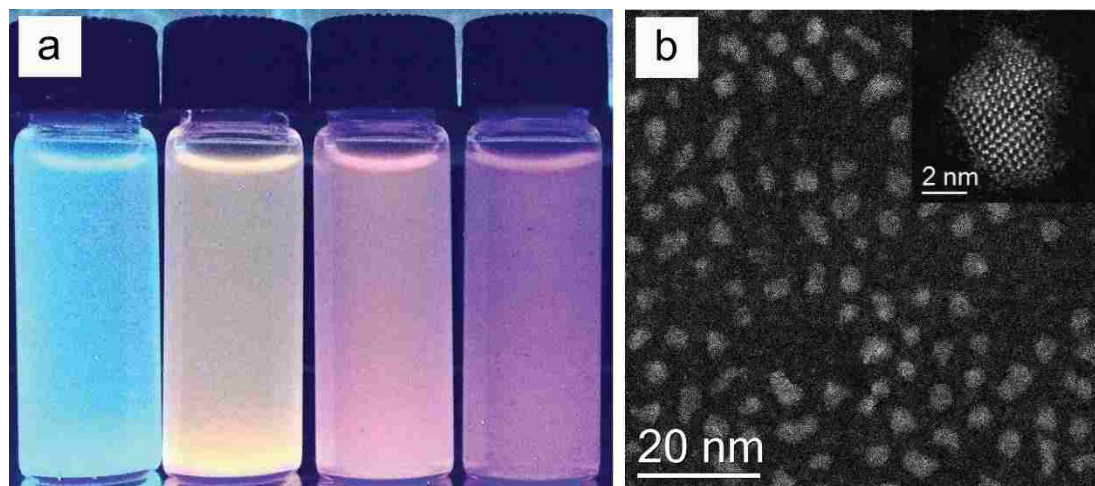
## Introduction

### 1.1 Overview of quantum dots

Quantum dots (QDs) are semiconductor nanomaterials with their size in nanoscale, typically from 1 to 10 nm, comprising hundreds to a few thousands of atoms. An important parameter of semiconductor materials is the band gap which separates the conduction from the valence bands. In bulk semiconductor materials, the bandgap is fixed. However, as the size of the material goes down to the nanoscale which results in quantum confinement, and the band gap varies with the particle size. The larger the particle size, the smaller the band gap. This phenomenon is known as the quantum size effect.<sup>[1,2]</sup> Owing to their size dependent properties, the fluorescence of QDs can be tuned by changing their particle sizes (Figure 1.1.a) and high magnification electron microscopy characterizations reveal that they are nanocrystals (Figure 1.1.b).

QDs have attracted significant attention in the past three decades since they were discovered by Louis Brus in the early 1980s.<sup>[1]</sup> Different types of QDs, such as CdSe<sup>[3]</sup>, PbS<sup>[4]</sup> and InP<sup>[5]</sup>, have been extensively studied. QDs can be synthesized from a variety of different materials and procedures. There are two major routes for nanocrystal synthesis: aqueous route and organic route. The former generally achieves QD synthesis from appropriate reagents and surfactant-type stabilizers (also referred as capping agents) in homogenous aqueous phase.<sup>[6]</sup> Compared to aqueous route, the organic route exhibits better qualities (e.g. high quantum yield) of the synthesized nanocrystals with well controlled

particle size and shape.<sup>[3,7,8]</sup> Classical studies have demonstrated that the synthesis of monodispersed colloids requires a temporal separation of nucleation and growth of the seeds.<sup>[9]</sup> There are two major techniques for nanocrystal synthesis in organic solvent: hot-injection method and heating-up method.<sup>[10]</sup> Hot-injection method realizes the separation of nucleation and growth by rapid injection of the reagents into the hot solvent and shows good control over the growth. The heating-up method is a batch process with gradually elevating the reaction temperature slightly above the decomposition of the precursors. The hot-injection method for QDs synthesis was first introduced by Bawendi and co-workers in their report for metal chalcogenides synthesis and later widely adopted owing to its precise control over the quality of nanocrystals.<sup>[3]</sup> A typical hot-injection method is usually carried out at high temperature ( $\sim 300$  °C) and inert atmosphere with argon or nitrogen control is required.



*Figure 1.1. Photoluminescence of quantum dots and electron microscopy characterizations. (a) CdS quantum dots solutions with different sizes illuminated under UV lamp; (b) TEM images of CdS quantum dots, inset b is a high magnification image of a single quantum dot.*

Subsequent processes relying on the surface modification of the as-synthesized QDs, are frequently used to manipulate the surface chemistry, such as capping ligand



exchange, and improve the properties of QDs for photovoltaics and optoelectronics applications.<sup>[3,11,12]</sup> The surface chemistry of the nanocrystal particles plays an important role on the physical and chemical properties of the nanocrystals and the right type of the capping ligand binding with the surface atoms is essential.<sup>[13]</sup> With different types of capping ligand, the QDs can be either hydrophobic, hydrophilic or amphiphilic. Therefore, phase transfer of QDs from polar solvent to nonpolar solvent or vice-versa can be realized by capping ligand exchange or introducing a new capping ligand coexisting with the primary ligands on the nanocrystal surface<sup>[14-17]</sup>. Commonly used capping ligands, such as tri-n-octylphosphine oxide, trioctylphosphine, amines (e.g. oleylamine), fatty acids (e.g. oleic acid) and thiols (e.g. L-cysteine) have been widely reported for QDs production and surface modification.<sup>[18]</sup> The binding between the capping ligand molecule and the nanocrystal undergoes a dynamic binding and unbinding processes. For capping ligand exchange, the incoming ligand molecule should bind more strongly than the primary one. Murray et al. reported a successful surface exchange of CdSe QDs by repeated exposure of the QDs precipitation to an excess of a competing capping group, pyridine, at slightly elevated temperature.<sup>[3]</sup> Comparelli et al. realized the capping exchange of CdS QDs by mixing the QDs in a small quantity of chloroform with a large excess of degassed amines at 50-80 °C for 24-96 h.<sup>[11]</sup> Gaponik et al. proposed an efficient phase transfer protocol applicable for a variety of II-VI nanocrystals synthesized in water and capped with different short-chain thiols (CdS, CdSe, HgTe, etc.).<sup>[14]</sup> It has been reported that after phase transfer, the photoluminescence emission quenches significantly and can be restored to initial values by further treatments such as a heating step. By introducing capping exchange/phase transfer, the as-synthesized QDs become more versatile for further applications.

Core/shell QDs structures have also been widely studied and as a very important strategy to modify the surface structure and passivate the surface of the nanocrystals<sup>[19–25]</sup>. Methods for overcoating a semiconductor nanocrystal with a second semiconductor material with a larger band gap are well developed owing to their significant improvements on luminescence efficiency. With a shell growth, the excitons, both electrons and holes, are confined in the core material, promoting the radiative recombinations. ZnS is usually utilized as the shell material for other types of QDs (CdSe, CdS or InP) since ZnS has a larger band gap, ~3.61 eV, and meanwhile it is environmentally benign. Steckel et al. successfully overcoated CdS QDs with ~ 3 monolayers of ZnS shell.<sup>[25]</sup> The deep-trap emission was suppressed and the quantum yield was improved from 3~6 % to 20~30 %. The procedure by Steckel uses a variety of solvents and precursors, including a highly pyrophoric compound, diethylzinc, which makes it difficult to handle. Peng's group proposed successive ionic layer adsorption and reaction method for core/shell CdSe/CdS QDs synthesis and achieved a large-scale batch synthesis.<sup>[22]</sup> They also introduced a facile approach, denominated as thermal-cycling coupled single precursor, which uses a single precursor for core/shell CdS/ZnS QDs synthesis at relatively low temperature (below 200 °C).<sup>[24]</sup> Core/shell structure promotes the optical properties, reduces the toxicity and also improves the stability of QDs against photooxidation. Thus, shell structure growth over nanocrystals has been considered as a requirement for their further applications.

Due to their size-dependent photoluminescent properties, semiconductor quantum dots (QDs) have showed great potential applications in a number of devices, including display technologies, *in-vivo* or *in-vitro* biomedical imaging/detection and QDs based solar cells.<sup>[12,26–29]</sup> As materials for display devices, QDs (e.g. CdSe) show great potential for

next generation display technology. Quantum dots can be simply tuned to different sizes during synthesis and emit different colors as described before. They have very narrow emission peaks indicating pure colors. It has been reported that electrically driven quantum dot light-emitting devices have increased in external quantum efficiency from less than 0.01% to about 18% in the past few decades.<sup>[30-32]</sup> Quantum dots have been also emerged in solar cell studies, known as quantum dot sensitized solar cell. So far, a certified power conversion efficiency of 11.6 % has been reported by Du et al.<sup>[33]</sup> by using Zn-Cu-In-Se QD. Though the efficiency is still lower than that of commercial silicon products, considering the improvement from less than 1 % to 10 % in the past decade, there still exists a large space to further enhance the efficiency. Another potential application of QDs is their use in biology. QDs have appeared as *in vivo* and *in vitro* fluorophores in a variety of biological investigations owing to their unique optical properties. Compared to traditional organic molecules as fluorescent labels, quantum dots exhibit long-term stability and simultaneous detection of multiple signals.<sup>[12]</sup> They can be easily manipulated with different ligands for various requirement in biology. Besides these, QDs have also been introduced to assist photocatalysis reactions in biology systems. Sakimoto et al. developed a hybrid approach using a nonphotosynthetic bacterium, *Moorella thermoacetica*, with cadmium sulfide nanoparticles, for photosynthesis of acetic acid from carbon dioxide.<sup>[34]</sup> Brown et al. also demonstrated that cadmium sulfide nanocrystals acting as the light harvesting source can photosensitize the nitrogenase molybdenum-iron protein to drive the enzymatic reduction of N<sub>2</sub> into NH<sub>3</sub>.<sup>[35]</sup>

Most current methods to produce CdS QDs utilize elevated temperature, organic solvent based processes. For example, the method of Murray et al. utilizes

bis(trimethylsilyl)sulfide reacting with dimethylcadmium ( $\text{Me}_2\text{Cd}$ ) at 300 °C in an anhydrous environment. Note that  $\text{Me}_2\text{Cd}$  is expensive, toxic, and pyrophoric.<sup>[3]</sup> The alternative method of Peng and Peng utilizes trioctylphosphine oxide,  $\text{CdO}$ , and hexylphosphonic acid or tetradecylphosphonic acid at 300 °C, again in anhydrous environment.<sup>[7]</sup> In addition to environmental issues related to scale-up of these solvent based reactions, the reactants themselves must be synthesized. These high costs inhibit their widespread commercial adoption. Therefore, to pursue economical and environmentally feasible applications, there are still challenges. To address these challenges, it is desirable to develop alternative methods to produce QDs under mild conditions with low costs. QDs fabricated from an aqueous route usually are biologically compatible and exhibit great potential on biomedical applications. Biosynthesis methods, owing to their good compatibility of the products and simplicity of the process, have attracted great interests and attentions.<sup>[36,37]</sup> Using low cost sources combined with room temperature, bio-based aqueous synthesis conditions may provide a route to lower the cost of QDs synthesis to a level commensurate with their potential use in consumer products. Thus, biosynthetic approach to QDs production may provide a viable pathway to overcome the primary cost barrier to their utilization in optoelectronics and other commercial technologies.

## **1.2 Biomineralization/biosynthesis of quantum dots**

Biomineralization is a promising route toward the scalable biomanufacturing of functional materials. It involves multiple biomolecules which mediate the mineralization and control the crystal structure. Prokaryotes have evolved several response mechanisms to solutions containing toxic levels of heavy metals such as cadmium. These include the

production of cysteine-rich peptides to direct growth of insoluble metal precipitates<sup>[38,39]</sup> and the formation of glutathione-metal complexes to trap intracellular metals<sup>[40,41]</sup>. This has inspired the pursuit of a range of novel, biological approaches, including using peptides, glutathione or other cellular components to direct the synthesis of QD's.<sup>[40,42,43]</sup>

With regard to metal sulfide nanocrystals, a number of groups have demonstrated the potential of engineered or natural biomolecules or biological systems as structure directing agents during the chemical synthesis of CdS nanocrystals.<sup>[40,42–45]</sup> In these cases, a reactive sulfur source, typically sodium sulfide, is added to a cadmium containing solution. For example, Sweeney et al. achieved intracellular CdS nanocrystal synthesis within *E. coli* upon addition of reactive sodium sulfide to a solution of the bacteria and cadmium chloride.<sup>[40]</sup> In this report, the bacterial system served to direct the formation of CdS nanocrystals. Flynn et al. utilized the same reactants in the presence of engineered peptide-phage constructs to direct the nucleation and growth of CdS nanocrystals.<sup>[45]</sup> A similar viral assembly approach was also utilized to achieve control over orientation during crystal growth to yield nanowire morphologies.<sup>[44]</sup> The majority of the reports have used biological components to template structure during synthesis from reactive sulfur precursors, typically Na<sub>2</sub>S.

Biosynthesis of CdSe QDs has also been widely studied because of their great potential in display applications. Cui et al. achieved intracellular CdSe nanocrystal synthesis within yeast cells.<sup>[46]</sup> They adopted a rational coupling strategy in an appropriate space and time sequence so that Cd can collide with low-valence selenium to yield CdSe QDs. They first reduced the selenium precursor (Na<sub>2</sub>SeO<sub>3</sub>) into organoselenium compounds in yeast cells and then at the appropriate moment added the cadmium precursor

(CdCl<sub>2</sub>). Fellowes et al. used a similar strategy but *Veillonella atypica* to reduce Na<sub>2</sub>SeO<sub>3</sub> for selenium source generation.<sup>[47]</sup> Kumar et al. developed a CdSe QDs biosynthesis protocol at room temperature by the fungus, *Fusarium oxysporum* when incubated with a mixture of CdCl<sub>2</sub> and SeCl<sub>4</sub>.<sup>[48]</sup> Suresh incubated the same precursors (CdCl<sub>2</sub> and SeCl<sub>4</sub>) with plant pathogenic fungus, *Helminthosporium solani*, and also synthesized CdSe nanocrystals with a mean diameter of  $5.5 \pm 2$  nm and 1 % quantum yield.<sup>[49]</sup> Park et al. reported a general strategy for in vivo synthesis of diverse nanocrystals by using recombinant *E. coli* expressing *Arabidopsis thaliana* phytochelatin synthase and/or *Pseudomonas putida* metallothionein. They accomplished a variety of metal/alloy and semiconductor nanocrystals synthesis, such as Au, FeCo, CdSe.<sup>[50]</sup> Table 1.1 lists some of the prior work on biosynthesis of CdS and CdSe QDs via different biosystems.

Many of these prior studies that utilize biosynthesis protocols clearly demonstrate nanocrystals formation, however, few investigations have focused on their photoluminescent properties and these reported biosynthesized QDs either experience poor optical properties or need a complicated fabrication and purification procedures. Thus, the key limitations in translating current biological approaches to commercial-scale QD production include (i) an inability to rationally alter intrinsic (genetic) or extrinsic (growth media) properties to reproducibly control QD size and (ii) the need for complex procedures to extract and purify the QDs from the culture.

**Table 1.1. Biosynthesis of quantum dots from different microorganisms or peptides.**

Type	Organism/peptide	Absorbance (nm)	Emission (nm)	Particle size (nm)	QY (%)	Ref
CdS	<i>Fusarium oxysporum</i>	~ 400	N	5 ~ 20	N	[51]
CdS	<i>Escherichia coli</i>	318	384	2 ~ 5	0.007	[42]
CdS	<i>Escherichia coli</i>	~ 420	445~ 510	6	N	[52]
CdS	<i>Rhodobacter sphaeroides</i>	282 ~ 506	382 ~406	2.3 ~ 36.8	N	[53]
CdS	<i>Candida glabrata/Schizosacc haromyces pombe</i>	300 ~ 365	460	1.8 ~ 2.9	N	[38]
CdS	<i>Rhodopseudomonas palustris</i>	425	N	8.01	N	[54]
CdS	dendritic peptides	340 ~ 380	496 ~556	2.6 ~ 5.9	N	[43]
CdSe	<i>Saccharomyces cerevisiae</i>	N	520 ~ 670	2.7 ~ 6.34	4.7	[46,55,56]
CdSe	<i>Veillonella atypica</i>	380 ~ 520	500 ~ 520	2 ~ 4	10.33	[47,57]
CdSe	<i>Fusarium oxysporum</i>	~ 370	~ 440	11	N	[48]
CdSe	<i>Helminthosporium Solani</i>	~ 350	~ 430	5.5	1	[49]
CdSe	<i>Escherichia coli</i>	555 ~ 605	710	3.31 ~ 5.1	N	[50]

### 1.3 Objectives and outline of the thesis

The overall objective of this research is to develop a continuous, cell-based process that produces extracellular, water-soluble cadmium chalcogenide nanocrystals in high yield from low-cost precursors by direct fermentation. An engineered strain of *Stenotrophomonas maltophilia* (SMCD1) is chosen due to its intrinsically high resistance to a variety of heavy metals, including cadmium.<sup>[58–60]</sup> The enzyme associated with the nanocrystal formation has been identified as cystathionine  $\gamma$ -lyase and further overexpressed in engineered *E. coli* cells. This enzyme can solely direct nanocrystal synthesis equivalent to SMCD1 cells. Cadmium chalcogenide nanocrystals have been successfully synthesized by either SMCD1 or the enzyme with precisely controlled properties which are comparable to chemically synthesized QDs. The outline of this thesis is presented below:

- Chapter 1 gives a general introduction of quantum dots.
- Chapter 2 presents the results for biosynthesis of CdS QDs by SMCD1 cells and the techniques for characterizing CdS nanocrystals.
- Chapter 3 inspects the growth conditions for CdS synthesis, such as precursor concentrations, pH and growth temperature. Post treatments, e.g. capping exchange, core/shell growth, have also been discussed.
- Chapter 4 demonstrates the capability of cystathionine  $\gamma$ -lyase for CdSe synthesis and their photoluminescence enhancement by CdS shell growth and UV illumination.



- Chapter 5 discusses the growth mechanism of CdS and CdSe QDs formation by cystathionine  $\gamma$ -lyase and provides preliminary results for other types of nanocrystals synthesis.
- Chapter 6 summaries the major findings of this thesis and future work.

## Chapter 2

# Biom mineralization of CdS Quantum Dot from *Stenotrophomonas Maltophilia*

---

Harnessing nature's unique ability to achieve cost effective and scalable manufacturing solutions with reduced environmental impact is integral to realizing a future biomanufacturing economy. To address this challenge, we described a cell-based process using an engineered strain of *Stenotrophomonas maltophilia* (SMCD1) that produces high yields of extracellular, water-soluble CdS QDs from low-cost precursors in aqueous media. Strain SMCD1 enables controlled growth of CdS QDs over a period of 6 hours in culture, allowing precise, extrinsic control of QD size and optical properties with emission maxima ranging from 460 to 560 nm. The as-grown CdS QDs show both zinc-blende and wurtzite type structures with a quantum yield of up to 2.08 %. Our results demonstrate the feasibility of a scalable, biological process to produce low-cost CdS QDs.

---

### 2.1 Introduction

Biosynthesis of CdS QDs have been widely studied as discussed in Chapter 1. Several biological approaches have shown that biom mineralization of CdS and related semiconductor nanocrystals can occur, while these previous methods demonstrate only limited control over the final particle size. Since the opto-electronic functionality of QDs is largely due to their size dependent band gap, any application relevant synthesis route

must allow reproducible control over the nanocrystal size within the quantum confinement size range.

Bai et al. utilized immobilized *Rhodobacter sphaeroides* to demonstrate a progressive increase in CdS particle size with increasing cell incubation time, but did not provide information on the size distribution of the particles or the evolution of particle size over time.<sup>[61]</sup> Other reports of biosynthesized CdS nanocrystals show broad size distributions. For example, Borovaya synthesized CdS particles with sizes ranging from 2 to 8 nm within a single growth batch.<sup>[62]</sup> These previous reports demonstrate a mixture of both intracellular QDs<sup>[42,63–65]</sup> and extracellular QD<sup>[49,62,66,67]</sup> production. Extracellular production is preferable as it removes a requirement for cell lysis during harvesting, decreasing protein and other biomacromolecule contamination of the product nanocrystals. However, no previous report has demonstrated the combination of size controlled, reproducible, and extracellular biomanufacturing of CdS QDs.

In this chapter, we described an alternative aqueous-based, bacteria mediated, biosynthetic procedure for CdS nanocrystal synthesis at 37 °C. We utilized the relatively inexpensive precursor cadmium acetate ( $\text{Cd}(\text{CH}_3\text{CO}_2)_2$ ) as a Cd source and the amino acid L-cysteine as the sulphur source and capping agent. The resulting quantum dots show quantum yield (QY) approaching those of the chemical synthesized materials. We also demonstrated the control over the mean particle size in the 2-4 nm range which provides access to a wide range of quantum confined band gap energies. While the mean size and distribution width increases with increasing growth time, the as-synthesized standard deviation in mean size is demonstrated to be still less than 1 nm. The nanocrystals produced

are confirmed to be crystalline CdS via high resolution scanning transmission electron microscopy, X-ray energy dispersive spectroscopy (XEDS), and X-ray diffraction.






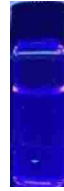
## **2.2 Biosynthesis of CdS quantum dots**

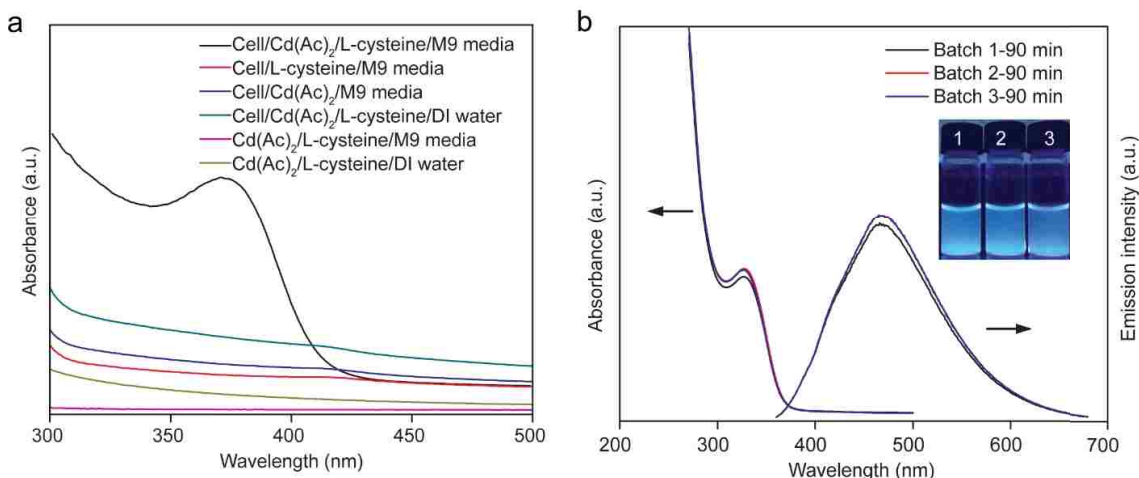
SMCD1 was isolated from soil as described above and iteratively selected for variants in culture that were tolerant to cadmium acetate at concentrations in excess of 1 mM. Cadmium-tolerant colonies were selected from cadmium-containing plates, and cultures grown in M9 minimal media containing 8 mM L-cysteine. From the observed photoluminescence (Table 2.1) and absorption spectra (Figure 2.1.a) with 6 h growth, only SMCD1 cells grown in the presence of both cadmium acetate and L-cysteine in M9 minimal media result in fluorescence consistent with the formation of CdS QDs with a well-defined first excitonic peak. Other combinations of ingredients lacking bacterium strain SMCD1, cadmium acetate or L-cysteine do not show any fluorescence, thus demonstrating that CdS formation and luminescence only occurs under culture conditions containing cadmium acetate, L-cysteine and SMCD1 cells in M9 media buffer. Furthermore, the procedure is reproducible, with essentially identical QD optical properties observed from independent cultures using optimized growth media and the same growth time (Figure 2.1.b). The absorbance and emission spectra are nearly the same and the inset photo also confirms that they have identical particle size.

Using the identified optimized growth conditions (Table 2.1), we find that photoluminescence is retained in the culture supernatants after removal of the cells by centrifugation, indicating that the water-soluble fluorescent particles are produced extracellularly (Figure 2.2.a). Compared to intracellular synthesis, it makes further purification of the nanocrystals much easier that simple centrifugation and dialysis can be

used to purify the as-grown nanocrystals without any cell lysis steps. The color clearly exhibits red-shift from blue to orange with increasing growth time. We also find that both absorption and fluorescence peaks shift systematically with increasing growth time in culture. Absorption spectra for samples with various growth times demonstrate well-defined first excitonic peaks (Figure 2.2.b) with maxima that shift to higher wavelengths with increasing growth time. The normalized fluorescence emission spectra (Figure 2.2.c) also show a shift to higher wavelength with increasing growth time. For the absorption spectra, the peak wavelength increases from 312 nm to 378 nm, while the corresponding emission spectra peak wavelength moves from 460 nm to 562 nm as the growth time is increased from 30 min up to 360 min.

**Table 2.1. Comparison of different growth conditions for CdS QDs synthesis.**

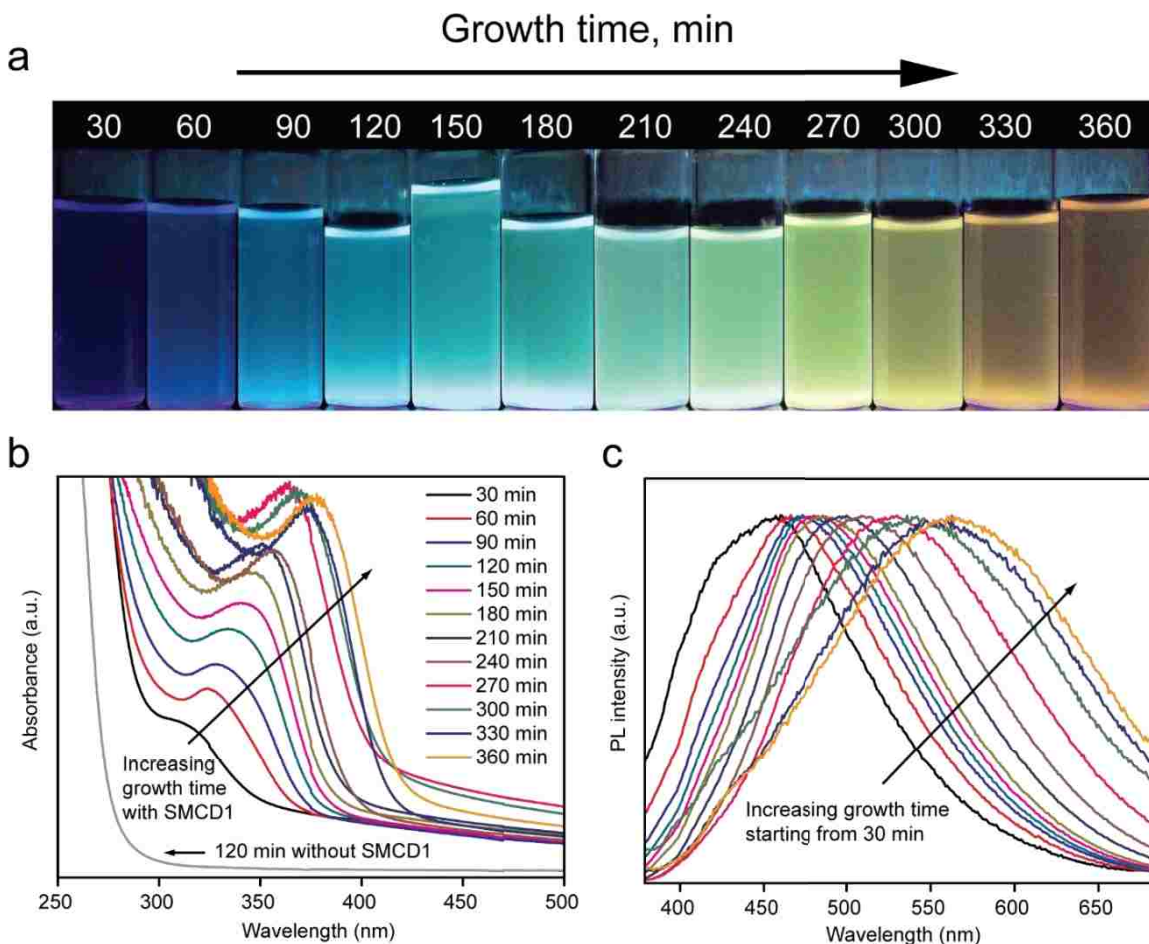
Ingredient	Sample 1	Sample 2	Sample 3	Sample 4	Sample 5	Sample 6
SMCD1 [OD <sub>600</sub> ]	0.5	0.5	0.5	0.5	–	–
Cd(Ac) <sub>2</sub> [mM]	1	–	1	1	1	1
L-cysteine [mM]	8	8	–	8	8	8
Growth media	M9 media	M9 media	M9 media	DI water	M9 media	DI water
Photoluminescence under UV light						



*Figure 2.1. Absorption and emission spectra of the as-grown cultures. (a) Absorption spectra of a series of samples prepared using different growth. (b) Optical properties of three different batches of CdS QDs prepared using the same growth conditions showing good reproducibility. Inset is a photograph of the culture supernatants illuminated under UV light. The emission spectra were recorded using a 350 nm excitation wavelength.*

While it may be hypothesized that another biosynthesized fluorescent species is responsible for the observed optical properties, all of this data is consistent with the biosynthetic formation of water soluble CdS quantum dots. Firstly, both cadmium acetate and L-cysteine are required for fluorescence to be observed in culture, indicating that the fluorescent species is CdS (Figure 2.1 and Table 2.1). Secondly, strain SMCD1 growing in M9 minimal media is necessary for fluorescence to appear indicating that this bacterial strain facilitates the biomineralization of CdS. Thirdly, the measured absorption wavelength maxima are consistent with a blue-shift from the bulk CdS band edge value (~515 nm) as expected for quantum confined CdS nanoparticles (Figure 2.2.b). The emission wavelengths are consistent with broad trap emission from such particles. Fourthly, the observed red-shift in both adsorption and emission wavelengths are consistent with increasing mean size of quantum confined particles with increasing time in culture (Figure 2.2.c). The relatively large Stokes' shift is typical of L-cysteine capped CdS QDs in aqueous solution as reported previously.<sup>[68,69]</sup> It is likely that the as-produced QDs are

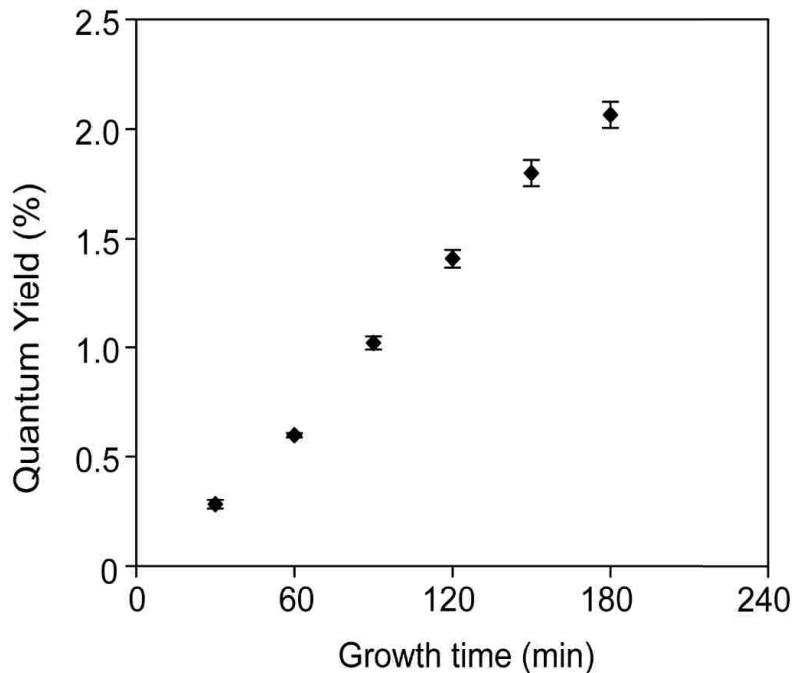
capped with L-cysteine due to the relatively high L-cysteine concentration in the media, as well as the requirement of L-cysteine for synthesis.



*Figure 2.2. Optical properties of the as-grown CdS QDs with different growth times. (a) Photograph of the culture supernatants from strain SMCD1 collected at various growth times when illuminated under UV light. (b) UV-vis absorption spectra of CdS QDs as a function of growth time. (c) Fluorescence emission spectra using a 350 nm excitation wavelength as a function of growth time.*

The QY of the purified CdS QDs which had growth times ranging from 30 min to 180 min were found to exhibit an approximately linear increase from 0.30 % to 2.08 % (Figure 2.3). Determination of the QY at longer growth times was inaccurate due to aggregation of the larger particles. The range of measured QY is once again consistent with other reports for L-cysteine capped QDs in aqueous solution and most importantly are

about three orders of magnitude greater than the QY (0.007 %) reported for previous biosynthetic CdS QDs.<sup>[42]</sup> The relatively low QY as compared to more standard inorganic preparation methods may be due to quenching by the L-cysteine or the dimer cystine.<sup>[70,71]</sup> Taking into account the measured systematic variation in particle size distribution with growth time, it can be concluded that the QY monotonically increases with increasing mean nanocrystal size in the 30-180 min growth time range. Similar size-dependent trends for the photoluminescence QY of semiconductor nanocrystals have been noted previously.<sup>[72-75]</sup> As the particle size decreases, the surface-to-volume ratio increases, which results in a higher proportion of surface defects. Therefore, it is likely that non-radiative relaxation at surface traps become more important with decreasing particle size.



*Figure 2.3. Quantum yields of CdS QDs as a function of growth time ranging from 30 min to 180 min.*

X-ray powder diffraction patterns (Figure 2.4) were also collected from powdered precipitated fractions of the as-grown CdS QDs and are consistent with CdS formation;



however peak broadening due to the nanoscopic nature of the particles results in just two broad peaks. Since the major peaks of commonly seen phases of CdS quantum dots, zinc-blende type and wurtzite type (there is also a high-pressure rock-salt phase, which is rarely reported) are very close to each other, it is impossible to identify the exact polymorphic structure of the as-grown CdS QDs from the XRD pattern.

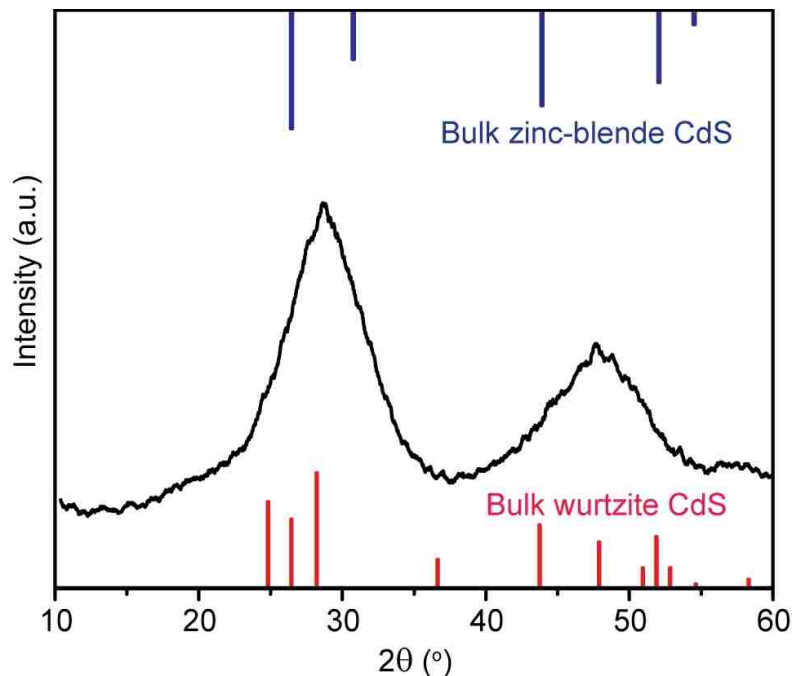


Figure 2.4. X-ray powder diffraction pattern of the precipitated CdS quantum dot powder after 360 min of growth. The stick patterns show the expected standard peak positions of the bulk wurtzite (bottom, PDF card no. 00-006-0314) and zinc-blende type CdS polymorphs (top, PDF card no. 00-010-0454).

### 2.3 Electron microscopy characterizations of CdS QDs

Electron microscopy characterizations provide us more crystal information of the as-grown nanocrystals, such as the crystal structure, particle size (distribution) and elemental analysis. For these nanocrystals, high resolution TEM (HRTEM) and high angle annular dark field - scanning transmission electron microscopy (HAADF-STEM) imaging are commonly used techniques. All the electron microscopy characterization work in this

thesis was carried out on two types of TEM instruments, JEOL 2000FX conventional TEM equipped with an Oxford Instruments XEDS system and aberration corrected JEOL ARM 200CF analytical electron microscope equipped with a Centurio XEDS system. The former has relatively low resolution and was used for pre-check of the samples. The latter allows a wider range of materials to be examined with atomic level resolution and was utilized for high magnification imaging of the nanocrystals. To achieve high resolution images, it is required that the samples meet a high level of purity. The most commonly encountered problem is the contamination which prevents the imaging especially at higher magnification.<sup>[76]</sup> The contaminations usually arise from the organic compounds left in the samples. Therefore, the samples need to be carefully prepared in order to eliminate the contaminations. As we have experienced a lot of failure when imaging these biosynthesized nanocrystals, here are several rules that would help to make the imaging easier:

(1) **Sample purifications.** To get rid of contaminations, the sample needs to be purified to a high extent. After synthesis, the culture was centrifuged at a high speed (8000 rpm for 10 min) to exclude large aggregates and cells. Then a syringe filter (0.2  $\mu\text{m}$ ) was used to filter large aggregates left (the cells should be completely removed after this step). After that, the solution was placed in a dialysis tubing (3500 MWCO) and dialyzed against deionized water for 24 h in 4 °C. The concentration of free thiol mostly from L-cysteine was detected by Ellman's reagent to determine the organic compound left in the solution, and it should decrease from ~ 8 mM to 0.2 ~ 0.5 mM after 24 h dialysis. After dialysis, another syringe filter was used to further remove the aggregates forming during dialysis and the solution is ready for TEM sample preparation. For aqueous sample preparation, 20 times dilution (initial absorbance peak intensity around 1) of the purified solution is proved

to be good for TEM imaging and it shows acceptable contaminations but with moderate particle concentration. For organic sample preparation, after one wash by anti-solvents, 50 times dilution (initial absorbance peak intensity around 1) was proven to work well. Multiple washes of the nanocrystals are recommended as long as the nanoparticles do not aggregate because of a loss of capping ligands.

(2) **TEM grid treatment.** Since the surface of carbon film on the grid is hydrophobic, the nanocrystal dispersion is non-ideal especially when preparing aqueous samples. To improve the dispersion of the nanoparticles deposited on the film, the TEM grids can be treated to form a hydrophilic surface by plasma cleaner. We use a chamber plasma cleaner and it can accommodate batch treatment of the TEM grids. The grids were placed in the chamber on a clean substrate and the plasma cleaner was set at a power of 10 W with air as the gas. The treatment last for 20 s and after that the TEM grids were ready for aqueous sample preparation. To test the hydrophilicity of the treated grid, simply loading a tiny drop of water (3  $\mu\text{L}$ ) onto the grid can be used to test whether the surface is hydrophilic or not. No treatment is needed if preparing with nanoparticles in organic solvent, such as chloroform or toluene.

(3) **Sample preparation and treatment before imaging.** The TEM sample was prepared by loading 3  $\mu\text{L}$  of the diluted solution onto the treated grid and placed in vacuum desiccator for 2 h. A wick-off technique is also useful to improve the dispersion of the nanoparticles. Right before loading the grid in the TEM instrument, a 10 s plasma treatment at 10 W was introduced to further eliminate the contamination. During imaging, 5 to 10 min beam shower is optional if necessary when contamination starts to appear. Beam

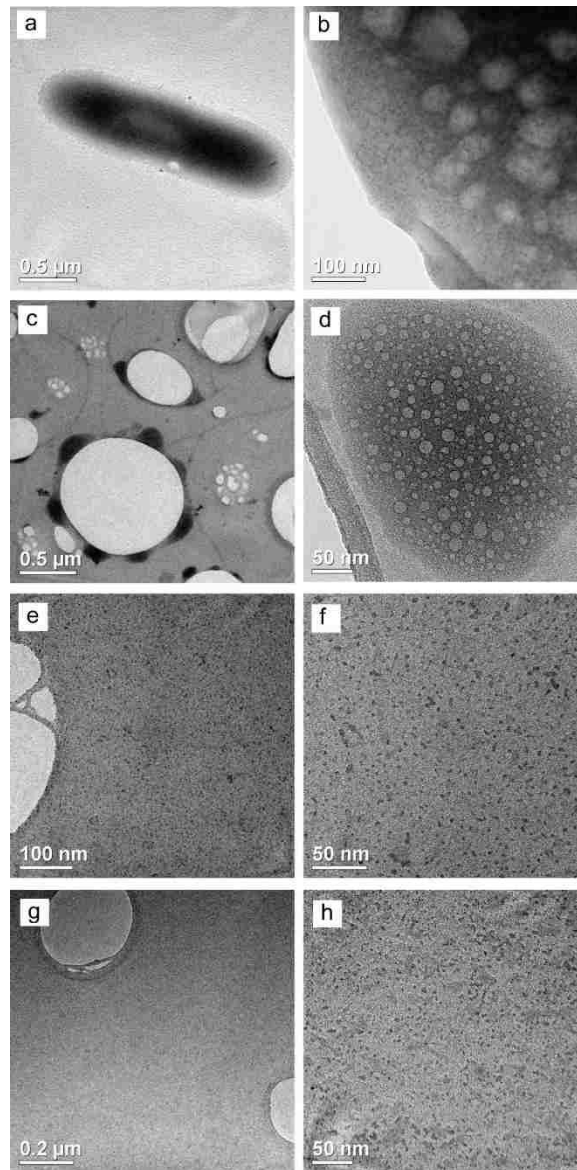
shower is commonly used to reduce the contamination by solidating the volatile organic compound on the specimen.<sup>[77]</sup>

(4) **Avoiding beam damage especially at high magnification.** Beam damage is clearly observable for small nanocrystals. There are not many actions to prevent the nanocrystals from damaged by intense electron beam. Generally, larger particles are much more stable compared to smaller particles especially under high magnification imaging. If imaging smaller particles, make sure to use lower magnification and meanwhile try to take images as quickly as possible, or else the particles would be damaged.

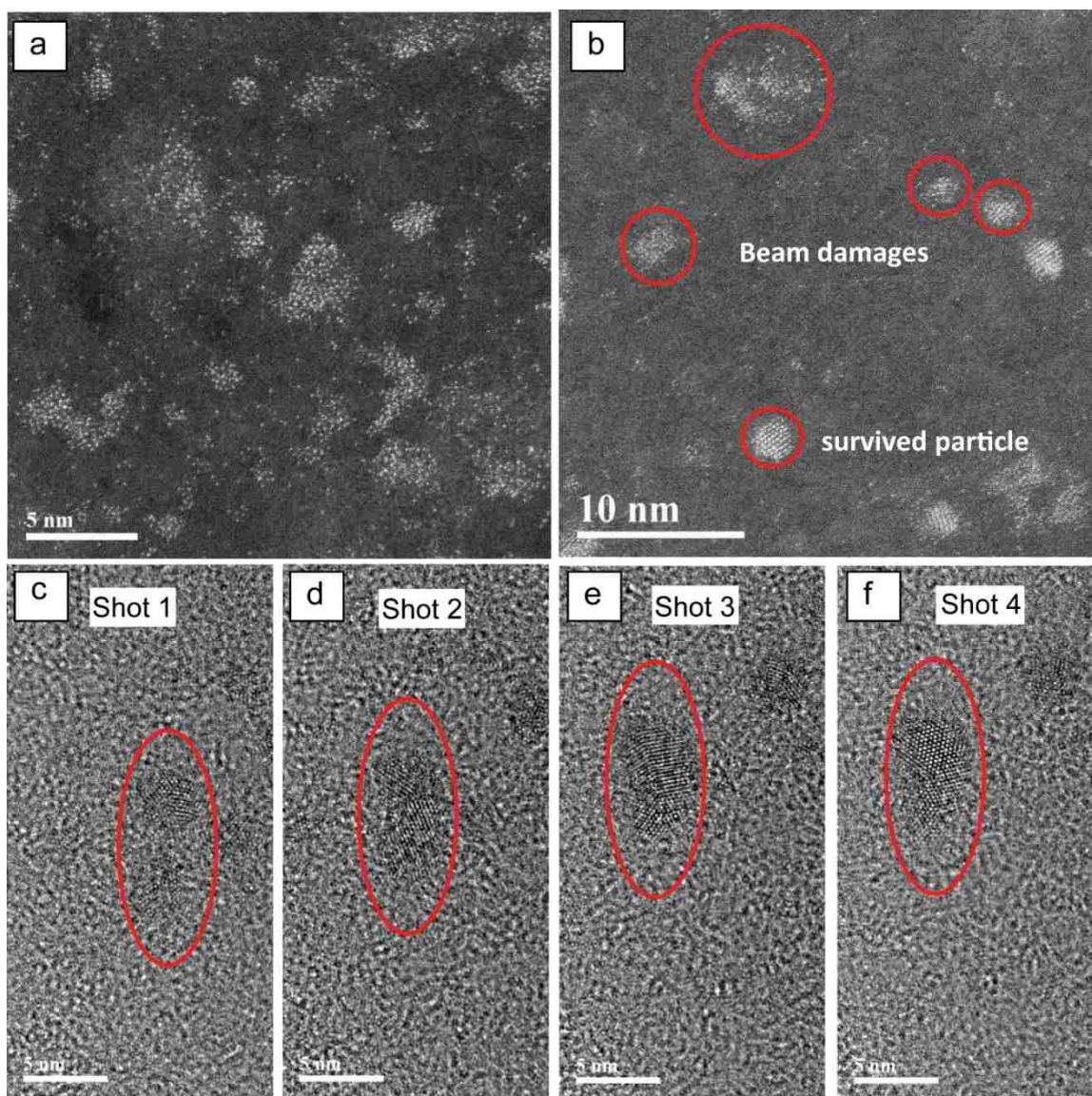
(5) **Single particle XEDS analysis.** It is very different to carry XEDS analysis on a single nanocrystal. To avoid serious detector drifts which bring the major error to the analysis, those isolated nanoparticles on the edge of the holes of the carbon film are better choices for testing. Then, the instrument can autocorrect effectively and reduce the test error. Meanwhile, line-scan analysis on a single particle always results in damage of the nanoparticles, thus line-scan analysis is not recommended.

Here, we demonstrate some typical TEM images of the samples prepared at different conditions. SMCD1 cells have a rod-like shape as shown in Figure 2.5.a. Without purification, the sample is very dense with cells found almost everywhere. We can also find that the nanocrystals are attached to the cells or organic matrix (Figure 2.5.b). After centrifugation, syringe filter and dialysis, the cells are barely found and the sample is much cleaner, however the nanoparticles are found embedded in loose organic matrix around the holes of the carbon film if no dilution applied (Figure 2.5.c and d). With 20 times dilution, the organic matrix is gone and the nanoparticles are well dispersed on the carbon film (Figure 2.5.e and f). The same as the samples prepared by wicked-off techniques, as shown

(Figure 2.5.g and h). All of these purification/treatment techniques improve the dispersion of these nanocrystals and meanwhile reduce the contamination to extremely low level. This also makes the high resolution imaging of the as-grown biosynthesized CdS nanocrystals feasible without serious contaminations.



*Figure 2.5. Electron microscopy characterization of SMCD1 cells and CdS QDs at different purification stage. (a) TEM image of SMCD1 cell. (b) TEM image of CdS QDs culture without purification. (c and d) TEM images of CdS QDs after purification but without dilution. (e and f) TEM images of CdS QDs after 20 times dilution. (g and h) TEM images of CdS QDs prepared by wicked-off technique.*

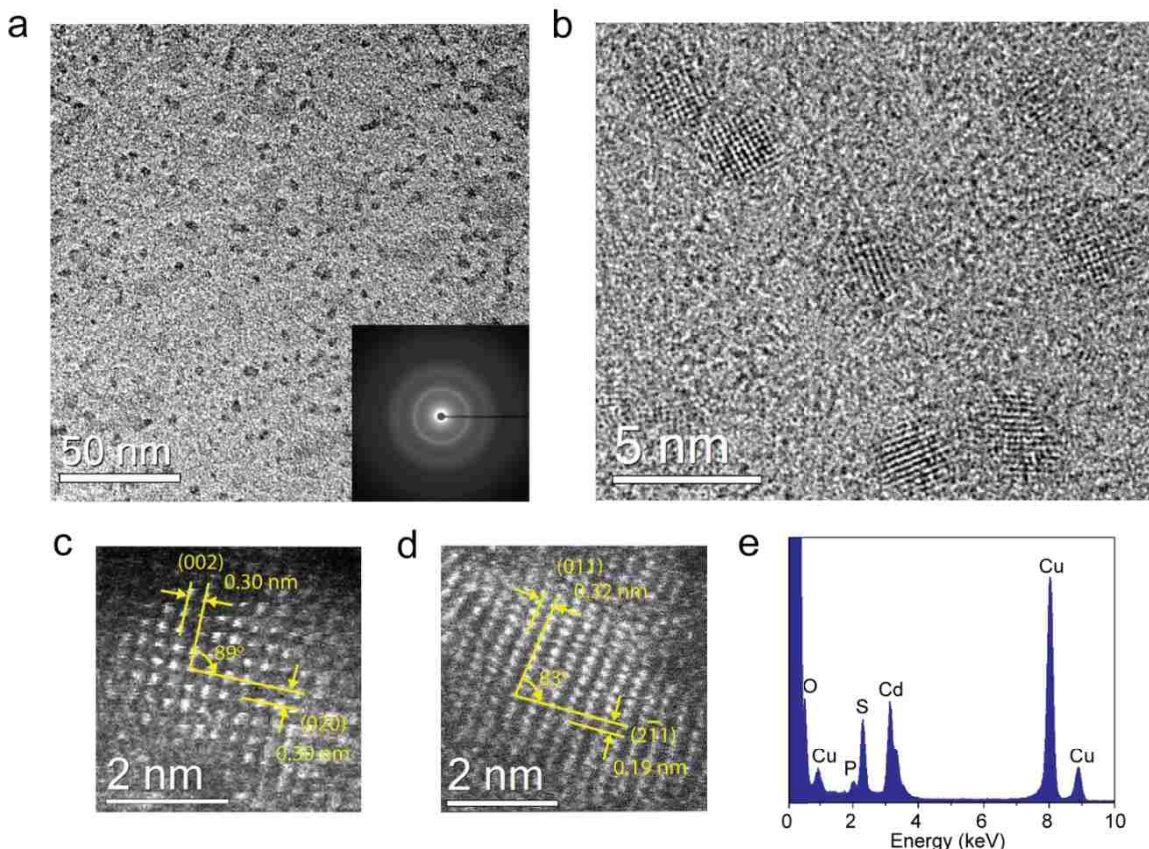


*Figure 2.6. Beam damage evidence of CdS QDs at high magnification imaging. (a) TEM image of atom clusters and dispersed atoms. (b) TEM image of survived and damaged CdS QDs. (c-f) TEM images of CdS QDs sintering after 4 images, sintering of two nanocrystals highlighted in red circles.*

We also found some evidence of beam damage during imaging at high magnifications. Some amorphous atom clusters or dispersed atoms are found frequently as shown (Figure 2.6.a). Nanoparticles with lattice fringes and nanosized atom clusters are also found (Figure 2.6.b). We attributed these atom clusters and dispersed atoms to the beam damage especially under intense electron beam at high magnifications. Direct



evidence of beam damage was caught by imaging the same area multiple times at high magnification (above 6 million). As is shown (Figure 2.6.c-f), two nanocrystals gradually sintered together and formed a single nanocrystal after 4 images. This reveals that these nanocrystals are very vulnerable under the electron beam and great caution should be paid when imaging them.



*Figure 2.7. Electron microscopy characterization of purified CdS QDs after 60 min growth. (a) Bright field TEM image of CdS QDs illustrating the typical particle dispersion, inset in (a) is the corresponding selected area electron diffraction (SAED) pattern. (b) Representative high resolution TEM image of CdS QDs. (c and d) High angle annular dark field (HAADF) images of particles exhibiting zinc-blende and wurtzite type structures respectively. (e) Energy-dispersive X-ray spectroscopy (XEDS) analysis confirming the co-existence of Cd and S in the QDs.*

By optimizing the TEM sample preparation and operation, we have succeeded in imaging the as-grown CdS quantum dots by HTEM and additional evidence to support

biosynthesis of CdS QDs from strain SMCD1 was obtained. Specifically, to evaluate the crystal structure and particle size distribution of the CdS materials, nanocrystals produced at a representative growth time of 60 min were purified and characterized by HRTEM (Figure 2.7). The highly dispersed QDs are clearly observable (Figure 2.7.a) by phase contrast imaging. From electron diffraction (Figure 2.7.a, inset), two broad but distinct rings corresponding to interplanar spacings of 0.33 nm and 0.21 nm are observed, which are consistent with expected lattice spacings of CdS. However, selected area electron diffraction cannot unequivocally distinguish between the possible CdS polymorphs (i.e. the zinc-blende and wurtzite type structures), as they both have lattice spacings similar to those measured within the limits of experimental error.

HRTEM and STEM-HAADF (high angle annular dark field) images were acquired to obtain more localized crystallographic information from the biosynthesized QDs. The HRTEM (Fig. 2.7.b) and STEM-HAADF images (Figure 2.7.c and d) exhibit lattice fringes within individual particles, whose spacings and intersection angles are consistent in some particles with the sphalerite form of CdS whereas in others they match the wurtzite form. The measured d-spacing value of 0.30 nm (Figure 2.7.c) for the two planes indicated match those of the (002) and (020) planes in zinc-blende type CdS viewed along the [100] projection; the measured interplanar angle is  $89^\circ$ , which matches the expected  $90^\circ$  angle between these two planes. In Figure 2.7.d the measured d-spacing values of 0.20 nm and 0.32 nm corresponds to those of the  $(2\bar{1}1)$  plane and (011) plane of wurtzite-type CdS, respectively; the measured interplanar angle between these two planes is  $83^\circ$ , which is also consistent with the expected value of  $82.0^\circ$  calculated from the cross product of  $(2\bar{1}1)$  and (011) when viewed along  $[\bar{1}\bar{1}1]$ . Detailed lattice fitting information can be found in Table



2.2 and 2.3. Therefore, we conclude that both zinc-blende and wurtzite type structures co-exist for CdS QDs produced by strain SMCD1. X-ray energy dispersive spectroscopy (XEDS) analysis confirmed that the particles are primarily comprised of cadmium and sulfur (Figure 2.7.e); some traces of phosphorus and oxygen are also present, most likely due to residual phosphate from the M9 minimal growth media; the copper peaks are artefacts of the TEM support grid.

**Table 2.2. Lattice fitting of nanocrystals in Figures 2.6.c to zinc-blende type CdS.**

Nanocrystal identification as zinc-blende type CdS		
Figure 2.6.c: [100] projection		
Plane	Measurement	Matching
Plane 1	d=3.01 Å	2.92 Å ( $2\bar{1}1$ )
Plane 2	d=3.03 Å	2.92 Å (011)
<1, 2> angle	89.4°	90°

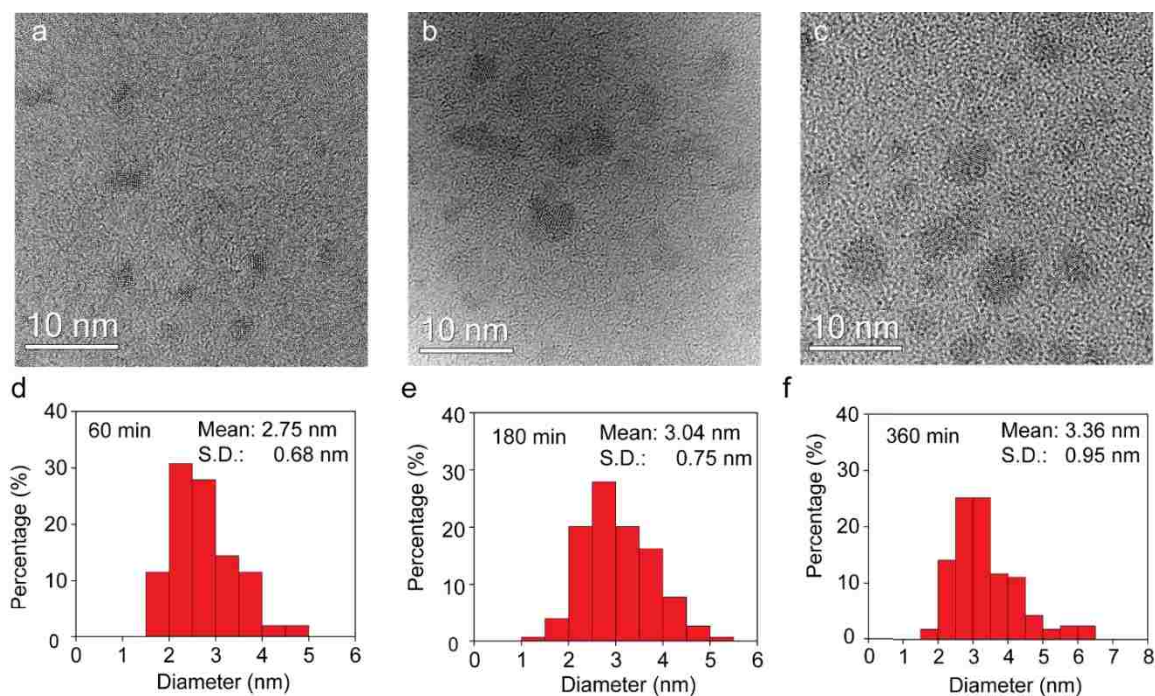
**Table 2.3. Lattice fitting of nanocrystals in Figures 2.6.d to wurtzite type CdS.**

Nanocrystal identification as wurtzite type CdS		
Figure 2.6.d: $[\bar{1}\bar{1}1]$ projection		
Plane	Measurement	Matching
Plane 1	d=1.93 Å	1.98 Å ( $2\bar{1}1$ )
Plane 2	d=3.22 Å	3.16 Å (011)
<1, 2> angle	82.7°	82°

## 2.4 Particle size control of CdS quantum dots

### 2.4.1 Particle size control by varying the growth time

Owing to their unique size dependent optical properties, tuning the particle size of QDs is very important. Here, we described a simple approach to control the average particle size of CdS nanocrystals synthesized from SMCD1 by varying the incubation time of the growth culture. Using the optimized growth conditions, we find that the absorbance peaks shift systematically with increasing growth time in culture (Figure 2.2.b).



*Figure 2.8. TEM images and particle size distributions of CdS QDs as a function of growth time. (a-c) Representative TEM images for growth times of 60, 180 and 300 min respectively; (d-f) Particle size distributions for growth time of 60, 180 and 300 min respectively (the mean values were derived from measurements of at least 100 particles).*

Typical TEM images of the CdS QDs with different growth time of 60, 180 and 300 min are shown (Figure 2.8.a-c) and exhibit well dispersion with lattice fringes indicating of nanocrystals. Particle size distributions (Figure 2.8.d-f) after 60, 180 and 300 min growth times were determined from analysis of these phase contrast images. The mean

particle size increases from 2.75 to 3.04 to 3.36 nm after 60, 180 and 300 min, respectively. The breadth of the distribution also increases with increasing growth time with the standard deviation increasing from 0.68 to 0.95 nm between 60 and 300 min growth. The observed relationship between size and adsorption peak wavelength are in-line with other reports for L-cysteine capped CdS QDs.<sup>[69,78]</sup>

#### **2.4.2 Particle size selection by gel filtration chromatography**

A post treatment of the purified CdS QDs was also introduced to select different size of these nanocrystals. Unlike size-selective precipitation procedure, which has been widely used in quantum dots especially synthesized from organic routes<sup>[3,79]</sup>, we introduced a precise and effective gel filtration chromatography purification technique for QDs size selection. This technique has been widely used for protein purification and has recently been reported for nanocrystals purification and size selection.<sup>[80]</sup> In gel filtration chromatography, the stationary phase consists of porous beads with a well-defined range of pore sizes allowing molecules within that molecular weight range to be separated. The elution volumes directly correlate with the hydrodynamic size of the analytes.

We used a commercial product, PD-10 desalting columns (GE Healthcare) containing *Sephadex G-25* medium, which allows rapid separation of high molecular weight substances from low molecular weight substances. Large particles are eluted first with a small retention time, while small particles are eluted last with a high retention time. In a typical procedure, 2.5 mL purified CdS QDs was loaded on top of the resin in the column, then deionized water was added continuously from the top to elute the nanoparticles. The eluates were collected in 0.5 mL aliquots as the elution started. The free thiol concentration, which indicates the level of L-cysteine in the solution, was also

checked. The absorbance spectra of the elution were collected (Figure 2.9.b) and they exhibit different excitonic peaks. As expected, the samples eluted first had larger peak wavelength, while the ones eluted later showed smaller peak wavelength. This reveals that eluted samples have different particle sizes. The photoluminescence under UV lamp also confirms the size selection (Figure 2.9.a). The nanoparticles are mainly distributed in elution 2 to 7 and shows blue-shift with increasing retention time. The free thiol concentration results show that the concentration of L-cysteine can be controlled to less than 0.3 mM from initial  $\sim 1.2$  mM in all of the elution samples containing CdS QDs.

Through gel filtration chromatography, the as-grown synthesized CdS QDs can be divided into portions with different sizes. Multiple runs of gel filtration chromatography were tried to further purify the samples, but the nanoparticles aggregated after 2 runs. We attribute the agglomeration of the nanoparticles to the low level of L-cysteine (free thiol), which also acts as the capping ligands stabilizing the nanoparticles. Once the concentration of free thiol is below a certain level, desorption of L-cysteine from the QDs surface results in a low coverage of the surface, eventually leads to the aggregation of the nanoparticles. In summary, gel filtration chromatography provides a simple method to select the as-grown nanocrystals with different sizes. It also helps to reduce the concentration of salts, for example, L-cysteine, left in the solution and can be used to purify the nanocrystals.

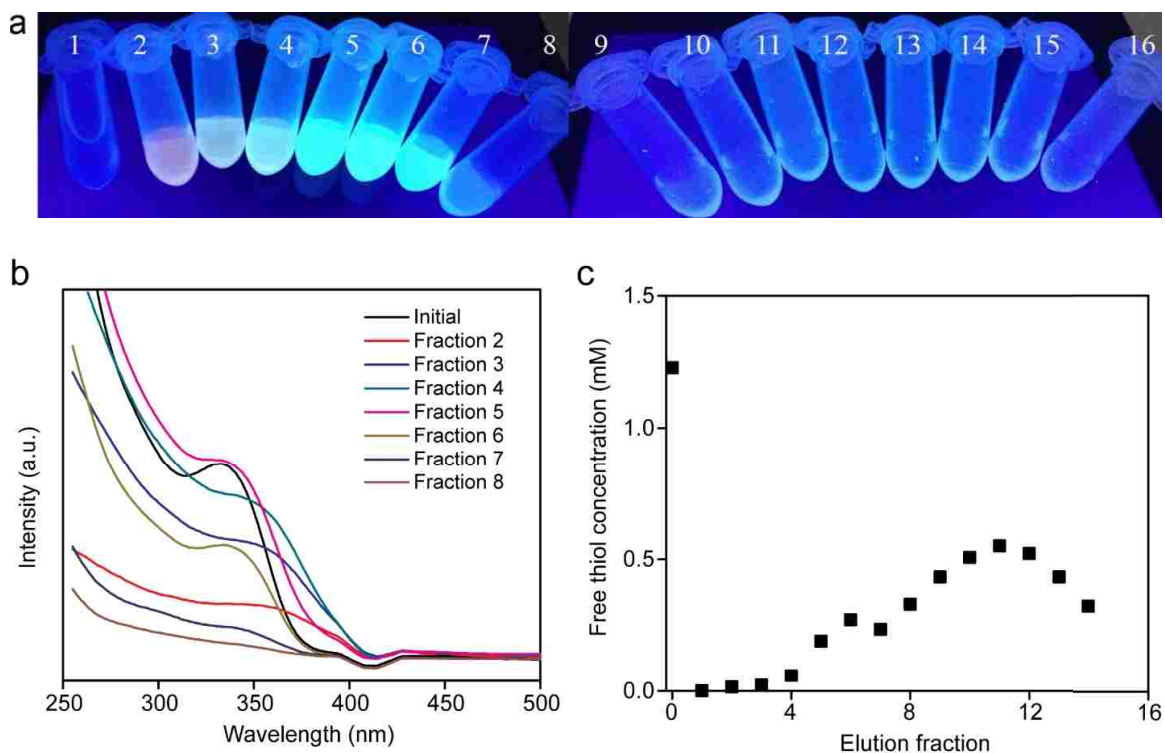


Figure 2.9. Size selection of CdS quantum dots by gel filtration chromatography. (a) Photo of different elutions under UV lamp; (b) absorbance spectra of different elution compared with initial CdS QDs; (c) Free thiol concentration profile of the eluted portions compared to the initial value.

## 2.5 Conclusions

We presented a novel approach for the reproducible biosynthesis of extracellular, water-soluble CdS QDs using an engineered strain of *Stenotrophomonas maltophilia* (SMCD1). The selected strain is capable of producing brightly fluorescent CdS QDs of different mean sizes, with emission maxima ranging from 460 to 560 nm and a quantum yield up to 2.08 %. Gel filtration chromatography was introduced to select the nanocrystals with different sizes. This biosynthetic approach to CdS QD production provides a viable pathway to realize the promise of green biomanufacturing of these materials for optoelectronic, energy, medicine and other emerging technological applications. Further optimizing the surface, structural and optical properties of the biosynthetic CdS QDs, as

well as investigating the cellular factors underlying the regulated biosynthesis will be discussed in next chapter.

## Chapter 3

# Optimizing Synthesis Conditions and Improving Functional Properties by Surface Modification of CdS Quantum Dots

---

Extracellular biomineralization of CdS quantum dot nanocrystals from buffered aqueous solution of cadmium acetate and L-cysteine were studied. CdS QDs synthesis is strongly influenced by the L-cysteine:cadmium acetate ratio, pH of the solution and the growth temperature. The observed trends are consistent with L-cysteine acting as both a sulfur source and nanocrystal capping agent. Enzymatic turnover of L-cysteine forms reactive sulfur in solution, removing the requirement for addition of reactive sodium sulfide of most other biomineralization approaches. The utility of the biomineralized quantum dots is demonstrated by phase transfer from the aqueous to the organic phase and subsequent incorporation into a quantum dot sensitized solar cell and chemical growth of a ZnS shell onto the biomineralized CdS core. QDs and reduced graphene oxide composite was also studied.

---

### 3.1 Introduction

Last chapter, we reported an engineered strain of the bacteria *Stenotrophomonas maltophilia* (SMCD1) capable of promoting extracellular CdS nanocrystal formation in the quantum confined size range. In biosynthesis processes, the growth conditions, such as the

reactant concentrations, pH of the buffer, and growth temperature, all play very important roles on the nanocrystal formation. In this case, cadmium acetate, as the Cd source, is toxic to bacteria, resulting in expressions of certain enzymes anticipated in transforming cadmium to nontoxic forms. The enzyme was identified as cystathionine  $\gamma$ -lyase, which is detailed discussed in chapter 5. L-cysteine, as the sulfur source and capping agent for CdS QDs, facilitates the formation of CdS nanocrystals and stabilizes them in the culture. The buffer, especially the pH, is also critical since enzymatic reactions are usually pH dependent. Growth temperature is also generally considered as an important factor influencing chemical reactions.

In this chapter, the sensitivity of SMCD1-mediated CdS biomineralization to reactant concentrations, buffer pH and temperature is systematically investigated to provide further insight into the QD formation mechanism. To the best of our knowledge, none of these previous reports describe the utilization of biomineralized CdS nanocrystals in any specific application. The outstanding question as to whether or not these biomineralized CdS nanocrystals can be utilized for optical applications is specifically addressed. A facile route for aqueous to organic phase transfer of the biosynthesized CdS nanocrystals is demonstrated which further broadens their scope for practical utilization as functional nanomaterials. The now organic soluble biomineralized CdS nanocrystals are integrated into a functioning quantum dot sensitized solar cell and also utilized in a chemical synthesis procedure to generate CdS/ZnS core-shell nanocrystals.



## 3.2 Influence of synthesis conditions on CdS QDs growth

### 3.2.1 Growth dependency on the concentration of cadmium acetate

We first investigated the influence variable cadmium acetate concentration between 0.25 mM and 4 mM with constant L-cysteine (8 mM) and cell ( $OD_{600} = 0.5$ ) concentration, and constant buffer pH of 9.0. This yields a theoretical range of (L-cysteine:cadmium acetate) ratio from 32:1 to 2:1. The absorbance and emission spectra of the harvested aqueous solutions after certain incubation time at 37 °C are shown in Figure 3.1. The first excitonic absorption peaks, Figure 3.1.a, shift to longer wavelength with increasing S:Cd ratio. No absorbance peak is observed at a S:Cd ratio of 2:1 as the peak is obscured by the absorbance of the buffer solution below 300 nm. The corresponding emission peak positions, Figure 3.1.b, shows the same red-shift trend with increasing S:Cd ratio, consistent with the change in visible photoluminescence under UV light, inset in Figure 3.1.b. The absorbance spectra as a function of incubation time were also collected at S:Cd ratios of 32:1 and 8:1. The absorption peak wavelength systematically increases as a function of incubation time up to 90 min in both cases, Figure 3.1.c; however, the peak intensity is much greater and the peak wavelength is clearly larger at decreased S:Cd ratio, which are consistent with the result of Figure 3.1.a. The optical properties reported here are all within the quantum confinement range for CdS, indicating the formation of CdS nanocrystals.

The observed red-shift in our samples is attributable to an increase in the average size of the quantum dots as the S:Cd increases, suggesting that the enzymatic production of  $H_2S$  may be the limiting factor in particle growth. Last chapter, the correlation of optical and electron microscopy data reveals that adsorption peak maxima of 324, 334 and 344 nm,

correspond to biomineralized nanocrystal sizes of  $2.75 \pm 0.68$ ,  $3.04 \pm 0.75$ , and  $3.36 \pm 0.95$  nm, respectively. Therefore, with S:Cd = 2, the nanocrystal size is believed to be larger than that of S:Cd = 32. Considering the same concentration of L-cysteine, the only difference is the concentration of cadmium acetate. From the peak intensity data, we can also roughly estimate the nanoparticle concentration from the peak intensity and it is reported that lower intensity implies lower particle concentration.<sup>[81]</sup> Thus, with lower cadmium acetate concentration, fewer CdS nanocrystal nuclei form, resulting in a lower nanoparticle concentration. While the turnover of L-cysteine to form H<sub>2</sub>S is almost identical owing to the same concentration of L-cysteine, it is not surprising that the size of the nanoparticles is larger with low S:Cd ratio. In summary, lower cadmium acetate concentration (S:Cd ratio) results in lower nanocrystal concentration, while the average nanoparticle size is larger and the as-grown CdS QDs culture exhibits larger absorbance peak wavelength and the same as emission.

### **3.2.2 Growth dependency on the concentration of L-cysteine**

L-cysteine acts as both the sulfur source and capping agent during nanocrystal biomineralization. The optimization of growth conditions is thus highly dependent on the interplay of factors influencing this dual role. Firstly, the concentration of L-cysteine will influence reactant availability and the growth rate. Secondly, L-cysteine is also the capping agent stabilizing the nanocrystals in the solution. The dynamic absorption and desorption of the capping agent on the nanocrystal surface during synthesis is also critical. In order to elucidate the influence of L-cysteine concentration, the CdS QDs growth at different L-cysteine concentration were inspected.

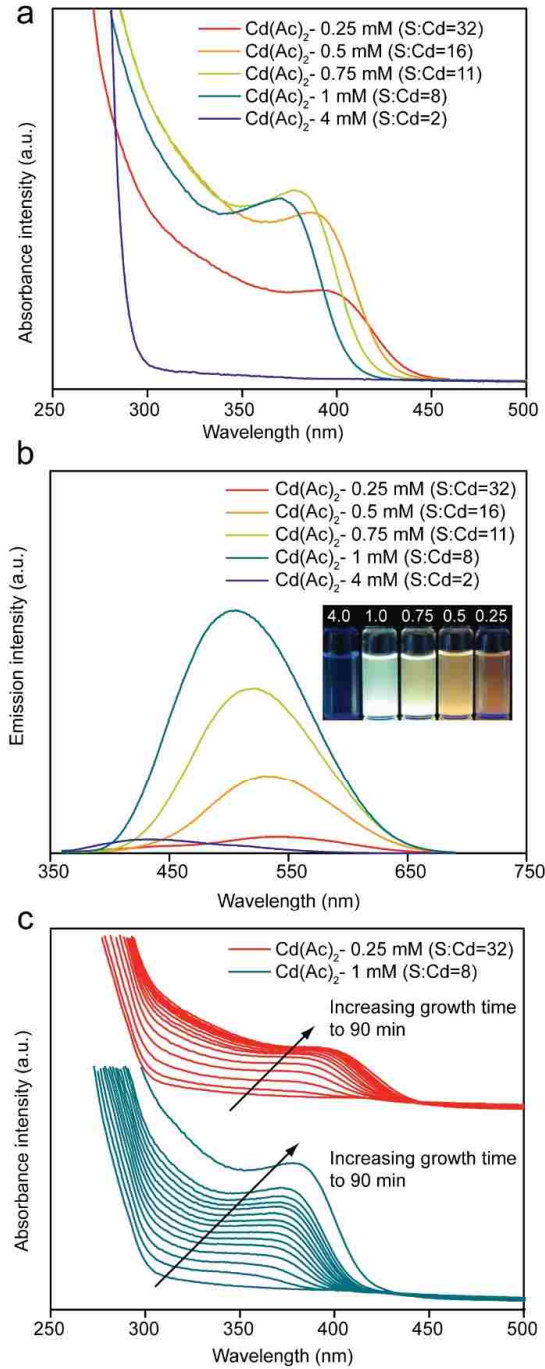
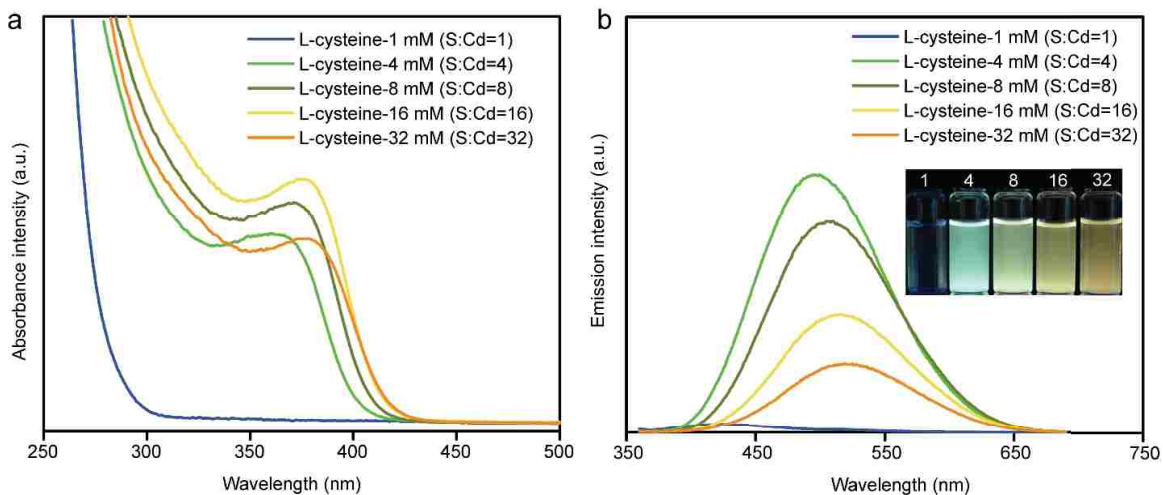


Figure 3.1. Aqueous phase optical properties of harvested CdS nanocrystal solutions grown with different concentrations of cadmium acetate ( $\text{Cd}(\text{Ac})_2$ ) ranging from 0.25 mM to 4 mM. a) UV-vis absorption spectra. b) Fluorescence emission spectra using a 350 nm excitation wavelength. Inset is a photograph of the cultures illuminated under UV light showing the evolution of fluorescent color. c) Temporal evolution of absorbance spectra using 0.25 mM and 4 mM concentrations of  $\text{Cd}(\text{Ac})_2$ . Each line is separated by a 4 minutes incubation time interval up until 50 mins, and after that the spectra were sampled at 60 and 90 mins.

Figure 3.2 shows absorption and photoluminescence properties respectively of CdS nanocrystals grown as a function S:Cd ratio induced by varying the L-cysteine concentration, from 1 mM to 32 mM, at constant cadmium acetate (1 mM) and cell ( $OD_{600} = 0.5$ ) concentration and a pH of 9.0. The absorbance spectra (Figure 3.2.a) show well-defined peaks with maxima showing a red-shift trend with increasing S:Cd ratio, corresponding to increasing L-cysteine concentration. As with the lowest S:Cd ratio in Figure 3.1.a, the absorption peak for S:Cd ratio is obscured by the absorption of the buffer solution. The emission spectra (Figure 3.2.b) show the same systematic trend with the peak maxima wavelength progressively red-shifting with increasing L-cysteine concentration, consistent with the visible photoluminescence observed under UV light, inset of Figure 3.2.b.



*Figure 3.2. Aqueous phase optical properties of CdS QDs harvested after 30 min incubation time with varying initial concentration of L-cysteine varying between 1 mM and 32 mM. (a) UV-vis absorption spectra of the as-grown cultures; (b) Fluorescence emission spectra using a 350 nm excitation wavelength. Inset is a photograph of the visible fluorescence from these cultures under UV illumination.*

### 3.2.3 Growth dependency on the pH of the buffer

The pH of the Tris-HCl buffer also plays very important role on CdS QDs formation in this biosynthesis process. As we know, most enzymatic reactions are pH dependent by exhibiting maximum activity in a narrow pH range. In addition, the solution pH will influence both the protonation/deprotonation of the thiol group on L-cysteine (with pKa = 8.3),<sup>[82]</sup> and the potential formation of the dimer, cystine, which can quench fluorescence.<sup>[70,83]</sup> To investigate how pH effects CdS QDs formation, we inspected the growth under different pH values.

Figure 3.3 shows the influence of buffer pH during growth on the optical properties of the nanocrystals at a fixed initial concentration of cadmium acetate (1 mM), L-cysteine (8 mM) and cells ( $OD_{600} = 0.5$ ). Figure 3.3.a shows that the nanocrystal absorbance peak wavelength of 372 nm at a growth pH of 9.0, is red-shifted by 51 nm when compared to that obtained from a synthesis carried out at pH 7.2. The corresponding emission peak wavelengths (Figure 3.3.b) are similarly red-shifted; i.e. 512 and 440 nm at growth pH 9.0 and 7.2, respectively. The corresponding quantum yields of these harvested particles are 0.7 and 1.9 %, for the pH 7.2 and 9.0 solutions, respectively. The reported optimal activity of cystathionine  $\gamma$ -lyase enzymes is above pH 8.0 which is in agreement with the observed red-shift upon increasing pH in our experiments.<sup>[84–86]</sup> This observation further supports the concept of the growth rate being dependent on the availability of reactive sulfur, most likely in the form of  $H_2S$ .

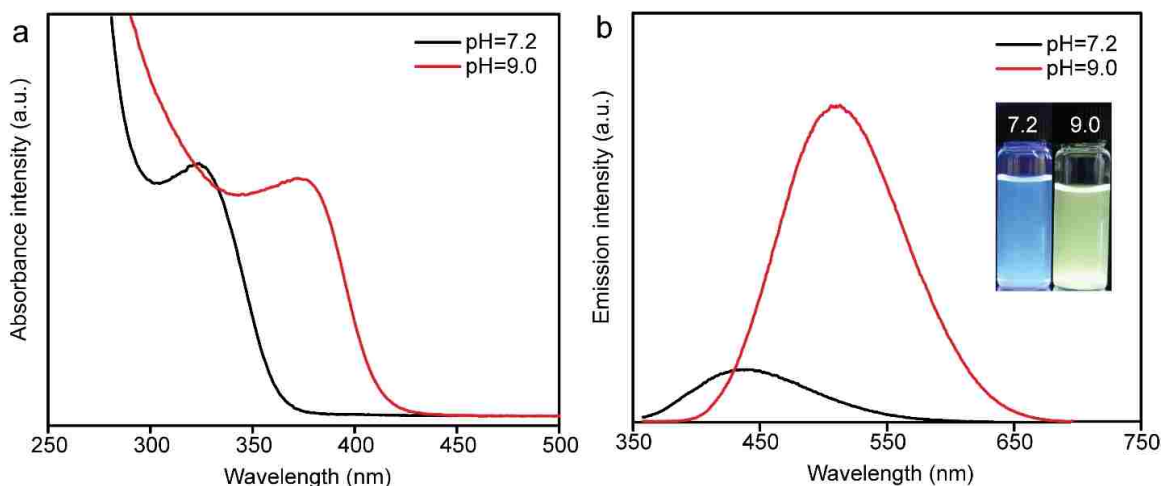
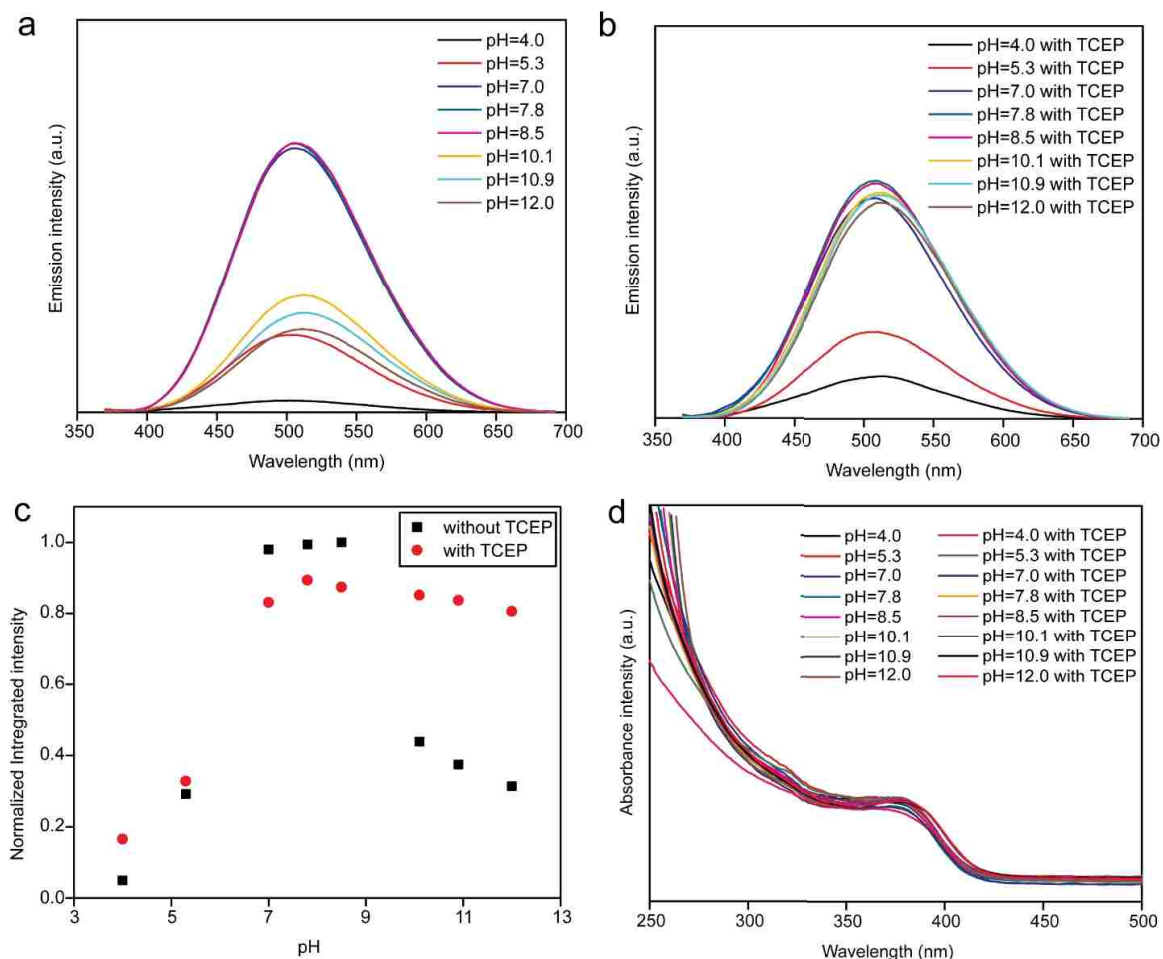


Figure 3.3. Aqueous phase optical properties of harvested CdS nanocrystal solutions after 30 min incubation time with varying initial pH. (a) UV-vis absorption spectra; (b) Fluorescence emission spectra using a 350 nm excitation wavelength. Inset is a photograph of the visible fluorescence from the cultures when illuminated under UV light.

Besides the growth evaluation at different pH, we also investigated the photoluminescence dependence of the purified CdS QDs solution on the solution pH. Figure 3.4 shows the photoluminescence intensity of various purified aqueous QD samples as a function of solution pH adjusted after synthesis. The synthesis was carried out at a pH of 9.0. The corresponding absorbance spectra peak maxima wavelength and intensity are unaffected by changing the pH after synthesis (Figure 3.4.d). The pH was adjusted with acetic acid or tetramethylammonium hydroxide. The optimal (maximum) photoluminescence intensity was obtained by adjusting the pH after synthesis to between 7.0 and 8.5, which is consistent with the pKa of the thiol group in L-cysteine being 8.3. The corresponding quantum yield in this pH range was determined to be 2.3%. The increased quantum yield of the post-treated sample when compared to the as-harvested solution is most likely due to the purification of the aqueous phase via dialysis. Decreasing the pH even further to 4.0 leads to a significant decrease in photoluminescence intensity and a corresponding decrease in quantum yield to 0.1%. This degradation is in-line with

previous reports, where a pH value significantly below the pKa of the thiol group in the QD capping agent leads to suppression of the photoluminescence in the absence of any specific cadmium-capping agent complex formation.<sup>[87–89]</sup>



*Figure 3.4. Aqueous phase optical properties of purified CdS nanocrystal solutions after 30 min incubation time with varying pH of the purified solution. (a) UV-vis absorption spectra of the as-grown cultures; (b) Fluorescence emission spectra using a 350 nm excitation wavelength; (c) Normalized integrated photoluminescence intensity; (d) Absorbance spectra of CdS QDs at different pH with and without TCEP.*

The photoluminescence intensity similarly decreases upon increasing the pH above 8.5 and the quantum yield drops to 0.7 % at pH 12. This is probably due to the dimerization of L-cysteine to cystine which has been previously reported to quench photoluminescence.<sup>[70]</sup> Cystine can be reduced upon the addition of tris(2-

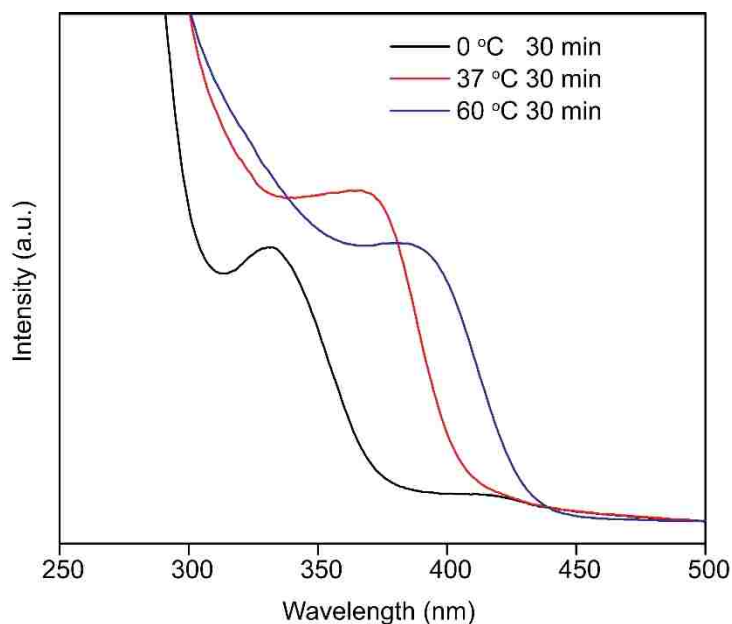
carboxyethyl)phosphine hydrochloride (TCEP) to the elevated pH solution, leading to an increase in photoluminescence (Figures 3.4.b and c). All of this data clearly demonstrates the role of L-cysteine as a capping agent in this biomineralized CdS QD system. This is in addition to its role as a sulfur source for the likely enzymatic turnover of L-cysteine to form H<sub>2</sub>S.

The quantum yield of these biomineralized CdS QDs is broadly comparable to the majority of other reports on aqueous phase chemically synthesized CdS solutions<sup>[90,91]</sup> although occasionally quantum yields up to 15%<sup>[92,93]</sup> have been obtained. In aqueous solution, the quantum yield may be limited by the relatively poor capping of L-cysteine; indeed, L-cysteine has been reported to quench the photoluminescence of aqueous CdS QDs.<sup>[71]</sup> Certainly a value of around 2.3 % when capped with L-cysteine in the aqueous phase appears to be the maximum achievable quantum yield through the current cell-based biomineralization route.

### **3.2.4 Growth dependency on the temperature**

We also investigated the temperature dependence of CdS biosynthesis. Figure 3.5 shows the influence of incubation temperature (0 °C, 37 °C and 60 °C) on the optical properties of the nanocrystals at a fixed initial concentration of cadmium acetate (1 mM), L-cysteine (8 mM), and cells (OD<sub>600</sub> = 0.5) at pH 9 Tris-HCl buffer for 30 min incubation. The peak wavelength of the absorbance spectra clearly exhibits red-shift with elevating temperature from 335 nm to 390 nm, while the intensity remains similar. The peak shift indicates that the particle size increases at higher temperature. This also means that at higher temperature, CdS QDs growth is favored, likely owing to higher activity of the enzyme associated with the CdS growth.





*Figure 3.5. Aqueous phase optical properties of CdS nanocrystal solutions after 30 min incubation time with varying temperature. (a-c) UV-vis absorption spectra of the as-grown cultures at 0 °C, 37 °C and 60 °C, respectively.*

### **3.2.5 Discussions**

The CdS nanocrystal growth rate is clearly sensitive to the S:Cd ratio, with values between 4:1 and 16:1 yielding stable nanocrystal solutions after 30 minutes of incubation that show optical properties consistent with CdS particles in the quantum confined size range. Figures 3.1 and 3.2 also reveal practical limitations in both the upper Cd concentration and lower limit of L-cysteine concentration. A Cd concentration of 4 mM leads to minimal nanocrystal growth, most likely due to the toxicity of Cd to the cell. The original directed evolution approach selected a viable bacterial strain at 1 mM Cd. An L-cysteine concentration below 4 mM also leads to minimal nanocrystal growth, which in this case is due to a combination of low availability of reactive sulfur and utilization of the amino acid in unrelated cellular processes.

Within the range of stable solutions, increasing the S:Cd ratio leads to a red-shift of optical properties, consistent with an increase in nanocrystal size and consistent with

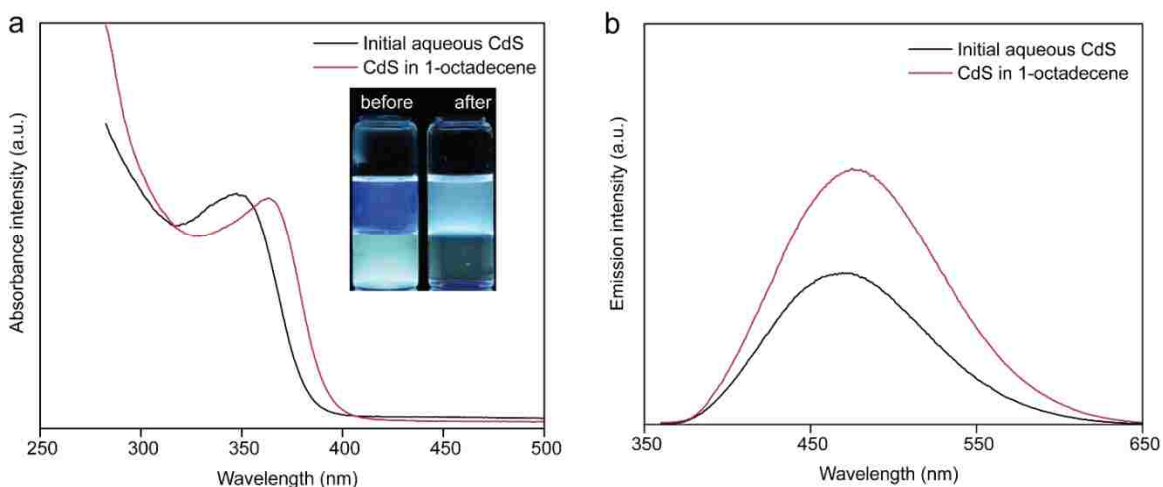
other reports of varying S:Cd ratio during chemical synthesis with reactive chemical precursors added to solution.<sup>[94,95]</sup> Wang et al. proposed that at low cysteine/Cd ratio, the Cd precursor is primarily in the form of reactive Cd-cysteine monothiol-complexes that initiate large population of nuclei, and consequently a larger number of smaller particles are formed during synthesis. In contrast, at higher cysteine/Cd ratio, they suggest that the Cd precursor is mainly in the form of a lower reactivity dithiol-complex, leading to a smaller number of nuclei and subsequent increased average size of QD. Critically Wang et al also discuss that increased cysteine concentration also favors the formation of the cysteine dimer. The potential formation of this dimer is likely of increased importance to our biomineralization process as cysteine acts as both capping agent and sulfur precursor. No reactive chemical precursor such as Na<sub>2</sub>S is added for biomineralization, instead strain SMCD1 produces the putative cystathionine  $\gamma$ -lyase enzyme previously identified as responsible for mineralization and templating.<sup>[96]</sup> This class of enzyme converts L-cysteine or L-cystine to H<sub>2</sub>S, pyruvic acid and NH<sub>3</sub>,<sup>[97]</sup> thereby providing the reactive sulfur required for solution phase CdS biomineralization. It may be that the presence of the dimer reduces the number of initial nuclei through slower enzymatic turnover.

### **3.3 Surface modification of biosynthesized CdS quantum dots**

#### **3.3.1 Phase transfer and capping exchange of the biosynthesized CdS QDs**

A facile method was developed to transfer the CdS QDs from the aqueous phase to organic solvent. The protocol is very efficient that simply mixing two phases result in successful phase transfer. In a typical procedure, 10 mL 1-octadecene (solvent) and 5 mL oleylamine (capping agent) were mixed with 15 mL purified CdS QDs solution. Then the mixture was vigorously stirred to ensure successful phase transfer. After that, phase

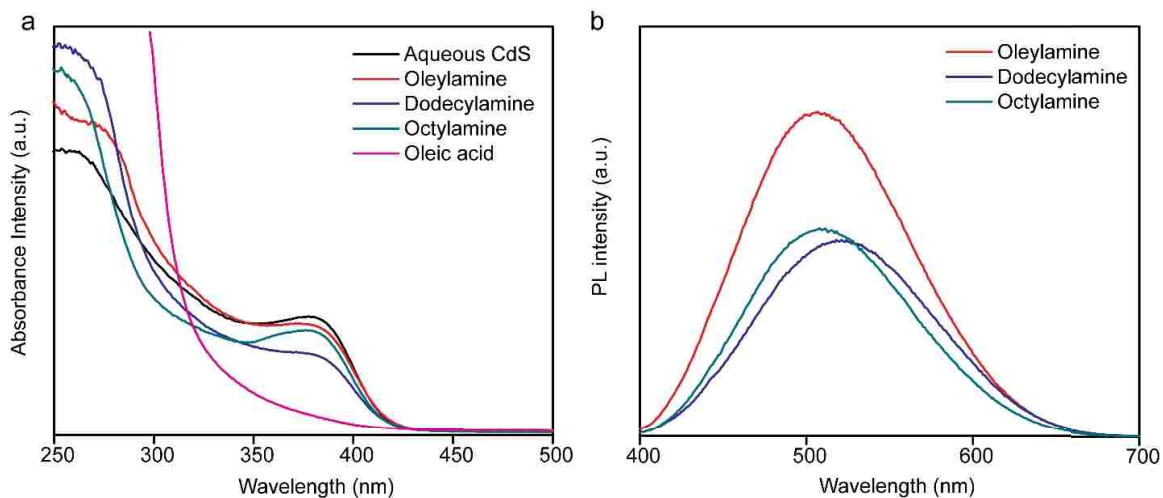
separation by centrifugation was used and the top organic phase with CdS QDs was collected. Multiple washes by anti-solvents were introduced if necessary.



*Figure 3.6. Optical properties of CdS QDs in aqueous phase and 1-octadecene after phase transfer. (a) UV-vis absorption spectra; (b) Fluorescence emission spectra using a 350 nm excitation wavelength. Inset in (a) is a photograph of the bi-phase solution illuminated under UV light before and after transfer.*

The absorbance and photoluminescence emission spectra of the QDs in the aqueous phase and in the organic phase after phase transfer are shown in Figures 3.6.a and b respectively. The efficiency of the phase transfer procedure is confirmed by the low level of photoemission observed under UV illumination for the (lower) aqueous phase after transfer, and correspondingly high level of photoemission from the (upper) organic phase, inset in Figure 3.6.a. The peak intensity before and after phase transfer are nearly the same, which in the other way confirms the high efficiency of this phase transfer protocol. The maxima of the absorbance and photoemission peaks both red-shift, by 15 and 5 nm, respectively, upon transfer to the organic phase due to the change of capping agent. The quantum yield of the CdS QDs in the organic phase increases to 2.9 % from an initial value of 1.5 % in the aqueous phase, most likely due to more efficient QD capping in the organic

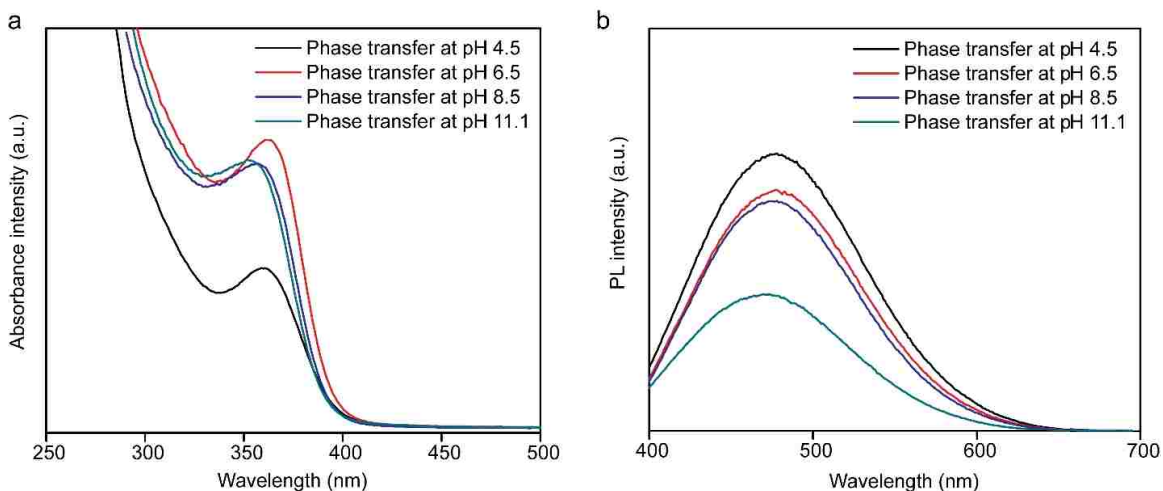
phase. This facile procedure for aqueous to organic phase transfer enables integration of the biomineralized QDs into more standard processing procedures.



*Figure 3.7. Optical properties of CdS QDs in aqueous phase and organic phase after phase transfer with different capping agent, oleylamine, dodecylamine, octylamine and oleic acid. (a) UV-vis absorption spectra; (b) Fluorescence emission spectra using a 350 nm excitation wavelength.*

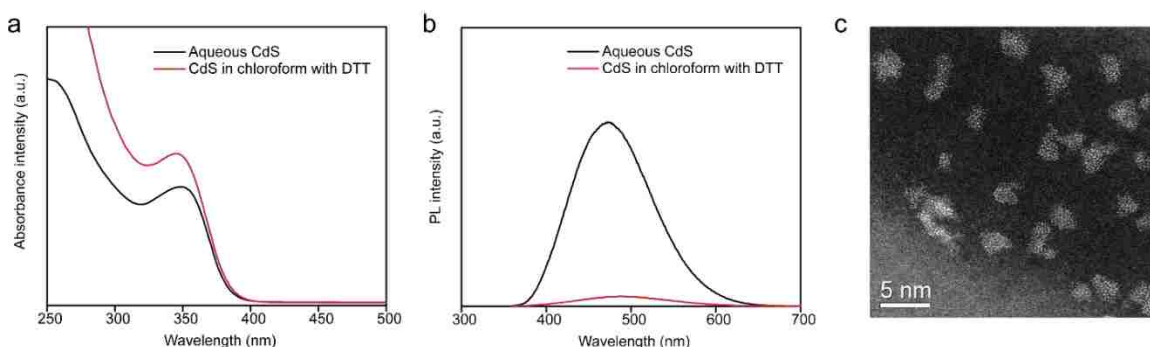
Besides oleylamine (C<sub>18</sub>), other capping agents have also been introduced for phase transfer, such as dodecylamine (C<sub>12</sub>), octylamine (C<sub>8</sub>) and oleic acid. Except oleic acid, other amines also show efficient phase transfer according to the absorbance spectra (Figure 3.7.a). The absorbance spectrum from oleic acid does not show a characteristic peak which indicates existence of CdS QDs, while others show nearly identical spectra as the aqueous CdS sample. The emission spectra of the transferred CdS QDs reveal that with oleylamine as the capping agent, the intensity is the highest, indicating better passivation or coverage of the nanocrystals' surface. Therefore, it is safe to conclude that amines exhibit better affinity to CdS QDs and can be used for phase transfer of L-cysteine capped CdS QDs with high efficiency. Among these amines, oleylamine exhibits the best transfer efficiency and highest photoluminescence.

We also investigated the pH effect on this phase transfer protocol. The pH of the purified CdS QDs solution was adjusted from 4.5 to 11.1 by either acetic acid or sodium hydroxide, and then identical conditions were used for phase transfer. At acidic condition, e.g. pH 4.5, the phase transfer is not as efficient as that with higher pH (Figure 3.8.a). For the sample with pH 4.5, the transferred absorbance peak intensity is much lower. However, the emission intensity is the highest indicating the highest quantum yield. As we discussed before, low pH favors the protonation of L-cysteine, resulting in desorption of the capped ligands. The coverage of CdS nanocrystals' surface decreases at acidic conditions and this promotes the absorption of amines. More amine but fewer L-cysteine on the nanocrystals' surface enhance their photoluminescence with high emission intensities. It is worth to note that poor capped nanocrystals in the aqueous phase at acidic conditions have the trend to aggregate since there are fewer ligands left on the surface to stabilize them. This can explain that lower pH has a lower absorbance intensity.



*Figure 3.8. Optical properties of CdS QDs after phase transfer at different pH. (a) UV-vis absorption spectra; (b) Fluorescence emission spectra using a 350 nm excitation wavelength.*

Another protocol reported by Gaponik et al. has also been used for CdS QDs phase transfer. Instead of amines, 1-dodecanethiol is the capping agent.<sup>[14]</sup> In a typical procedure, 10 mL 1-dodecanethiol and 20 mL acetone was mixed with 15 mL purified CdS QDs solution. Then the mixture is vigorously stirred and heated up to the boiling point of acetone around 60 °C to ensure successful phase transfer. After that, phase separation by centrifugation was used and the top organic phase enriched with CdS QDs was collected. Further precipitation and resuspension steps were used to purify the QDs. The purified CdS QDs are then soluble in solvents, like hexane or chloroform and ready for characterizations.



*Figure 3.9. Characterizations of CdS QDs before and after phase transfer with 1-dodecanethiol. (a) UV-vis absorption spectra; (b) Fluorescence emission spectra using a 350 nm excitation wavelength; (c) Typical HAADF-STEM images of CdS QDs after phase transfer.*

This protocol is also very efficient and the nanocrystals can be transferred to the organic phase in minutes. The absorbance spectra also confirm the efficiency of the phase transfer (Figure 3.9.a) and the peak wavelength doesn't shift. However, the emission is significantly quenched compared to the initial one (Figure 3.9.b). We attribute the quenching of photoluminescence to the capping ligand, 1-dodecanethiol. Thiols were widely reported to quench the emission of CdS or CdSe quantum dots.<sup>[98,99]</sup> CdS QDs after phase transfer are also characterized by STEM (Figure 3.9.c). Interestingly, the nanoparticles turn to be amorphous clusters rather than nanocrystals, while the shapes of

the particles are maintained. It is hypothesized that 1-dodecanthiol capped CdS QDs are very sensitive to electron beam and can be easily damaged.

### 3.3.2 ZnS shell growth on CdS via chemical route

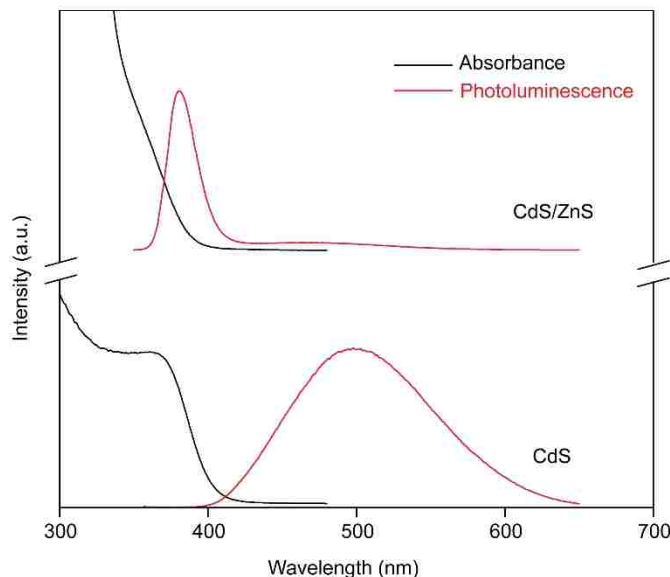


Figure 3.10. Normalized optical characteristics of the core CdS QDs capped with oleic acid and resultant core-shell CdS/ZnS QDs. Black lines are UV-vis absorption spectra; red lines are fluorescence emission spectra using a 350 nm excitation wavelength.

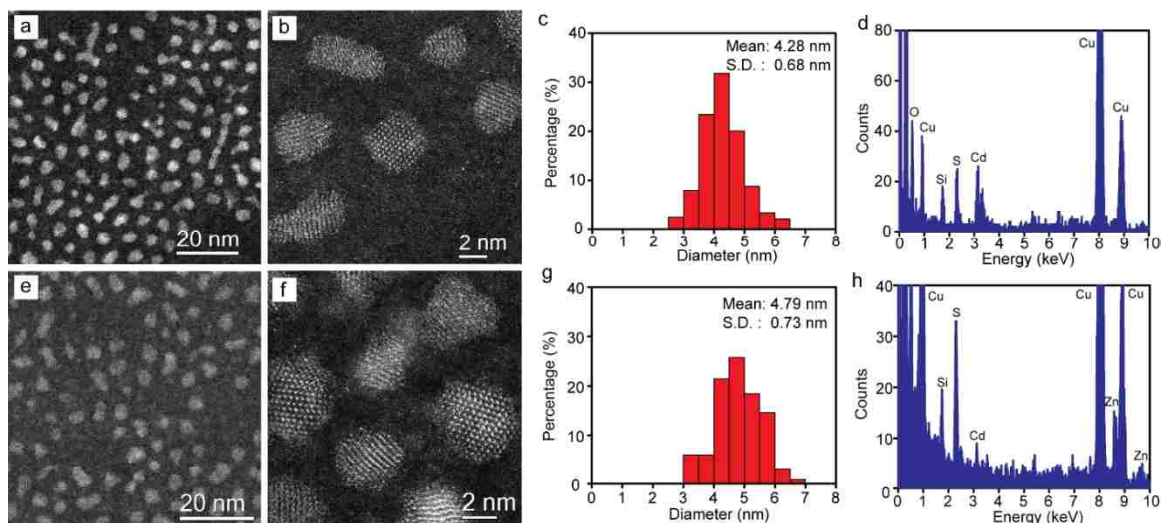
To further demonstrate the possible utility of these biomineralized QDs, CdS/ZnS QDs were synthesized from the phase transferred CdS by following a single precursor method previously developed by Chen et al.<sup>[24]</sup> The absorbance and emission spectra of the QDs before and after ZnS shell growth are shown in Figure 3.10. While the emission spectrum of the CdS core material shows a broad trap-state emission with a large Stokes' shift of 135 nm, the CdS/ZnS QDs exhibit a dominant band-edge emission with a Stokes' shift of 20 nm. This indicates that the growth of a ZnS shell on the biomineralized QDs eliminates the majority of the surface traps and is consistent with previous reports for chemically synthesized materials.<sup>[24,25,100,101]</sup> The ZnS growth procedure requires capping agent exchange on the seed QD to oleic acid which causes an accompanying quenching of

CdS photoluminescence, as compared to the original oleylamine capped CdS QDs. The quantum yield of oleic acid capped biomineralized CdS QDs prior to ZnS growth is only 0.8 %, but increases to 2.7 % after ZnS shell growth, suggesting effective passivation of CdS surface trap states.

High angle annular dark field - scanning transmission electron microscopy (HAADF-STEM) was utilized to visualize the size and crystalline nature of the CdS and CdS/ZnS QDs, and complementary X-ray energy dispersive spectroscopy (XEDS) analysis was performed to confirm the co-existence of Cd and Zn within individual core-shell QDs. Well dispersed CdS QDs prior to ZnS growth are observable in Figure 3.11.a. Corresponding higher resolution images are able to resolve atomic structure within individual particles (Figure 3.11.b). Previous fitting of lattice fringe spacings and intersections angles indicate that the biomineralized CDs QDs are in fact a mixture of the hexagonal wurtzite and cubic zinc-blende phases. Comparable particle dispersion, crystal quality and polymorph distribution are observed for the CdS/ZnS QDs, as shown in Figures 3.10.e and f, respectively. XEDS analysis from individual QDs confirmed that the as-synthesized CdS particles contain only Cd and S (Figure 3.11.d) while the XEDS spectrum of a single CdS/ZnS particle confirms the presence of Cd, Zn and S (Figure 3.11.h). Although there is not enough contrast to directly observe a distinct core-shell structure in these images, the thickness of the ZnS layer can be estimated by comparison of the particle size distributions acquired before and after ZnS shell deposition as measured from analysis of at least 200 particles per sample. The mean particle size of the CdS only QDs is  $4.28 \pm 0.68$  nm with a dispersion of 16 % (Figure 3.11.c). After ZnS growth, the mean size



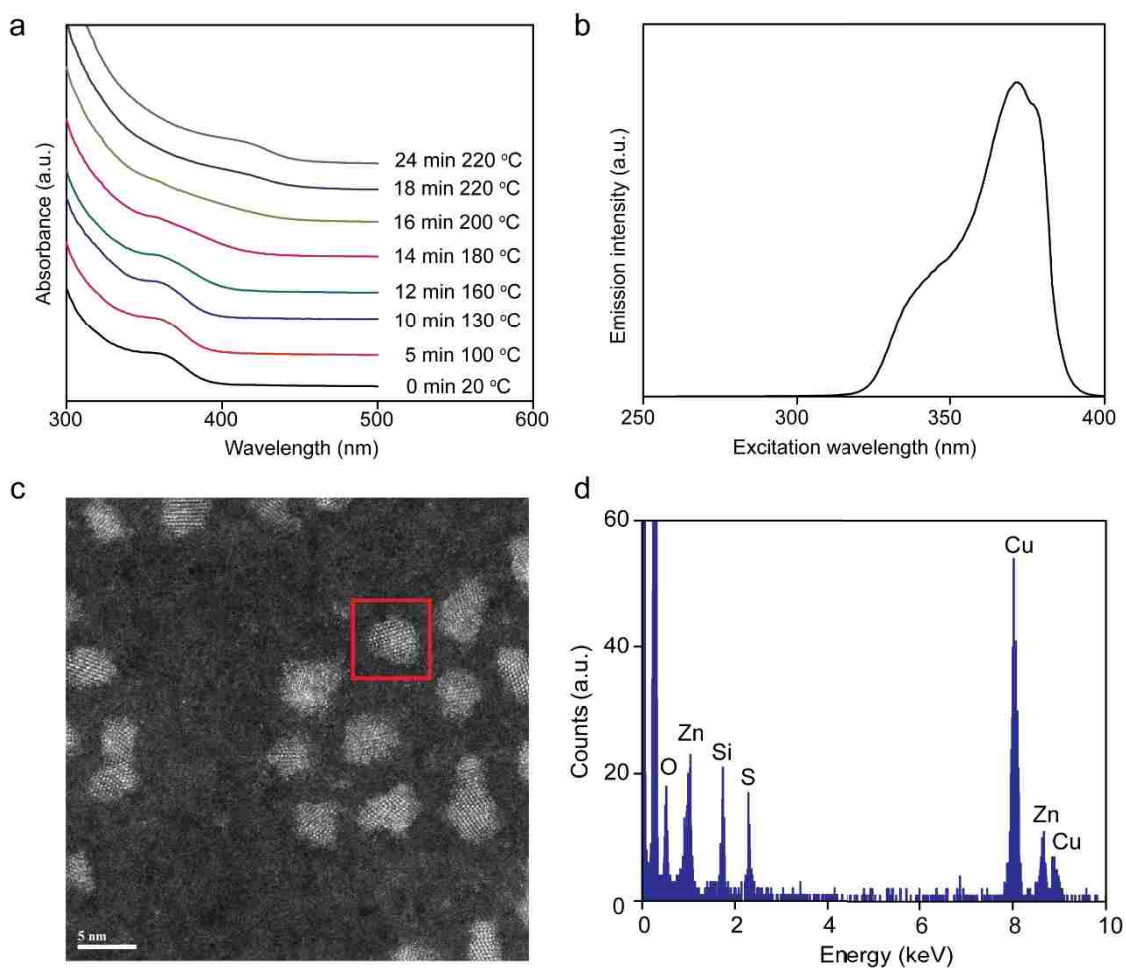
increases to  $4.79 \pm 0.73$  nm with a dispersion of 15 % (Figure 3.11.g). This is consistent with the deposition of about a monolayer of ZnS on the exterior surface of a CdS core. [25]



*Figure 3.11. Electron microscopy characterizations of CdS and CdS/ZnS quantum dots. (a and b) HAADF-STEM images of the CdS QDs; (c) Particle size distribution of the CdS QDs; (d) XEDS analysis from an individual CdS QD. (e and f) HAADF-STEM images of the CdS/ZnS QDs. (g) Particle size distribution of the CdS/ZnS QDs. (h) XEDS analysis of the CdS/ZnS QDs. A small Si-escape peak from the detector material is present in the XEDS spectra; the copper peaks arise from the TEM support grid.*

As described in the experimental session, the method used for ZnS shell growth is a low temperature procedure, which is chosen owing to the thermal stability of the biosynthesized CdS. Figure 3.12.a shows the absorbance evolution of CdS QDs when heated up to 220 °C and it clearly demonstrates that the absorbance peak red-shifts above 180 °C. This indicates that these nanocrystals are not stable at high temperature and procedures for shell growth with temperature beyond 180 °C is not feasible. We also checked the excitation spectrum emitted at 380 nm of the CdS/ZnS QDs after shell growth and from the spectrum we cannot find the evidence supporting considerable population of ZnS nanocrystals (Figure 3.12.b). ZnS has a bulk band gap of 3.6 eV corresponding to ~ 344 nm wavelength. For quantum confined ZnS nanocrystals, the absorbing wavelength

should be even smaller. This excitation spectrum confirms that no significant population of ZnS nanocrystals form. However, from single nanocrystal XEDS analysis, we find some nanoparticles with composition of Zn and S but not Cd, which indicates few populations of ZnS nanocrystals (Figure 3.12.c and d). Therefore, there are some ZnS nanocrystals forming during the core/shell growth, which are difficult to avoid, but the population is not massive.



*Figure 3.12. More characterizations of CdS/ZnS quantum dots. (a) Absorbance evolution of CdS QDs after phase transfer when heated up to 220 °C. (b) Excitation spectrum of CdS/ZnS QDs emitted at 380 nm. (c) HAADF-STEM images of the CdS/ZnS QDs sample. (d) XEDS analysis from an individual nanocrystal (red frame highlighted), indicating the composition of Zn and S; the copper peaks arise from the TEM support grid and the silicon peak is from the instrument.*

The formation of a chemically synthesized ZnS shell on the biomineralized CdS core is clearly demonstrated by the change in mean particle diameter, XEDS analysis from individual particles and a shift from trap-state to band-edge emission after the ZnS shell growth. All of these combined observations are in agreement with prior reports of ZnS shell growth on CdS. Direct imaging of a ZnS shell was not feasible but the measured diameter increase indicates a single ZnS layer has been deposited. While the quantum yield increases upon phase transfer to the organic phase with oleylamine capping, it decreases again upon capping with oleic acid. Growth of ZnS again increases the quantum yield. The biomineralized QDs are crystalline, and the surface traps are significantly decreased upon ZnS shell growth; however, the maximum quantum yield achieved in all conditions is below three percent. Improvement in quantum yield is hence a fertile area for further work in these biomineralized systems.

### **3.4 CdS QDs sensitized solar cell**

We also demonstrated that the phase transferred CdS QDs can be utilized in a quantum dot sensitized photovoltaic cell by drop casting the solution into a TiO<sub>2</sub> electrode, Figure 3.13. Addition of the biomineralized CdS QDs leads to both increased open circuit voltage,  $V_{OC}$ , from 0.32 to 0.60 V, and increased short circuit current density,  $J_{SC}$ , from 0.41 to 0.55 mA/cm<sup>2</sup>. In addition, there is an increase in fill factor from 41 % to 50 %, which translates to a corresponding increase in device efficiency to 0.17 %. These performance improvements upon integration of biomineralized CdS quantum dot nanocrystals into the solar cell are in line with prior reports utilizing chemically synthesized materials.<sup>[102–104]</sup> It should be noted that these basic photovoltaic cells are not fully

optimized and here only serve to illustrate the potential for technological use of these biomineralized CdS QD materials.

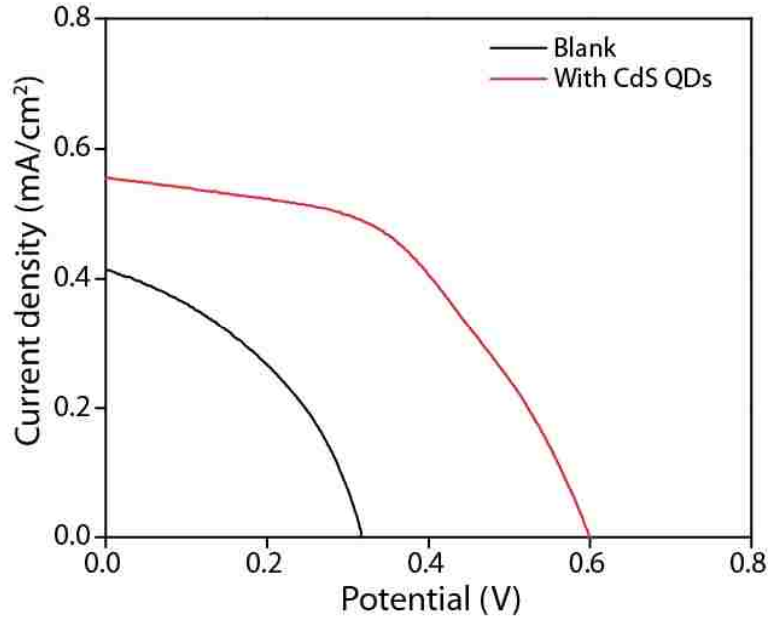
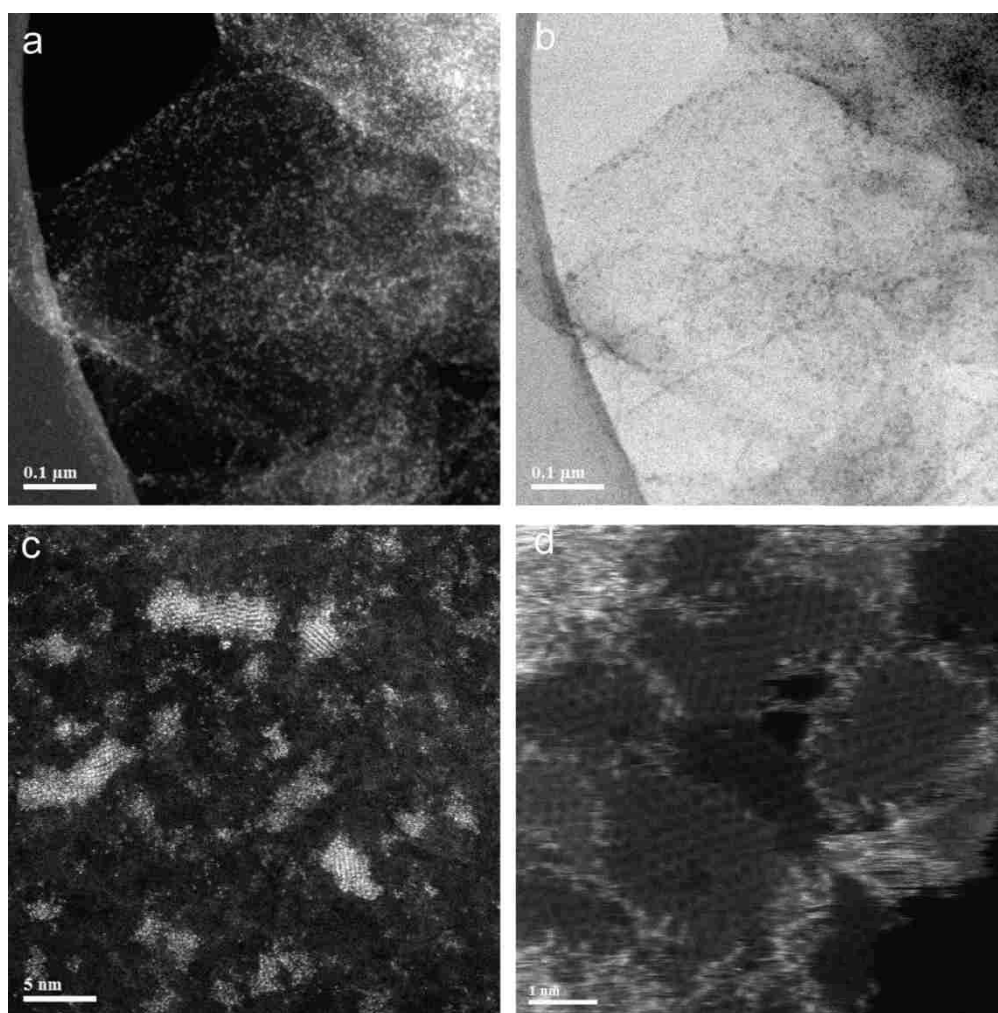


Figure 3.13. J-V characteristics of the CdS quantum dot based cells measured under one-sun illumination (AM 1.5 G,  $100 \text{ mW/cm}^2$ ).  $V_{\text{Open Circuit}} = 0.60 \text{ V}$ ,  $J_{\text{Short Circuit}} = 0.55 \text{ mA/cm}^2$ , Fill Factor = 50 %, Efficiency = 0.17 %.

### 3.5 CdS and reduced graphene oxide composite

Aqueous CdS QDs has been also studied to form a CdS and reduced graphene oxide (rGO) composite for further applications. Here, the biosynthesized CdS QDs and rGO were mixed together to fabricate CdS-rGO composite by a simple sonication step. The graphene oxide was synthesized via the improved Hummers' method.<sup>[105]</sup> Then the graphene oxide was reduced by sodium borohydride to form rGO precipitations. The composite product was characterized by STEM and the images are shown in Figure 3.14. The STEM images of rGO clearly shows single or fewer layer carbon sheets (Figure 3.14.d). The dark field and bright field images clearly confirm that CdS QDs are attached on rGO sheets rather than carbon film of the TEM grid (Figure 3.14.a and b). High magnification images provide

more detailed information of the nanocrystals on rGO (Figure 3.14.c). They are well dispersed on the sheets and maintain the crystal structure. Since the composite has been aggressively washed by either water or acetone, we believe that the CdS QDs are firmly attached on the rGO sheets with strong bindings. The quenching fluorescence also confirms the interaction of CdS QDs with rGO. This simple procedure opens a door for exploring the functions of biosynthesized CdS QDs with rGO. Future work could be carried out based on this simple method for preparing biosynthesized CdS-rGO composite.



*Figure 3.14. Electron microscopy characterizations of CdS and reduced graphene oxide (rGO) composite. (a and b) HAADF-STEM dark field and bright field images of the CdS-rGO composite; (c) High magnification image of CdS-rGO composite; (d) High magnification image of rGO.*

### 3.6 Conclusions

We presented a detailed study of the biosynthesized CdS QDs from *Stenotrophomonas maltophilia* (SMCD1). The growth parameters, such as the concentrations of cadmium acetate and L-cysteine, the pH of the buffer, and the growth temperature have been systematically investigated. The optical properties can be controlled and tuned by varying the growth conditions. In addition, the biosynthesized water soluble CdS QDs can be efficiently transferred to organic solvents with a concurrent improvement in their optical properties. Furthermore, CdS/ZnS quantum dots with core-shell morphologies have also been successfully generated which display suppression of CdS surface trap states. By utilizing such post-growth treatments on the as-grown cell-derived CdS particles (i.e. solvent exchange, stabilizing ligand exchange, and ZnS shell formation), QD materials have been produced which show comparable properties to their chemically synthesized CdS QD counterparts. Potential functions of the biosynthesized CdS QDs have been tested on solar cell which exhibits the improvement of the efficiency with loading of these nanocrystals. Meanwhile, CdS QDs and reduced graphene oxide composite has been fabricated by a simple sonication step and it can be used for further applications.

While the solar cell performance results and ZnS shell growth are in good agreement with previous reports utilizing CdS and CdS/ZnS core-shell QDs, what is remarkable about this study is that an optimized biomineralization procedure can produce crystalline CdS QDs of sufficiently high enough quality that they can be utilized in a similar manner to chemically synthesized materials. While clearly there is still some way to go in optimizing the biomineralization procedure to produce the highest quality QDs in terms of absolute quantum yield, the potential cost benefits over chemical synthesis routes are

considerable. The biomineralized materials are fabricated at 37°C in water in an open laboratory container from low-cost cadmium acetate and L-cysteine. There may well be an application space where the lower QY may be outweighed by the potential environmental and cost benefits of biomineralization.

## Chapter 4

# Biominingeralization of CdSe and Core/shell CdSe/CdS Quantum Dot from Cystathionine $\gamma$ - lyase

---

In this chapter, we demonstrated biominingeralization of CdSe and core/shell CdSe/CdS nanocrystals by cystathionine  $\gamma$ -lyase (smCSE) enzyme. The quantum yield of the core/shell CdSe/CdS is up to 12 % which is, to the best of our knowledge, the highest quantum yield reported of biominingeralized CdSe quantum dot and is comparable with that from chemical synthesis routes. The particle size of CdSe nanocrystals is precisely controlled by varying the incubation time up to 24 h and the mean size can be tuned from  $3.85 \pm 1.01$  nm to  $6.91 \pm 1.68$  nm. The CdSe nanocrystals are identified to be a wurtzite type crystal structure rather than zinc-blende type. This single-enzyme route to functional nanocrystals synthesis reveals the powerful potential of biominingeralization processes.

---

### 4.1 Introduction

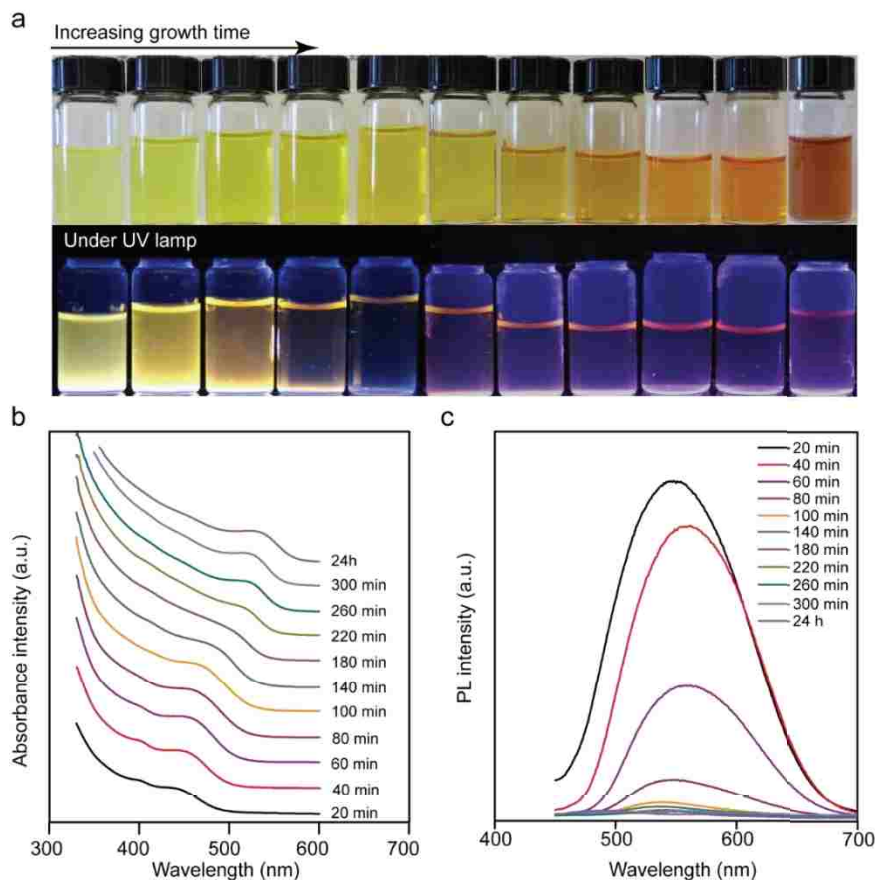
In chapter 2 and 3, an engineered strain of the bacteria, *Stenotrophomonas maltophilia* (SMCD1) are capable of promoting extracellular CdS nanocrystal formation in the quantum confined size range. The extracellular synthesis from SMCD1 is linked to



the expression of cystathionine  $\gamma$ -lyase (smCSE), which is a class of enzymes that catalyze the formation of pyruvate, ammonia, and hydrogen sulfide from L-cysteine.<sup>[106-108]</sup> The slower mineralization rate and intrinsic nanocrystal size control which smCSE enzyme facilitates demonstrates the important additional role of biological templating. Strain SMCD1 and smCSE have also been introduced for PbS nanocrystal formation and a CdS shell was successfully grown onto the purified PbS nanocrystals as the seeds, forming a core/shell PbS/CdS nanostructure.<sup>[109]</sup> Thereby, smCSE enzyme is a versatile enzyme for biomineralization of nanosized sulfides. We also speculate that this enzyme may be able to catalyze selenides formation.

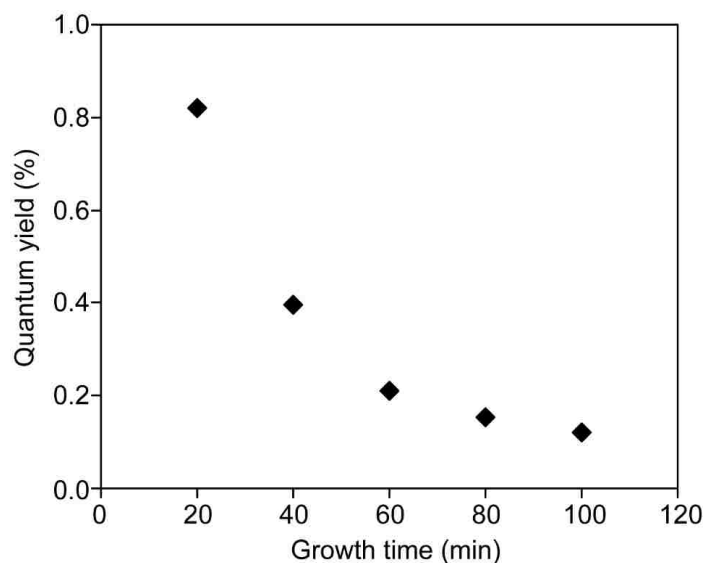
In this chapter, we described an enzyme-based biosynthetic procedure for CdSe nanocrystal synthesis at 37 °C. smCSE enzyme is the single enzyme intriguing the formation and templating of CdSe nanocrystals and selenocystine is the selenium source. The synthesis is as efficient as that of CdS QDs. The particle size of CdSe QDs can be tuned by varying the incubation time up to 24 h accompanied with evolution of optical properties. Though the as-grown CdSe nanocrystals show low quantum yields, a CdS shell was successfully grown onto the purified CdSe nanocrystals and formed core/shell CdSe/CdS structure, which significantly enhances the quantum yield. The most important feature of shell growth is that the shell material with a larger band gap than the core material can efficiently passivate the surface of the core nanoparticle. The quantum yield of CdSe/CdS nanocrystals by smCSE enzyme approaches those of chemical synthesized materials.

## 4.2 Biosynthesis of CdSe quantum dots



*Figure 4.1. Optical properties of the as-grown CdSe QDs with increasing growth time. (a) Photos of the CdSe QDs under ambient light (top) and UV lamp (bottom); (b) UV-vis absorption spectra of CdSe QDs as a function of growth time. (c) Fluorescence emission spectra using a 420 nm excitation wavelength as a function of growth time.*

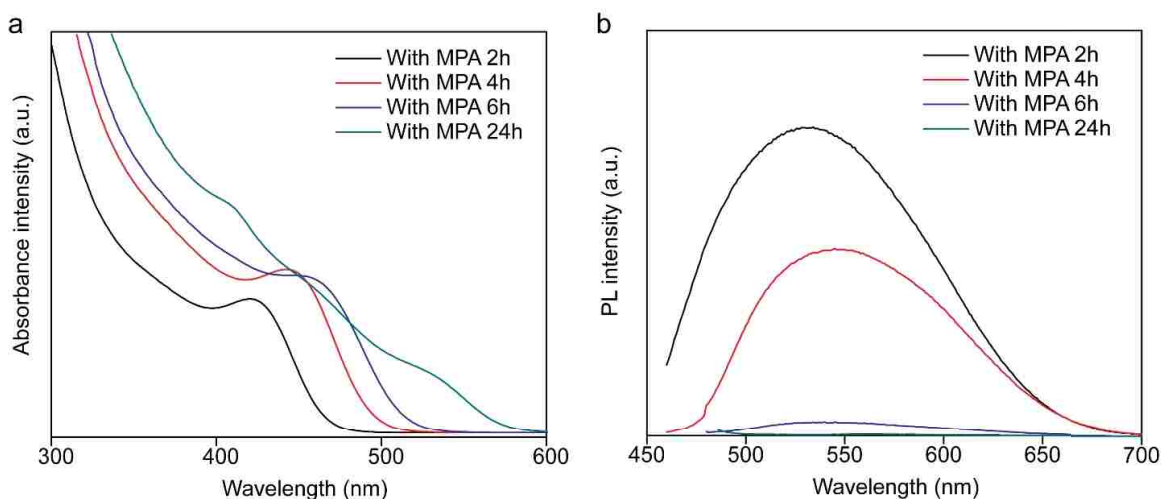
We have previously demonstrated that smCSE is capable of biomineralization of CdS quantum dots utilizing cadmium acetate as the cadmium source and L-cysteine as the sulfur source and capping agent. Selenium containing compounds, such as selenocysteine or selenocystine, were studied for CdSe nanocrystals synthesis. Selenocysteine is a cysteine analogue with a selenium-containing selenol group in place of the sulfur-containing thiol group, while selenocystine is the dimer. Our results clearly show that CdSe nanocrystals were successfully synthesized by smCSE enzyme using selenocystine as the Se source.



*Figure 4.2. Quantum yield of CdSe QDs with increasing growth time from 20 to 100 min.*

Selenocystine, the dimer, was chosen as the selenium source because it is stable, while selenocysteine can be easily oxidized. A similar protocol as for CdS biosynthesis was utilized. In short, 1 mM cadmium acetate, 8 mM selenocystine and 0.04 mg/mL smCSE in Tris-HCl buffer (pH = 9) was prepared in a glovebox with nitrogen controlled and then transferred to 37 °C incubator with shaking. Samples with different growth time starting from 20 min to 24 h were collected and inspected. The color of the culture turns from light yellow to brown after several hours' incubation, indicating the growth of CdSe nanocrystals (Figure 4.1.a top). The samples under UV lamp show strong photoluminescence especially for the samples within 2 h growth (Figure 4.1.a bottom), while with long time incubation, the photoluminescence quenches significantly. Absorbance and emission spectra were also collected. The absorption spectra for samples with various incubation times demonstrate well-defined first excitonic peaks (Figure 4.1.b) with maxima that shift to higher wavelengths with increasing growth time. After about 5 h growth, the peak shifts very little, indicating slow growth rate probably owing to the

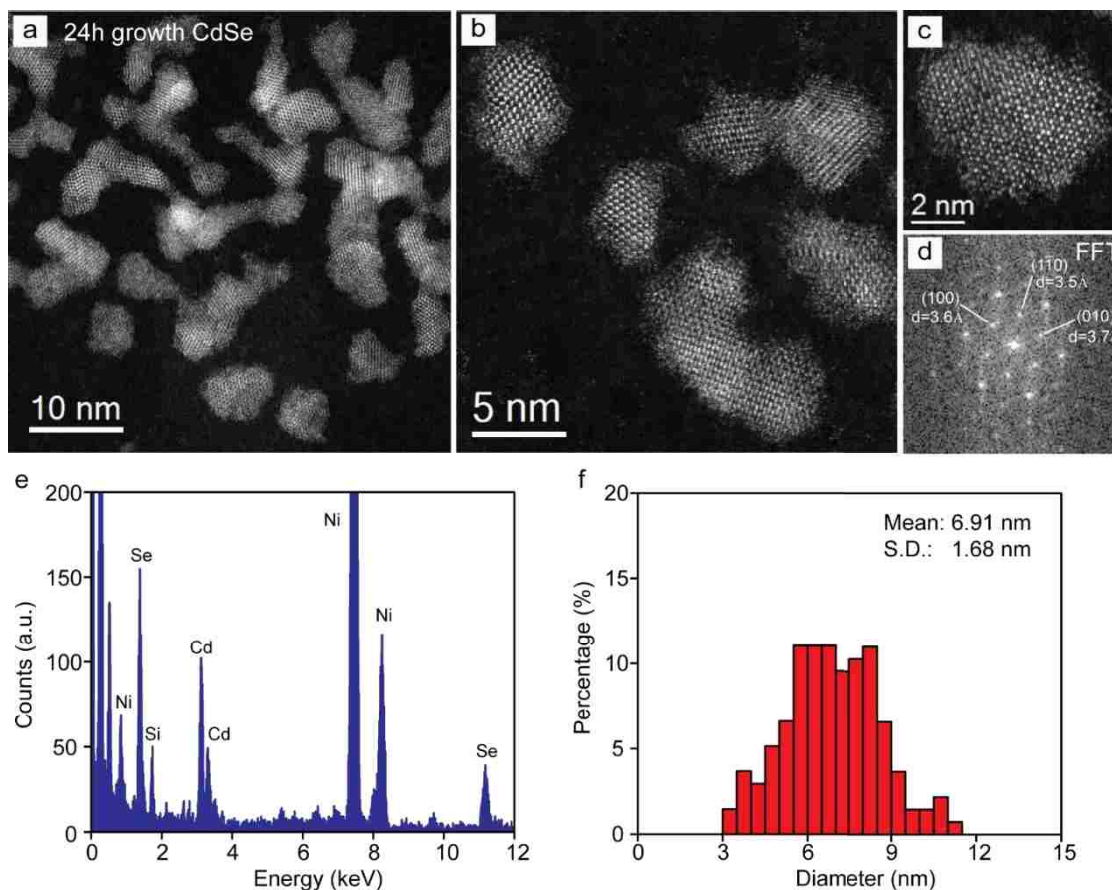
consumption of the precursors and deactivation of smCSE enzyme. The fluorescence emission spectra (Figure 4.1.c) reveal a broad trap-state emission with a large Stokes' shift, indicating poor surface passivation of CdSe QDs. The emission intensity decreases sharply with increasing growth time and after about 80 min, there is almost no photoluminescence detected. For the absorption spectra, the peak wavelength increases from about 438 nm to 535 nm as the growth time increased from 20 min up to 24 h; the emission peak wavelength of 20 min growth is about 550 nm and shows a red-shift trend with increasing growth time, however, after 80 min the peak positions are difficult to identify because of the low intensities. The quantum yield of the as-grown CdSe QDs decreases from 0.8 % for 20 min growth to 0.1 % for 100 min growth (Figure 4.2). This is in agreement with the photoluminescence under UV lamp. The quenching of the photoluminescence with increasing growth time is attributed to more surface defects of CdSe nanocrystals generated when the size increases.



*Figure 4.3. Optical properties of the as-grown CdSe QDs with increasing growth time with addition of 3-mercaptopropionic acid. (a) UV-vis absorption spectra of CdSe QDs as a function of growth time. (b) Fluorescence emission spectra using a 420 nm excitation wavelength as a function of growth time.*

We also investigated the CdSe QDs growth in presence of 3-mercaptopropionic acid (MPA), which is a commonly used capping agent for aqueous nanocrystals reported elsewhere.<sup>[110,111]</sup> In the presence of 20 mM MPA, the growth rate apparently slows down according to the absorbance spectrum evolution (Figure 4.3.a). The absorbance spectra exhibit similar features as those from the cultures without MPA (Figure 4.1.b), while the peak wavelength shifts from 424 nm after 2 h growth to 530 nm after 24 h. The intensities of the emission spectra show similar decrease trend indicating fluorescence quenching with increasing incubation time. The peak wavelength of 2 h growth is about 531 nm and red-shifts with increasing incubation time. Same phenomenon has been reported by Wang et al.<sup>[94]</sup> It was also reported that increasing the ratio of MPA:Cd above 1.5, the majority of Cd precursors form Cd–MPA dithiolcomplex rather than monothiol-complex.<sup>[112]</sup> Since the release of Cd from dithiol-complex is more difficult compared to monothiol-complex, introducing excess MPA would reduce the nucleation and growth rate of QDs. No nanocrystals formed when further increasing the concentration of MPA to 200 mM.

The formation of CdSe nanocrystals by smCSE enzyme was further confirmed by STEM high angle annular dark field (HAADF) imaging and X-ray energy dispersive spectroscopy (XEDS) of phase transferred materials. The crystal structure and particle size distribution of the CdSe nanocrystals produced at a growth time of 24 h were purified and characterized. The well dispersed QDs are clearly observable (Figure 4.4.a and b) with clear lattice fringes by phase contrast imaging, while the shapes of the nanocrystals are irregular rather than spherical. This shape feature may be associated with different facet growth rate of the nanocrystals.



*Figure 4.4. Electron microscopy characterizations of the large core (24 h growth) CdSe QDs. (a and b) High angle annular dark field (HAADF) images of the core CdSe QDs. (c and d) High magnification HAADF image and FFT (fast Fourier transformed) images of a single CdSe QD, showing a wurtzite structure. (e) Energy-dispersive X-ray spectroscopy (XEDS) analysis, confirming the existence of Cd and Se. (f) Particle size distribution.*

A high resolution image and its FFT (fast Fourier transformed) image of a single CdSe nanocrystal are shown (Figure 4.4.c and d) for lattice fitting. Its spacings and intersection angles are consistent with the wurtzite form of CdSe. The measured d-spacing values of 0.35, 0.36 and 0.37 nm (Figure 4.4.d) match those of the  $(1\bar{1}0)$ ,  $(100)$  and  $(010)$  planes in wurtzite type CdSe, which is 0.37 nm when viewed along  $[001]$ , respectively; the measured interplanar angles of  $56.9^\circ$ ,  $65.2^\circ$ , and  $57.9^\circ$  are also in consistency with expected value of  $60^\circ$  (Table 4.1). More lattice fitting results support that the CdSe nanocrystals are wurtzite type rather than zinc-blende type. Thus, we conclude that only wurtzite type

structure of CdSe QDs are produced by smCSE enzyme. X-ray energy dispersive spectroscopy (XEDS) analysis confirmed that the particles are primarily comprised of cadmium and selenium (Figure 4.4.e); some trace of silicon is from the instrument and the nickel peaks are artefacts of the TEM support grid. Particle size of the as-grown CdSe QDs with 24 h growth has a broad distribution and its measured mean size is 6.91 nm (spherical equivalent) with a standard deviation of 1.68 nm (Figure 4.4.f).

**Table 4.1. Lattice fitting of nanocrystals in Figures 4.3.d to wurtzite type CdSe.**

Figure 4.3.d: [001] projection		
Plane	Measurement	Matching
Plane 1	d=3.60 Å	3.72 Å (100)
Plane 2	d=3.48 Å	3.72 Å (1 $\bar{1}$ 0)
Plane 3	d=3.73 Å	3.72 Å (010)
<1, 2> angle	56.9 °	60°
<1, 3> angle	65.2°	60°
<2, 3> angle	57.9°	60°

All the evidences provided above confirm the formation of CdSe QDs by smCSE enzyme. The as-grown CdSe QDs exhibits red-shift of the first excitonic peak with increasing growth time and this indicates the size of nanocrystals increasing with growth time. The electron microscopy characterizations reveal that the mean particle size changes from 3.85 nm after 20 min to 6.91 nm after 24 h with a dispersion of about 25 %, showing a broad size distribution (Figure 4.4.f and 4.8.c). This was also observed in the study of CdS QDs biosynthesis. When compared to the particle size with identical absorbance peak

position from chemically synthesized CdSe QDs, the mean particle size of these biosynthesized CdSe QDs from smCSE enzyme is clearly larger. Yu et al. has systematically studied the relation between mean particle size and absorbance peak wavelength and they provided a sizing curve of CdSe showing that the mean particle size is around 2.5 nm at absorbance peak of 530 nm.<sup>[81]</sup> We attribute the difference to the different shapes of CdSe nanocrystals. The chemical synthesized nanocrystals usually exhibit uniform spherical shapes and quantum confinement relies on the radius of the nanocrystals. If the nanocrystals have irregular shapes with different size on different dimension, for example, CdSe nanorod, the optical property would be very different. Peng et al. compared the optical properties of CdSe quantum dots and nanorods.<sup>[113]</sup> It reported that the absorbance spectra are very similar when the sizes along *a*-axis are nearly the same, however the sizes along *c*-axis are different. In addition, the reported quantum yield of nanorod is much smaller than that of quantum dots. From the TEM images of these biosynthesized CdSe nanocrystals (Figure 4.4.a-b), it is obvious that these nanocrystals have irregular shapes rather than spherical. When estimating the particle size, the particles were measured as spherical equivalent shape. The irregular shapes of these CdSe nanocrystals might explain the disagreement between the optical properties and the measured particle size. Meanwhile, it might also explain the low quantum yield.

## **4.3 Photoluminescence enhancement of CdSe quantum dots**

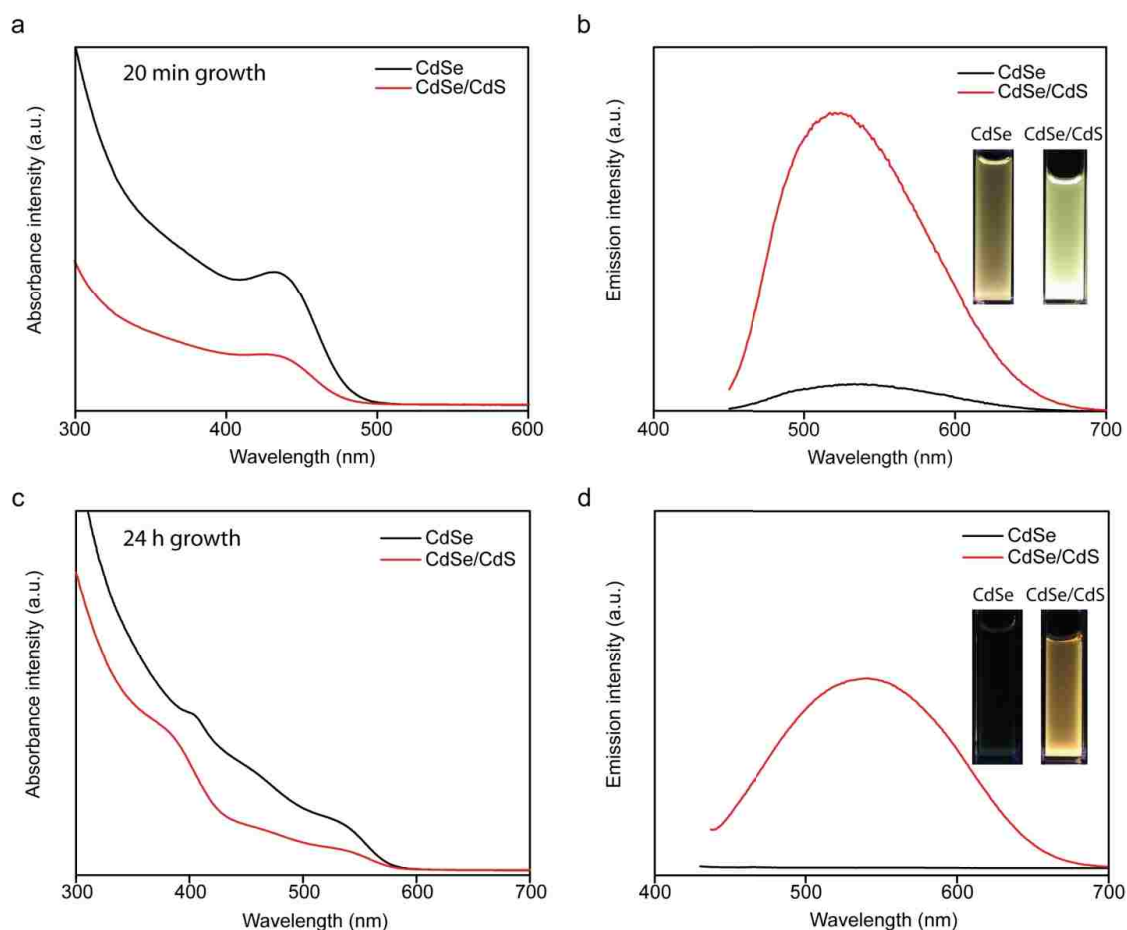
### **4.3.1 Core/shell CdSe/CdS growth via biosynthesis route**

Our previous study reveals that PbS and core/shell PbS/CdS QDs can be synthesized in the presence of smCSE enzyme.<sup>[109]</sup> Considering a mechanistic similarity between biomineralization of CdSe and CdS QDs using smCSE, we attempted to grow a



thin CdS shell onto the CdSe QDs by a sequential biomineralization process. In a typical procedure, biomineralized CdSe cores with 20 min growth were precipitated by acetone at high speed centrifugation and the supernatant was discarded. The CdSe nanocrystals were then re-suspended in a pH 9 Tris-HCl buffer solution with 8 mmol L-cysteine, 1 mmol cadmium acetate and 0.04 mg/mL smCSE enzyme. The solution was then incubated at 37 °C for 12 hours. The core/shell CdSe/CdS QDs solution exhibits significant enhancement of the emission and shows a quantum yield of as high as 12 %. Singh et al. reported an approach of core/shell CdSe/ZnS synthesis using a peptide template, however there are no quantum yield data reported and the ZnS shell growth only resulted in a 1.5-fold increase in photoluminescence.<sup>[114]</sup> To the best of our knowledge, this is the first report of biosynthesis of core/shell CdSe/CdS quantum dots with such a high quantum yield.

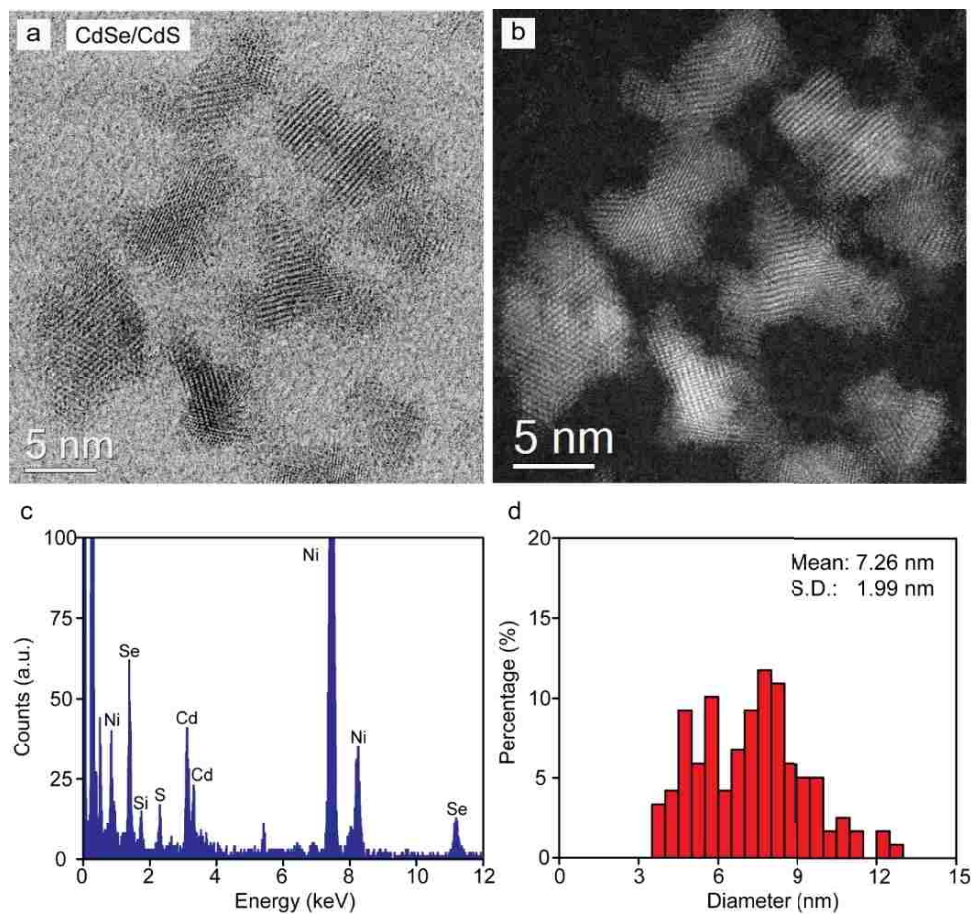
The optical properties of CdSe and core/shell CdSe/CdS QDs with different initial core sizes are shown in Figure 4.5. Small CdSe QDs with 20 min growth show a first excitonic peak around 436 nm (Fig 4.5.a) and a broad emission peak around 524 nm (Fig 4.5.b). The core/shell CdSe/CdS QDs exhibit very similar absorbance and emission spectra without notable peak shift except a significant increase of the emission intensity. The photo inset displays the fluorescence of the as-grown CdSe and core/shell CdSe/CdS under UV lamp. There is no sign of CdS population during the shell growth according to the optical spectra. The quantum yield of the CdSe QDs with 20 min growth is only 0.8 % initially, however, after CdS shell growth, it is improved up to 12 %, which confirms the formation of CdS shell.



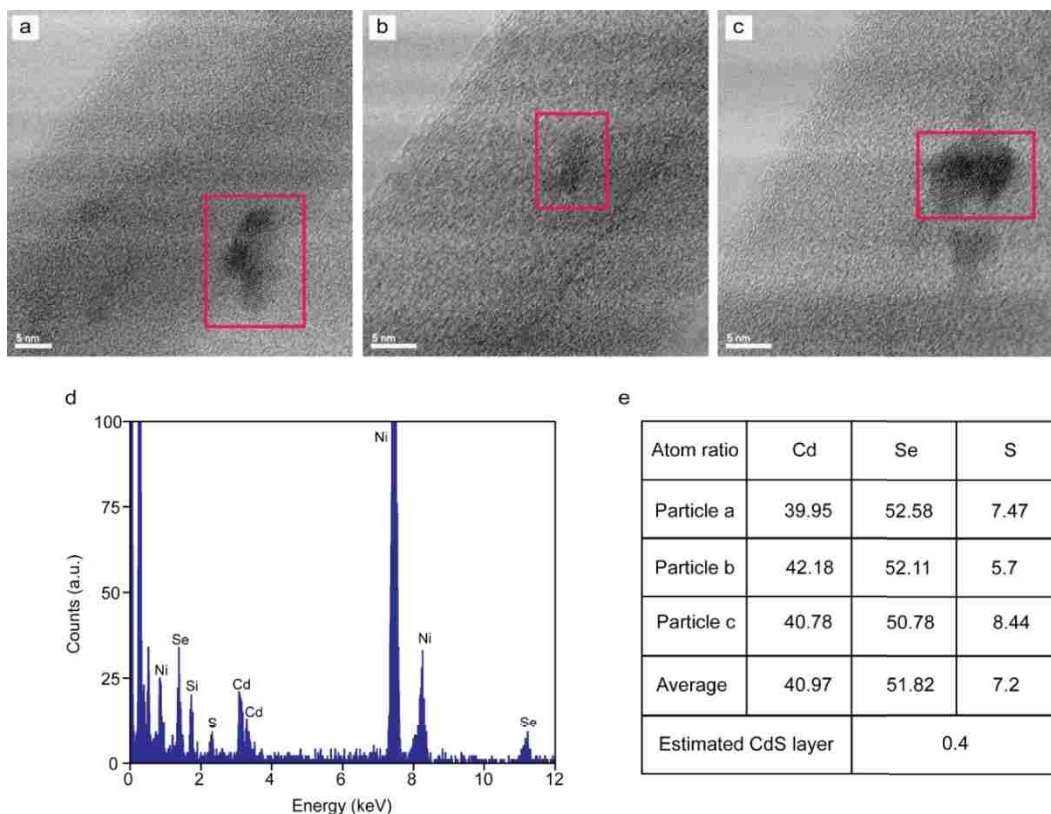
*Figure 4.5. Optical properties of CdSe and CdSe/CdS QDs. (a and b) UV-vis absorption spectra and fluorescence emission spectra of smaller particle size sample using a 420 nm excitation wavelength, inset is a photograph of the samples illuminated under UV lamp. Quantum yield increases from 0.8 % to 12.0 %. (c and d) UV-vis absorption spectra and fluorescence emission spectra of larger particle size sample using a 420 nm excitation wavelength, inset is a photograph of the samples illuminated under UV lamp. Quantum yield increases from almost 0 to 2.7 %.*

We also investigated larger CdSe with 24 h growth and carried out the same CdS shell growth. The absorbance of core CdSe shows the first excitonic peak around 532 nm (Fig 4.5.c) and almost nothing from the emission spectrum (Fig 4.5.d). After the shell growth, the absorbance shows similar features and the intensity of the emission peak at around 545 nm is clearly enhanced. The quantum yield of the larger core/shell CdSe/CdS is about 2.7 %. In summary, the as-grown CdSe QDs synthesized from smCSE enzyme

show poor photoluminescence, especially for large particle size samples. After CdS shell growth, there is as high as 15-fold increase of the quantum yield. The optical properties provide firm evidence of successful CdS shell growth.



*Figure 4.6 Electron microscopy characterizations of the large size (24 h core growth) core/shell CdSe/CdS QDs. (a and b) Bright field and dark field (HAADF) images of the core/shell CdSe/CdS QDs. (c) Energy-dispersive X-ray spectroscopy (XEDS) analysis of a single particle, confirming the existence of Cd, Se and S. (d) Particle size distribution (the mean value was derived from 122 particles), indicating ~0.5 layer of CdS.*



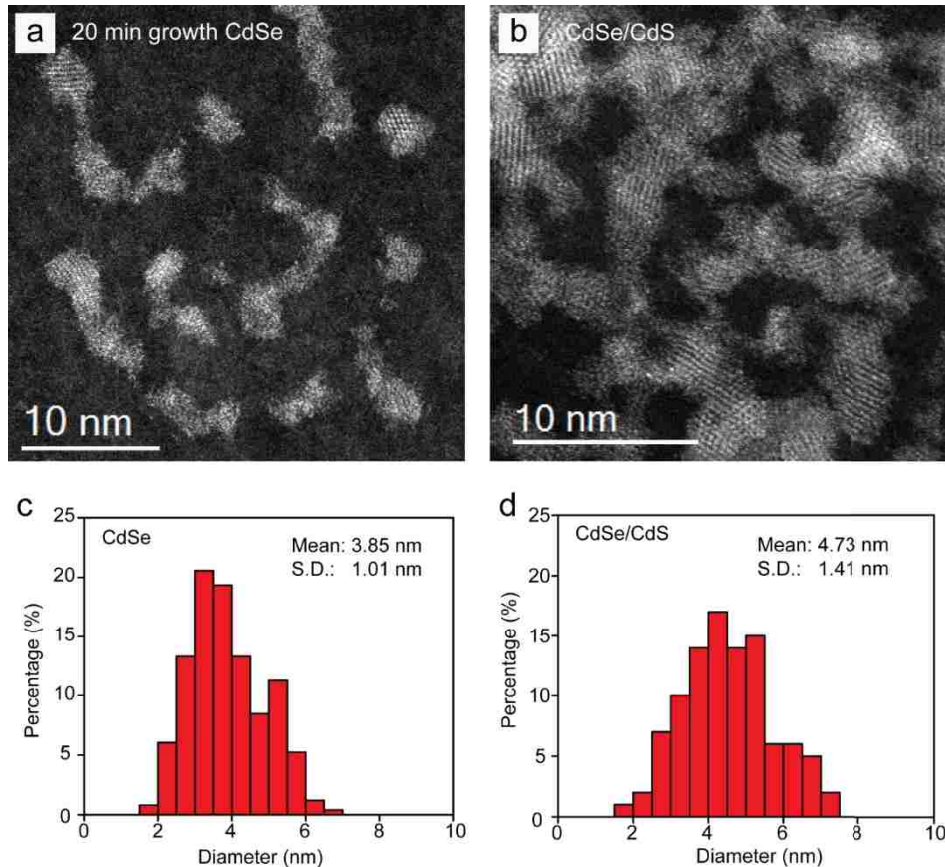
*Figure 4.7. Electron microscopy characterizations of the large size (24 h core growth) core/shell CdSe/CdS QDs. (a-c) Images of single core CdSe QDs (highlighted in red box). (d) Typical single particle energy-dispersive X-ray spectroscopy (XEDS) analysis. (e) Calculated atom ratio of Cd:Se:S from the XEDS spectra of a-c. The average estimated layer of CdS shell is about 0.4.*

In comparison, the core/shell CdSe/CdS QDs based on 24 h growth CdSe cores were characterized by STEM high angle annular dark field (HAADF) imaging and X-ray energy dispersive spectroscopy (XEDS). Typical bright field and dark field images of core/shell CdSe/CdS QDs samples are presented in Figure 4.6.a and b. The images show well dispersed nanocrystals with clear lattice fringes. Because the lattice parameters of bulk CdSe and CdS are very close with only 3.9 % lattice mismatch<sup>[20]</sup> and the shell thickness is also very small, it is difficult to distinguish shell structure from the core material within the images. Herein, we used XEDS analysis on a single nanocrystal to identify its composition. A typical spectrum collected from a single nanocrystal confirms that the

nanocrystal is primarily comprised of cadmium, selenium and sulfur (Figure 4.6.c), confirming a core/shell structure. Particle size of the core/shell CdSe/CdS QDs shows a broad distribution and the measured average particle size is 7.26 nm with a standard deviation of 1.99 nm (Figure 4.6.d). The mean size difference of the core and core/shell is about 0.35 nm corresponding to about 0.5 layer of CdS shell (a single layer a CdS shell increases the diameter of a nanocrystal by 0.7 nm). The simulated results of the atom ratio Cd:Se:S from the XEDS analysis were also obtained (Figure 4.7). The shell thickness calculation reveals that the thickness is about 0.4 layer, which is in good agreement with the particle size distribution result.

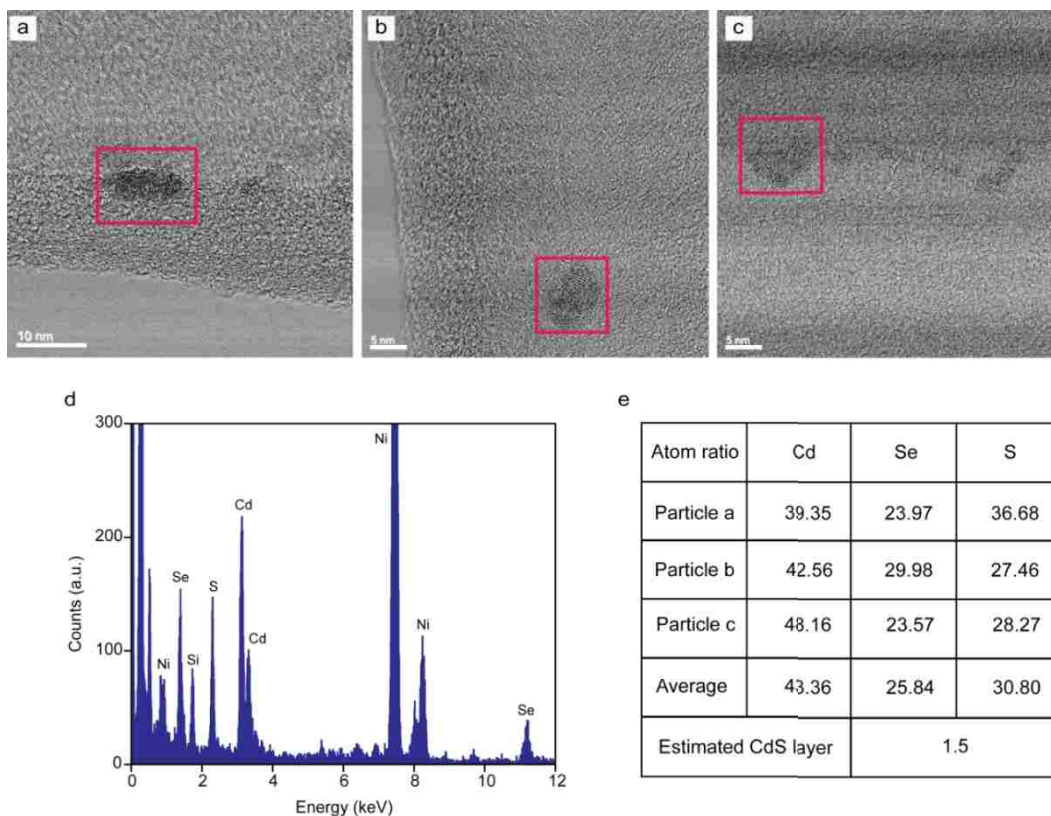
The small size CdSe QDs with 20 min growth and CdSe/CdS core/shell QDs were also investigated by STEM-HAADF imaging and XEDS. The dark field image (Figure 4.8.a) of the CdSe QDs reveals that they apparently have smaller particle size than that of 24 h growth sample. However, the crystallinity is not as good as that of 24 h growth sample and only part of them show clear lattice fringes. This is probably owing to their fragility under intense electron beam. The particle size of the CdSe QDs has relatively narrow distribution (Figure 4.8.c) and its measured mean size is 3.85 nm with a standard deviation of 1.01 nm. The dark field image (Figure 4.8.b) of the core/shell CdSe/CdS QDs shows that the nanocrystals tend to aggregate, though some dispersed nanoparticles were also found (Figure 4.9). Lack of surface capping or beam damage may result in the poor dispersion of the nanocrystals. The particle size distribution of the core/shell CdSe/CdS QDs (Figure 4.8.d) exhibits a mean size of 4.73 nm with a standard deviation of 1.41 nm. The mean size difference of the core and core/shell is about 0.88 nm corresponding to about 1.3 layer of CdS shell. Furthermore, similar XEDS analysis on single core/shell CdSe/CdS

QDs was carried out (Figure 4.9). The calculated shell thickness reveals that the thickness is about 1.5 layer and this is also in good agreement with the particle size distribution result. Therefore, electron microscopy characterization results from both small and large core CdSe and core/shell CdSe/CdS QDs confirm the successful growth of CdS shell. With identical shell growth condition, smaller cores are able to grow a thicker shell, probably because less amount of CdS crystallization per layer is required for small-sized nanoparticles. The higher quantum yield of the small-sized core/shell CdSe/CdS QDs also supports the thicker shell growth.



*Figure 4.8. Electron microscopy characterizations of the small size core CdSe and core/shell CdSe/CdS QDs. (a and b) Dark field (HAADF) images of the core CdSe and core/shell CdSe/CdS QDs, respectively. (c and d) Particle size distributions of the core CdSe and core/shell CdSe/CdS QDs (the mean values were derived from measurement of 236 and 100 particles), indicating ~1.3 layer of CdS.*





*Figure 4.9. Electron microscopy characterizations of the small size (20 min core growth) core/shell CdSe/CdS QDs. (a-c) Images of single core CdSe QDs (highlighted in red box). (d) Typical single particle energy-dispersive X-ray spectroscopy (XEDS) analysis. (e) Calculated atom ratio of Cd:Se:S from the XEDS spectra of a-c. The average estimated layer of CdS shell is about 1.5.*

Our previous study on core/shell PbS/CdS nanocrystals biosynthesis reveals that smCSE enzyme can encourage CdS shell growth onto purified PbS nanocrystal seeds, though it has not been ruled out whether it is a shell growth or cation exchange reaction. Singh et al. reported synthesis of core/shell CdSe/ZnS nanocrystals via a bi-functional peptide containing a CdSe domain and a ZnS domain. The peptides offer the possibility for layer-by-layer deposition to synthesis core-shell hybrid nanocrystals without any cross contamination.<sup>[114]</sup> In our case, CdSe and CdS can both be synthesized by smCSE enzyme probably at the same domain. The optical properties of the core/shell CdSe/CdS nanocrystals maintain similar features except for significantly enhanced emission intensity.

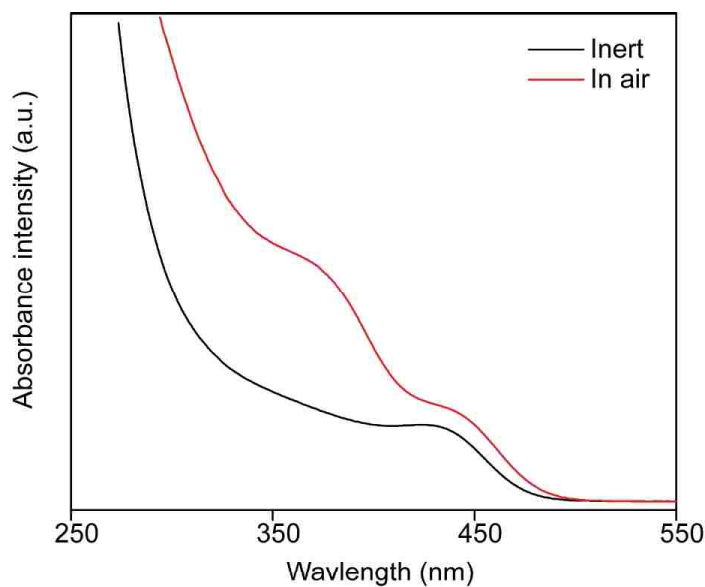
It has been widely reported that successful shell growth results in red-shifts of the absorbance and emission peaks especially for a thick shell growth<sup>[20–22]</sup>. If the shell thickness is small, no significant peak shift is observable. Our results are in good agreement with thin shell growth. Even though direct evidence of a core/shell structure either from TEM imaging or XEDS line-scan analysis on a single nanocrystal is lack because of the thin shell, the quantum yield improvement, mean size differences and XEDS analysis altogether provide strong evidences of successful CdS shell growth.

Another concern about the core/shell structure is that these nanocrystals might be CdSe/CdS alloy rather than core/shell structure. To exclude the possibility of alloy formation, we compared our results with those reported CdSe/CdS alloy synthesis. Qian et al. reported CdSe core and gradient CdSeS external shell synthesized in aqueous phase by microwave irradiation. The alloyed CdSeS shell growth significantly enhance the quantum yield from initially less than 0.1 % to 25 % with a strong band-edge emission.<sup>[115]</sup> Klimov's group studied the relation of Auger recombination of core-shell CdSe-CdS nanocrystals with the alloy CdSeS structure in the core-shell interface.<sup>[116,117]</sup> Their results indicate that the alloy layer forms rapidly during the initial growth of the shell (up to ~9 ML), and then its thickness stays nearly constant at the value of 0.5 nm, which corresponds to ~1.3 monolayer. The alloy layer formation result in significant increase in emission efficiencies of multiexciton states. Homogeneously alloyed  $\text{CdS}_x\text{Se}_{1-x}$  nanocrystals have also been reported by Swafford et al.<sup>[118]</sup> They investigated the size and composition of  $\text{CdS}_x\text{Se}_{1-x}$  nanocrystals and the dependence of the band gap on alloy composition is found to be slightly nonlinear, with a bowing constant of 0.29. Thus, the optical properties of alloy CdSe/S should intermediate between CdS and CdSe with identical particle size. In our case,



the optical spectra after CdS shell growth do not blueshift but the quantum yield is significantly improved. Therefore, they are more likely to be core/shell structure rather than a homogeneously alloy since no blue-shift is observed. While considering the shell structure, it is still unclear whether the shell is CdS or CdSe/S alloy or both.

It is also worth to point out the core/shell CdSe/CdS should be synthesized under an inert condition. When exposed to air (oxygen), with identical growth conditions, the absorbance spectrum has an additional peak at around 370 nm, which is very likely to be the population of CdS QDs which peaks in that range according to our previous result. With atmosphere control (inert condition), no such peak shows up and it indicates the absence of CdS QDs. Thus, we concluded that an inert environment inhibits the formation of CdS QDs and favors the shell growth.



*Figure 4.10. Absorbance spectra of core/shell CdSe/CdS growth under inert and in-air conditions.*

### 4.3.2 Photoenhancement of luminescence by UV illumination

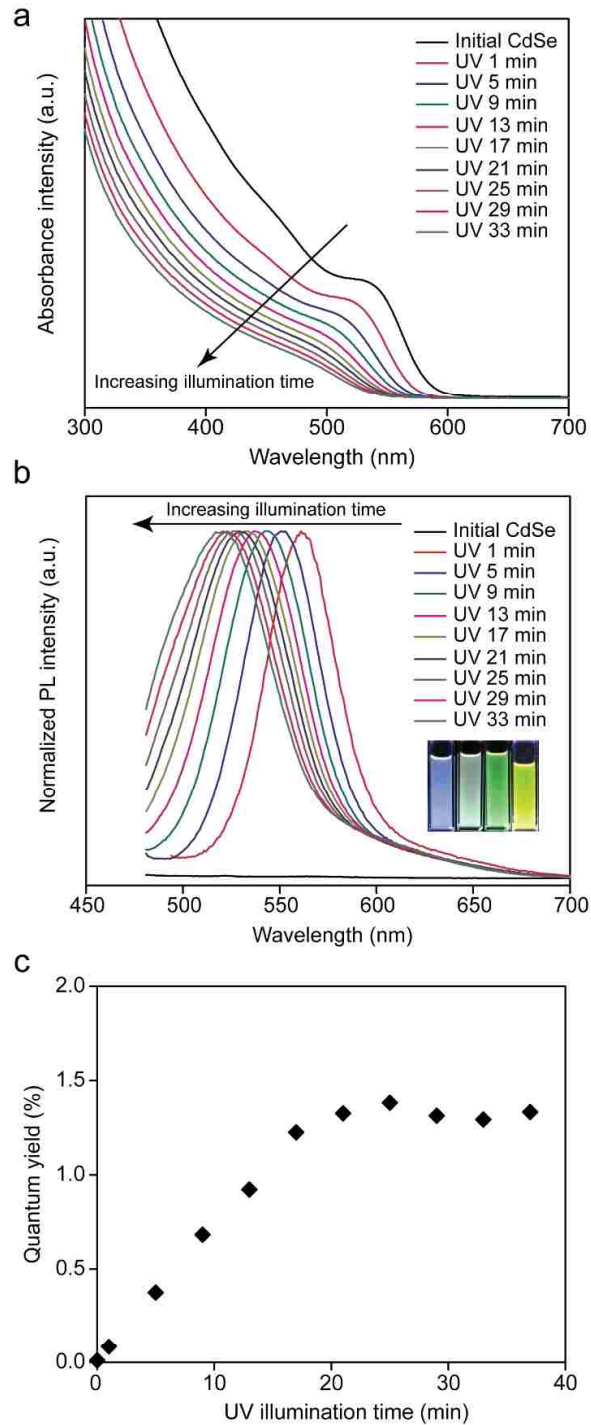


Figure 4.11. Optical properties of the core CdSe QDs under UV illuminations. (a) UV-vis absorption spectra of CdSe QDs as a function of time. (b) Fluorescence emission spectra using a 420 nm excitation wavelength as a function of UV illumination time, inset is a photograph taken at different time. (c) Quantum yield of the sample under different UV illumination time.

The photoluminescence of the as-grown CdSe QDs can be improved by either a CdS shell growth, which was described above, or UV illumination. UV illumination has been reported for photoluminescence enhancement of QDs.<sup>[119,120]</sup> Here, an 8W UV lamp with an excitation wavelength of 312 nm was introduced to study the UV-assisted photoluminescence enhancement. The as-grown CdSe QDs with 24 h growth were phase-transferred to organic solvent (chloroform) by the procedure described above and placed under the UV lamp. The absorbance and emission spectra (Figure 4.11.a and b) were collected at different illumination times from 1 min to 33 min. The absorbance peak shows a blue-shift trend and decreased intensity with increasing UV illumination time. The emission peaks also exhibit obvious blue-shifts. The quantum yield increases from initially nearly 0 to 1.3 % after 33 min illumination (Figure 4.11.c). The illuminated QDs solution exhibits strong band-edge emission with a small Stocks' shift of about 26 nm. The full-width at half maximum (FWHM) of the emission peaks are about 35 nm, which is similar to that of chemical routes.<sup>[19]</sup> It is believed that the UV illumination reconstructs the surface of the nanocrystals and improves the surface capping. In this case, the blue-shift of the absorbance peak indicates the decrease of the particle size of CdSe QDs, and the band-edge emission with higher quantum yield implies better surface passivation of the nanocrystals.

#### **4.4 Conclusions**

In summary, cystathionine  $\gamma$ -lyase enzyme is capable of controlled CdSe nanocrystal synthesis directly from aqueous solution by using selenocystine and cadmium acetate as reactants. The particle size of CdSe QDs can be tuned by varying the incubation time up to 24 h with average size from 3.85 nm to 6.91 nm. Furthermore, CdS shell is successfully grown on CdSe seeds in the presence of cystathionine  $\gamma$ -lyase and form

core/shell CdSe/CdS nanocrystals with significantly enhanced photoluminescence, a quantum yield up to 12 %. The photoluminescence of the as-grown CdSe QDs can be also improved by UV illumination at the expense of decreased particle size. This versatile enzyme demonstrates great potential for a variety of nanocrystal synthesis and can be exploited for large scale production of nanocrystals with high qualities.

## Chapter 5

# Proposed Biosynthesis Mechanism of CdS and CdSe Quantum Dots

---

The mechanism of CdS and CdSe synthesis by *Stenotrophomonas maltophilia* (SMCD1) and cystathionine  $\gamma$ -lyase (smCSE) was studied and proposed. Cystathionine  $\gamma$ -lyase was identified as the enzyme catalyzing the CdS and CdSe nanocrystal formation. For CdS formation, L-cysteine is the sulfur source; for CdSe formation, selenocystine (dimer of selenocysteine) is the selenium source. Although the precursors are different, they follow a similar mechanism. The proposed mechanism reveals that both processes rely on the cleavage of the dimers, either cystine or selenocystine, by the enzyme through multiple elimination reactions. Meanwhile, cystathionine  $\gamma$ -lyase was also proved to template the nanocrystal formation and control their sizes within quantum confined ranges.

---

### 5.1 Introduction

Cystathionine  $\gamma$ -lyase is widely distributed in prokaryotic and eukaryotic organisms and it plays an important role in the desulfuration pathway of cysteine and its derivatives, such as cystathionine and thiocysteine. In some bacteria and mammals, including humans, this enzyme takes part in generating hydrogen sulfide, which has been proved to be a physiologic vasodilator and regulator of blood pressure.<sup>[106-108,121]</sup> With its nominal substrate, L-cystathionine, the enzyme catalyzes a  $\gamma$ -elimination reaction and yield  $\alpha$ -

ketobutyrate, cysteine and  $\text{NH}_3$ . It also exhibits the ability to catalyze  $\beta$ -elimination reactions with several disulfides, such as cystine, to form persulfide and furthermore hydrogen sulfide.<sup>[122,123]</sup>

Since the 1950s, scientists have noticed that mammalian tissues contain enzymes, cystathionine  $\gamma$ -lyase and cystathionine  $\beta$ -synthase, capable of catalyzing the desulfhydration of cysteine. Stipanuk et al. studied the roles of these enzymes in rat tissues, and concluded that both enzymes catalyzed cysteine desulfhydration under physiologic conditions both *in vitro* and *in vivo*.<sup>[107]</sup> Steegborn et al. provided a deep insight of the catalytic mechanism of recombinant human cystathionine  $\gamma$ -lyase with different substrates, such as L-cystathionine, L-cysteine and L-cystine. It was demonstrated that the enzyme showed high  $\gamma$ -lyase activity toward L-cystathionine ( $K_m = 0.5 \text{ mM}$ ,  $V_{\max} = 2.5 \text{ units/mg}$ ) with an optimum pH of 8.2 and only marginal reactivity toward L-cystine and L-cysteine was detected.<sup>[84]</sup> Martin also inspected the mechanism of a cystathionine cleavage enzyme which shows much higher activity against L-cystine than L-cysteine. He also speculated that many cases of L-cysteine desulfhydrase reactions should be reinvestigated because of the extreme susceptibility to air oxidation of L-cysteine to form L-cystine.<sup>[124]</sup> Cavallini et al. suggested cystathionine  $\gamma$ -lyase is the single enzyme for cysteine and cystine desulfhydration. They pointed out that the actual substrate for the enzyme is cystine which is rapidly produced by cysteine oxidation.<sup>[125,126]</sup> They also suggested that cysteine is not a substrate of cystathionase but must contain a trace of cystine. Although L-cysteine acting as substrate of cystathionine  $\gamma$ -lyase has been widely reported, the exact mechanism is still unclear.

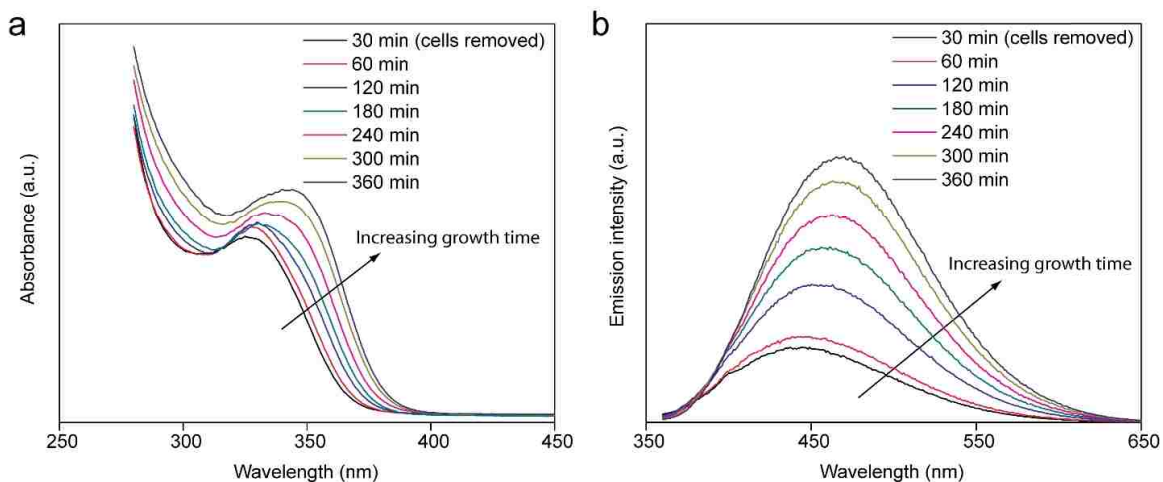
Cystine cleavage by cystathionine  $\gamma$ -lyase has been well studied. Yamanishi et al. proposed the mechanism of cystine cleavage reaction by cystathionine  $\gamma$ -lyase.<sup>[122]</sup> Cystine undergoes a  $\beta$ -disulphide elimination reaction that results in the production of pyruvate,  $\text{NH}^{4+}$  and thiocysteine. Then, thiocysteine interacts with a disulfide bond in the enzyme to form cysteine and a trisulfide structure on the enzyme side. Furthermore, the trisulfide structure is cleaved by consuming two cysteine to eliminate the S-atom as a sulfide ion, accompanied by the reformation of a disulfide bond in the enzyme and the oxidation of cysteines to cystine. This work provides a clear pathway of cystine to release  $\text{H}_2\text{S}$  in presence of cystathionine  $\gamma$ -lyase.

As an analogue, selenocystine is believed to experience the same reduction process. Esaki et al. investigated a variety of cysteine and selenocysteine related reactions with cystathionine  $\gamma$ -lyase in rat liver.<sup>[127]</sup> They reported that cystathionine  $\gamma$ -lyase can slowly eliminate selenocysteine to form  $\text{H}_2\text{Se}$  via  $\alpha$ -elimination reaction. They also reported a selenocysteine lyase enzyme from pig liver acting on selenocysteine.<sup>[128]</sup> Although they named the enzyme as selenocysteine lyase, they did not provide enough evidence to identify the enzyme structure. According to its absorbance spectrum, it exactly fits the spectrum of cystathionine  $\gamma$ -lyase.<sup>[96]</sup> It is skeptical that the selenocysteine lyase might have a high chance to be cystathionine  $\gamma$ -lyase. Thus, selenocystine and selenocysteine are believed to be able to act as the substrates for cystathionine  $\gamma$ -lyase.

## **5.2 Identification of cystathionine $\gamma$ -lyase**

To further elucidate the growth mechanism of nanocrystal formation, we investigated the nanoparticle growth following the removal of the bacterial cells from

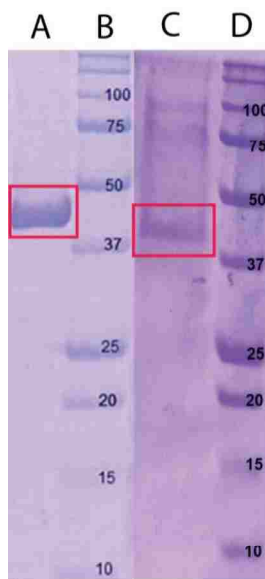
culture via centrifugation (Figure 5.1). The optical density at 600 nm ( $OD_{600}$ ) of the supernatant, a measure of cell concentration, after centrifugation was  $<2\%$  of the initial value, confirming removal of the cells. The CdS QDs in the free supernatant continued to grow in the absence of cells, although at a slower rate as characterized by a smaller red-shift in both adsorption and fluorescence peak maxima with increasing growth time. For example, after 360 minutes the absorbance and fluorescence maxima were at 343 and 469 nm, respectively, without cells and at 378 and 562 nm, respectively, with cells. This result confirms the extracellular production of the QDs, and indicates that QD growth does not require the continuous presence of cells throughout the entire growth process. We suggest that the presence of cells accelerates the rate of QD biosynthesis by continuously generating the extracellular components responsible for QD biosynthesis. Removal of the cells after an initial period reduces the rate of QD biosynthesis by reducing the concentration of extracellular components necessary for QD biosynthesis.



*Figure 5.1. Optical properties of the as-grown CdS QDs as a function of growth time in the supernatant following removal of cells via centrifugation at 30 minutes. (a) UV-vis absorption spectra; (b) Fluorescence emission spectra using a 350 nm excitation wavelength as a function of growth time.*



SDS-PAGE (polyacrylamide gel electrophoresis) analysis of the concentrated supernatant of CdS QDs culture clearly shows some traces of associated proteins (Figure 5.2, lane C), indicating that some enzymes may be involved in the formation of CdS nanocrystals. To compare, we also provide the purified cystathionine  $\gamma$ -lyase protein overexpressed by engineered *E. coli* cells in lane A. The bands on both lanes are very similar, which reveals that their molecular weights are in the same range. It is still not sure that the protein in the CdS culture is cystathionine  $\gamma$ -lyase protein. Thus, further qualitative analysis needs to be introduced to identify this protein.



*Figure 5.2. SDS-PAGE results of the CdS QDs culture comparing to pure cystathionine  $\gamma$ -lyase protein. Lane A, purified cystathionine  $\gamma$ -lyase (highlighted band); lane C, concentrated culture of CdS QDs; Lane B and D show molecular weight ladders.*

In order to identify what the protein is, the QD containing supernatant was dialyzed against distilled water to reduce the free Cd salt and L-cysteine concentration, then lyophilized and analyzed by electrospray ionization mass spectrometry (ESI-MS). This technique is significantly more sensitive than the SDS-PAGE and revealed several proteins associated with the QDs that may be responsible for the observed extracellular CdS QD

synthesis. Of particular note, a putative cystathionine  $\gamma$ -lyase (NCBI Accession Number WP\_012509966) was identified from independent QD samples analysed by ESI-MS (Figure 5.3). Cystathionine  $\gamma$ -lyase protein is a class of enzyme that produces H<sub>2</sub>S from L-cysteine, and prior work has shown that overexpression of a highly active cystathionine  $\gamma$ -lyase in *E. coli* confers resistance to otherwise toxic concentrations (0.1- 0.4 mM) of aqueous cadmium chloride by precipitation of bulk CdS through generation of H<sub>2</sub>S from 1 mM L-cysteine.<sup>[129]</sup> Consistent with these results, we find that in the presence of cystathionine  $\gamma$ -lyase protein, CdS QDs can be synthesized from cadmium acetate and L-cysteine with similar growth conditions (Figure 5.4). It clearly demonstrates the formation of CdS nanocrystals.

MSNATSQDRALALATLAIHGGQSPDPSTGAVMPPIYATSTYAQSSPGEHQGF EYSRTHNPTRFAY  
 ER**CVASLEGGTR**GF AFASGMAASSTVIELLDAGSHVAMDDIYGGSFRLF ERVRRRTAGLDFSFV  
 DLTDLAAFEASITPKTK**MVWIETPTNPMLKIVDIAA VAAIAK**RHGLIVVVDNTFASPMLQRPLEL  
 GADLVLHSATKYLNHGS DMVGGMVVVDNAELAEQMAFLQNSVGGVQGPFD SFLALRGLKTLPLR  
 MKAHCANALALAQWLEKHPAVEKVIYPGLASHPQHELAK**QMAGYGGIVSIVLK**GGFDAAKR FCE  
 KTELF TLAESLGGVESLVNH PAVMTHASIPVAR**REQLGISDALVR**LSVGVEDLGDLQVDLGEALK

*Figure 5.3. Sequence of the protein associated with the QDs. The identified protein sequence (NCBI accession number WP\_012509966), which corresponds to a predicted cystathionine  $\gamma$ -lyase, based on the results of ESI-MS (electrospray ionization mass spectrometry) is listed above. Specific peptide sequences from ESI-MS used in protein identification are given in bold and boxed for emphasis.*

In summary, all of our results point to a mechanism in which CdS QD biosynthesis occurs extracellularly via a cystathionine  $\gamma$ -lyase catalyzed conversion of L-cysteine to H<sub>2</sub>S. This enzyme is produced in culture by strain SMCD1 and is found to be associated with the CdS QD formation.

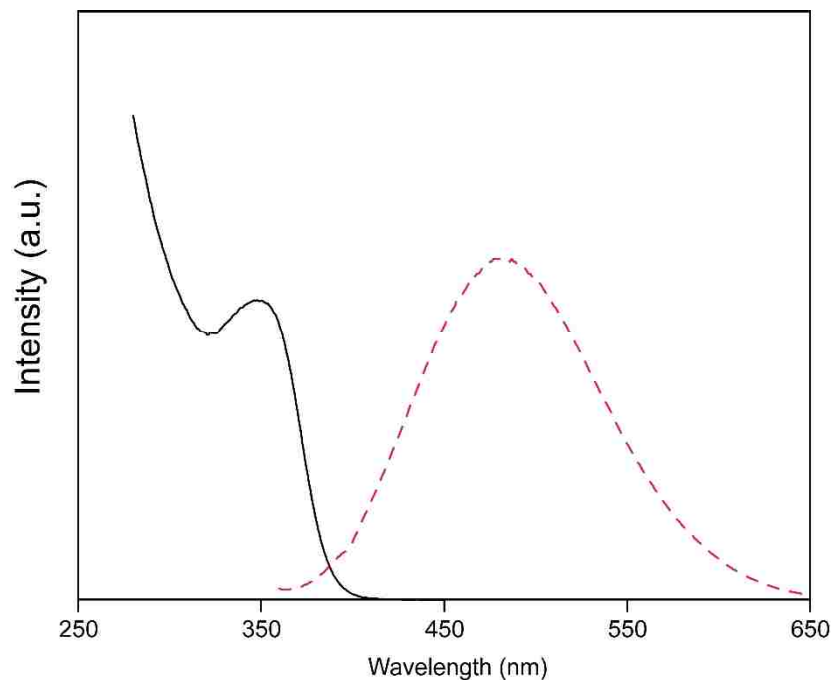


Figure 5.4. Optical properties of CdS QDs by cystathionine  $\gamma$ -lyase: absorbance spectrum (black solid line) and emission spectrum (red dash line).

### 5.3 The QD formation mechanism by cystathionine $\gamma$ -lyase

As we discussed before, cystathionine  $\gamma$ -lyase is widely reported to catalyze L-cysteine to release H<sub>2</sub>S both *in vivo* and *in vitro*. Here, we propose a mechanism that the enzymatic reactions of the dimers catalyzed by cystathionine  $\gamma$ -lyase generate the sulfur and selenium source for QDs formation. Meanwhile, the enzyme also anticipates in templating the nanocrystals growth. There are two major steps involved: enzymatic reactions of anion precursors for mineralization and growth templating. Coupled mineralization and templating by cystathionine  $\gamma$ -lyase results in precisely controlled nanocrystal formation.

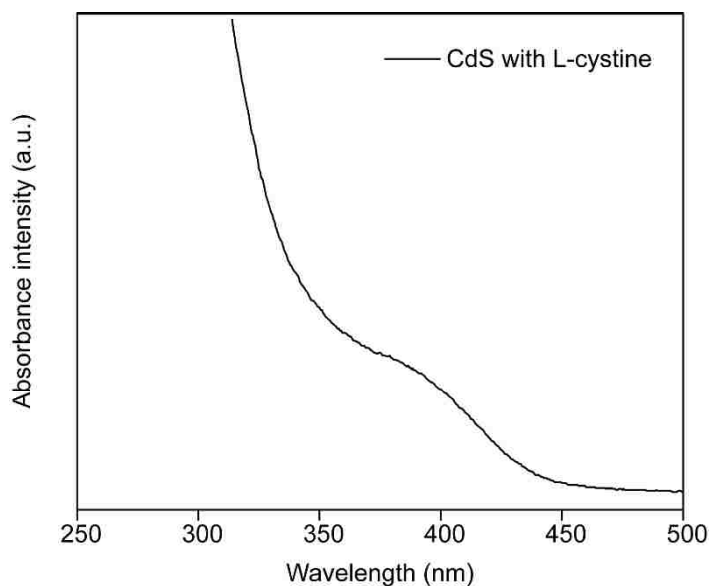


Figure 5.5. Absorbance of CdS synthesis by cystathionine  $\gamma$ -lyase using L-cystine as the sulfur source.

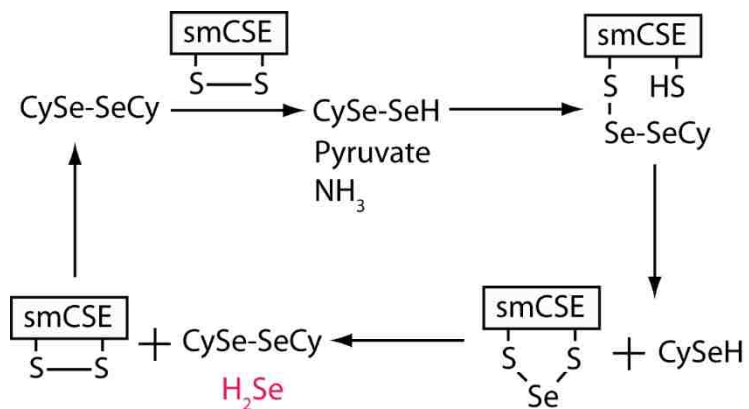


Figure 5.6. A proposed mechanism for selenocystine cleavage by cystathionine  $\gamma$ -lyase. (CySe-Secy, CySeH denote to selenocystine and selenocysteine, respectively; smCSE with disulfide bond denotes to cystathionine  $\gamma$ -lyase)

L-cysteine and cystine can be transformed to one another at specific conditions<sup>[130]</sup>.

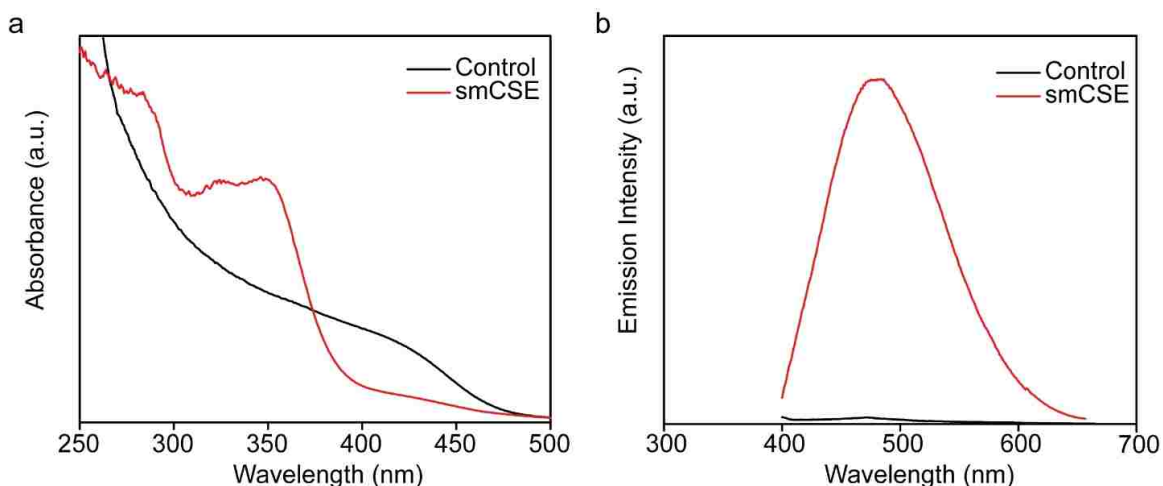
It is frequently noticed that the stock solution of L-cysteine in deionized water forms white precipitation, indicating the formation of cystine which is slightly soluble in water. Synthesis of CdS using L-cystine instead of L-cysteine as the sulfur source confirms the formation of CdS (Figure 5.5). The absorbance peak around 400 nm indicates the formation

of CdS nanocrystals. After 4 h incubation, the solution turns yellow and shows yellow precipitation after centrifugation. This directly proves the cleavage of L-cystine to form H<sub>2</sub>S by cystathionine  $\gamma$ -lyase. As an analogue, selenocystine has been reported to be reduced to form selenocysteine by multiple reducing agents, such as L-cysteine and glutathione.<sup>[131]</sup> Selenocystine is believed to follow the same pathway as cystine.

Both CdS and CdSe nanocrystal formation confirm the cleavage of L-cysteine and selenocystine to form H<sub>2</sub>S and H<sub>2</sub>Se, respectively. The enzymatic catalysis of L-cysteine and selenocystine by cystathionine  $\gamma$ -lyase is proposed to follow a mechanism similar to that of cystine cleavage. The proposed mechanism is as follows (Figure 5.6): L-cystine or selenocystine is cleaved to thiocysteine or Se-selenocysteine, pyruvate and NH<sub>3</sub>; thiocysteine or Se-selenocysteine binds with the disulfide bond in the enzyme to form a cystine trisulfide or S-Se-selenocysteine structure and cysteine or selenocysteine; the cystine trisulfide or S-Se-selenocysteine structure is cleaved by consuming two cysteine or selenocysteine molecules to form cystine or selenocystine and H<sub>2</sub>S or H<sub>2</sub>Se.

Cystathionine  $\gamma$ -lyase not only participates in the reduction of L-cysteine or selenocystine to form H<sub>2</sub>S or H<sub>2</sub>Se, but also templates and regulates the nanocrystals formation within the quantum confined size range. To further elucidate the templating role of the enzyme, our group carried out a study on the CdS QDs formation without generating H<sub>2</sub>S from L-cysteine.<sup>[96]</sup> To decouple the process, we introduced Na<sub>2</sub>S rather than L-cysteine as the sulfur source. Na<sub>2</sub>S is not a substrate for cystathionine  $\gamma$ -lyase, thus H<sub>2</sub>S is not produced under these conditions. Addition of Na<sub>2</sub>S to cadmium acetate solution at room temperature leads to nearly instantaneous formation of bulk CdS, with no distinct absorbance peak (Figure 5.7.a) or photoluminescence (Figure 5.7.b). Lack of a capping

agent to control nanocrystal growth leads to bulk CdS formation. However, when cystathionine  $\gamma$ -lyase was introduced, a distinct absorbance peak rapidly shows up at 360 nm (Figure 5.7.a) and a strong emission peak also shows up at 480 nm, indicating the formation of CdS nanocrystals. Therefore, cystathionine  $\gamma$ -lyase has the intrinsic ability to template CdS nanocrystal growth independently from its role on H<sub>2</sub>S generation. The formation of CdS nanocrystals in the absence of L-cysteine clearly indicates the role of cystathionine  $\gamma$ -lyase on templating and controlling the growth of CdS nanocrystals.



*Figure 5.7. Cystathionine  $\gamma$ -lyase forms CdS nanocrystals using Na<sub>2</sub>S as the sulfur source. (a) UV-visible absorbance spectra obtained upon the addition of Na<sub>2</sub>S to a preparation containing cadmium acetate in the presence of cystathionine  $\gamma$ -lyase; a solution of Na<sub>2</sub>S added to cadmium acetate is shown as a control. (b) Corresponding fluorescence (excitation at 340 nm) of solutions in a.*

In summary, we proposed the mechanism of CdS or CdSe nanocrystal formation by cystathionine  $\gamma$ -lyase. The cleavage of cystine (cysteine) or selenocystine by cystathionine  $\gamma$ -lyase results in the release of H<sub>2</sub>S or H<sub>2</sub>Se providing the source for CdS or CdSe formation in the presence of cadmium source. Cystathionine  $\gamma$ -lyase also templates the nanocrystal growth by controlling the growth rate of the nanocrystals and prohibits the formation of bulk materials.

## 5.4 Preliminary results for other types of quantum dots

In previous chapters, we reported the synthesis of CdS, CdSe and core/shell CdSe/CdS QDs by cystathionine  $\gamma$ -lyase. Other metal (such as Pb, Zn) sulfide or selenide nanocrystals were also considered for biosynthesis. Based on the detailed discussion of the mechanism for nanocrystals formation by cystathionine  $\gamma$ -lyase, we tried to exploit different types of nanomaterials. Here, some preliminary results for ZnS, PbSe, and ZnSe were demonstrated.

(1) **ZnS nanocrystals synthesis:** In a typical experiment, 1 mM zinc acetate, 8 mL L-cysteine and 0.05 mg/mL cystathionine  $\gamma$ -lyase were mixed in Tris-HCl buffer (pH = 9). The solution was then placed in the 37 °C incubator with shaking. The sample was taken at a certain time to check the absorbance. As we can see from Figure 5.8, the absorbance spectra clearly exhibit a characteristic peak around 280 nm with slight redshift with increasing incubation time, indicating the formation of quantum confined ZnS nanocrystals. The TEM images (Figure 5.8.c and d) show the nanocrystals with clear lattice fringes and the XEDS spectrum (Figure 5.8.b) shows that the composition of the nanocrystals to be Zn and S. These evidences confirm the formation of ZnS QDs.

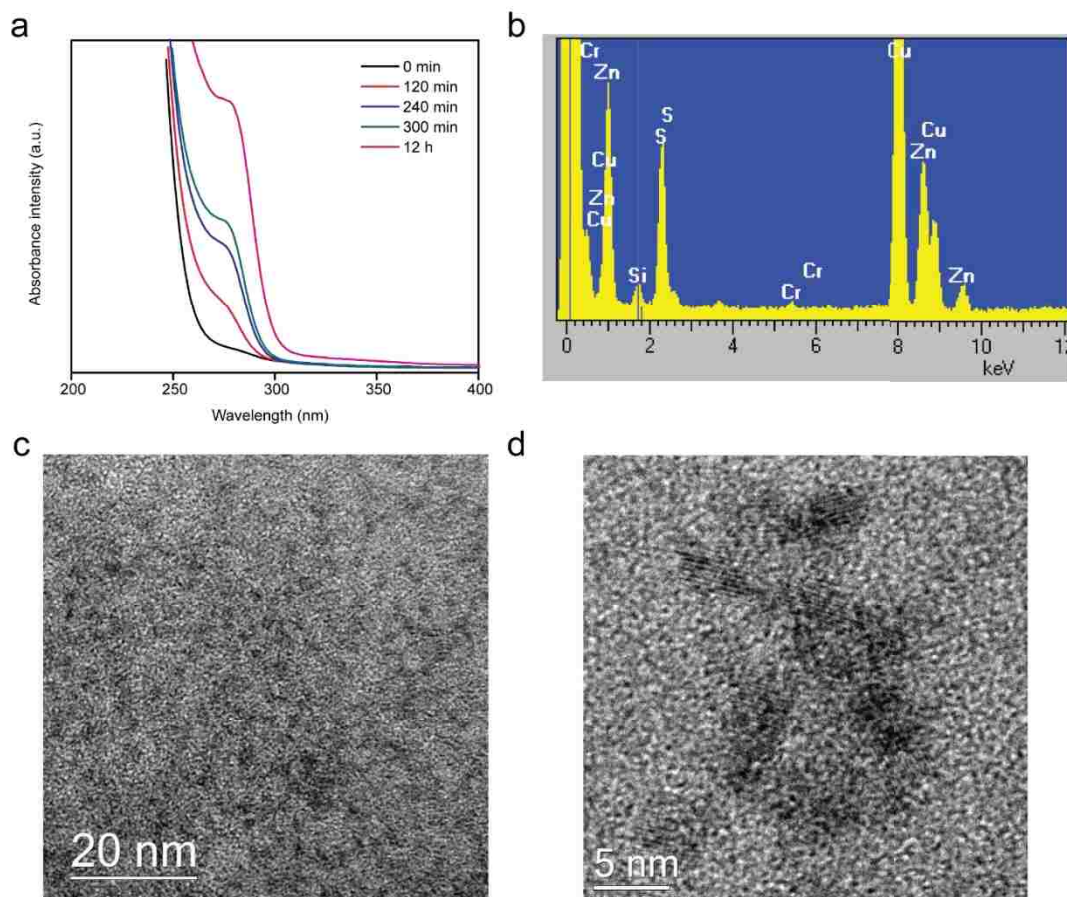


Figure 5.8. Preliminary result for ZnS QDs synthesis. (a) Absorbance spectra of the as-grown ZnS with increasing incubation time. (b) Energy-dispersive X-ray spectroscopy (XEDS) analysis, confirming the existence of Zn and S. (c and d) TEM images of the ZnS QDs.

(2) **PbSe nanocrystals synthesis:** In a typical experiment, 1 mM lead acetate, 8 mL selenocystine and 0.05 mg/mL cystathionine  $\gamma$ -lyase were mixed in Tris-HCl buffer (pH = 7). The solution was then placed at ice. The temperature is controlled at around 0 °C for a slow growth rate of the nanocrystals. As we can see, high resolution TEM images (Figure 5.9.a and b) clearly show the nanocrystals with lattice fringes and the XEDS spectrum (Figure 5.9.c) shows that the composition of the nanocrystals to be Pb and Se. PbSe synthesis is very sensitive to temperature. At higher temperature, the solution turns brown and turbid very quickly showing the formation of bulk PbSe materials. Decreasing the



temperature can slow down the growth rate and control the particle size in the nanoscale range.

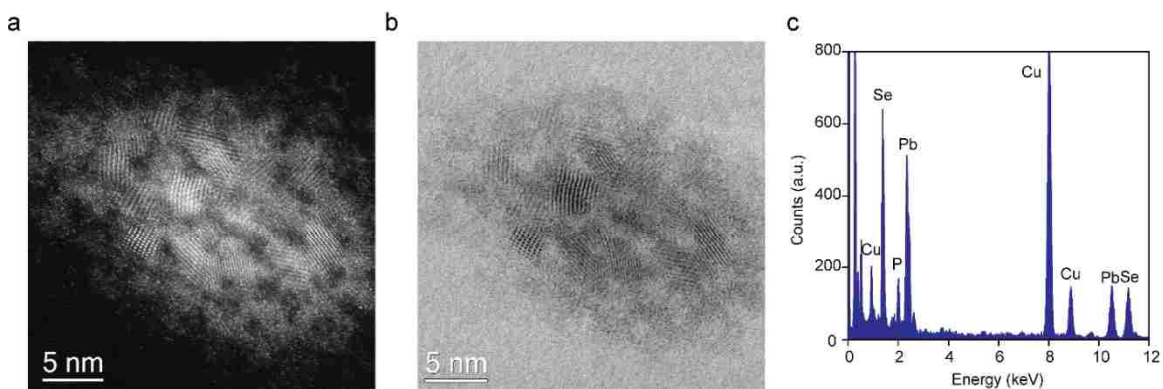


Figure 5.9. Electron microscopy characterizations of the PbSe nanocrystals. (a and b) Bright field and dark field (HAADF) images of the PbSe nanocrystals. (c) Energy-dispersive X-ray spectroscopy (XEDS) analysis, confirming the existence of Pb and Se.

(3) **ZnSe nanocrystals synthesis.** In a typical experiment, 1 mM zinc acetate, 8 mL selenocystine and 0.05 mg/mL cystathionine  $\gamma$ -lyase were mixed in Tirs-HCl buffer (pH = 9). The solution was then placed the 37 °C incubator with shaking. As we can see from Figure 5.10.a, the absorbance spectrum after 8 h growth shows a peak around 300 nm which is in consistence with the quantum confined range of ZnSe reported elsewhere.<sup>[132]</sup>

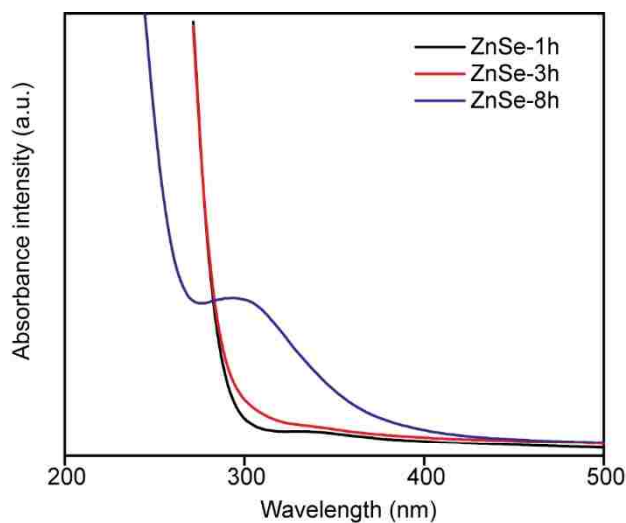


Figure 5.10. Preliminary result for ZnSe QDs synthesis with increasing incubation time.

These preliminary results, especially for ZnS and PbSe, clearly demonstrate the formation of nanocrystals. Although for ZnSe, the absorbance spectra are not enough to confirm the synthesis of nanocrystals, but they match with the reported optical properties. Ongoing work is focused on further proving the versatility of cystathionine  $\gamma$ -lyase for nanocrystal synthesis.

## 5.5 Conclusions

Cystathionine  $\gamma$ -lyase is identified from the culture for CdS QDs synthesis by bacteria *Stenotrophomonas maltophilia*. The analysis of SDS-PAGE and electrospray ionization mass spectrometry confirm its amino sequence. Cystathionine  $\gamma$ -lyase is capable of controlled sulfide or selenide nanocrystals formation through generating sulfur or selenium from the cleavage of L-cysteine or selenocystine. The cleavage is believed to happen at the active site of cystathionine  $\gamma$ -lyase with a disulfide bond from two cysteine residues. Meanwhile, cystathionine  $\gamma$ -lyase also templates the formation of these nanocrystals and controls the particle size within the quantum confined range. Attempts to synthesize different types of nanocrystals, such as ZnS, PbSe or ZnSe, show very positive results. Besides our previous reported PbS and core/shell PbS/CdS synthesis, this further reveals the versatility of cystathionine  $\gamma$ -lyase. This dual-function, single-enzyme, and aqueous route to functional material synthesis demonstrates the powerful potential of engineered functional material biomineralization.

## Chapter 6

### Summary

This dissertation focuses on biosynthesis of cadmium chalcogenide (CdS and CdSe) quantum dots from an engineered strain of *Stenotrophomonas maltophilia* (SMCD1) and cystathionine  $\gamma$ -lyase which is produced by SMCD1 cells and further overexpressed by engineered *E. coli* cells. CdS and CdSe QDs as well as core/shell CdSe/CdS have been successfully synthesized by either SMCD1 or the enzyme with precisely controlled properties which are comparable to chemically synthesized QDs. These nanocrystals were characterized by STEM, absorption and luminescence spectroscopy and powder XRD.

Strain SMCD1 enables controlled growth of CdS QDs over a period of 6 hours in culture, allowing precise, extrinsic control of QD size and optical properties with emission maxima ranging from 460 to 560 nm. This procedure exhibits high reproducibility. The mean particle sizes were tuned from 2.75 to 3.04 to 3.36 nm after 60, 180 and 300 min, respectively, with a dispersion of about 25 %. Gel filtration chromatography has also been introduced to further purify aqueous QDs and provided a simple method for size selection. The as-grown CdS QDs show both zinc-blende and wurtzite type structures with a quantum yield of up to 2.08 %.

Growth conditions, such as the concentration of cadmium acetate and L-cysteine, pH and growth temperature, were studied to elucidate the growth mechanism. High ratio of L-cysteine/cadmium acetate exhibits a high growth rate with absorbance peak red-shifting

compared to that with a lower ratio. High pH of the growth buffer favours the nanocrystal formation since the enzyme has high activity at basic conditions. Temperature also plays an important role on controlling the growth where high temperature favours the synthesis. Post treatments, such as capping exchange and ZnS growth, were introduced to manipulate the surface chemistry. After capping exchange, CdS QDs can be transferred to organic solvents and exhibit improved optical properties. ZnS shell growth suppressed the trap-state emission with an improved quantum yield up to 2.7 % from initial 0.8 %. For applications, CdS QDs solar cells were studied with a device efficiency of 0.18 %, though still very low; CdS-reduced graphene oxide composite was also fabricated and studied.

CdSe and core/shell CdSe/CdS nanocrystals by cystathionine  $\gamma$ -lyase (smCSE) enzyme were achieved. The quantum yield of the core/shell CdSe/CdS is up to 12 % which is the highest reported quantum yield of biomineralized CdSe quantum dots to date. It is comparable with that reported from chemical synthesis routes. The shell thicknesses were estimated either by mean particle size difference or elemental analysis to be about 0.5 ~ 1.5 layer. The particle size of CdSe nanocrystals was precisely controlled by varying the incubation time up to 24 h and the mean size can be tuned from  $3.85 \pm 1.01$  nm to  $6.91 \pm 1.68$  nm. The CdSe nanocrystals were identified to be a wurtzite type crystal structure rather than zinc-blende type. UV illumination was introduced to enhance the photoluminescence especially for larger CdSe QDs and quantum yield of about 2.5 % was achieved after several minutes of illumination.

The mechanism of CdS and CdSe synthesis by *Stenotrophomonas maltophilia* (SMCD1) and cystathionine  $\gamma$ -lyase was proposed. Cystathionine  $\gamma$ -lyase was identified as the enzyme catalyzing the CdS and CdSe nanocrystal formation from several techniques. Although the precursors are different, one being a monomer and the other a dimer, they are believed to follow a similar mechanism. Generation of H<sub>2</sub>S and H<sub>2</sub>Se from cleavage of the dimers, either cystine or selenocystine, by the enzyme through multiple elimination reactions, results in the nanocrystal formation. A detailed pathway of the reactions was provided to elucidate the mechanism. Meanwhile, cystathionine  $\gamma$ -lyase was also proved to template the nanocrystal formation and control their sizes within quantum confined ranges.

Exploiting different types of QDs is one direction for future work. Preliminary results clearly demonstrate various nanocrystal formation, such as ZnS and PbSe. Others, like ZnSe, are still unclear but show positive results. Pursuing potential applications, especially fuel production via photocatalysis assisted by these biosynthesized nanocrystals, could be another direction for study.

## Reference

- [1] L. E. Brus, *J. Chem. Phys.* **1984**, *80*, 4403.
- [2] A. P. Alivisatos, *Science*. **1996**, *271*, 933.
- [3] C. B. Murray, D. J. Norris, M. G. Bawendi, *J. Am. Chem. Soc.* **1993**, *115*, 8706.
- [4] R. J. Ellingson, M. C. Beard, J. C. Johnson, P. Yu, O. I. Micic, A. J. Nozik, A. Shabaev, A. L. Efros, *Nano Lett.* **2005**, *5*, 865.
- [5] O. I. Micic, C. J. Curtis, K. M. Jones, J. R. Sprague, A. J. Nozik, *J. Phys. Chem.* **1994**, *98*, 4966.
- [6] T. Rajh, O. I. Micic, A. J. Nozik, *J. Phys. Chem.* **1993**, *97*, 11999.
- [7] Z. A. Peng, X. Peng, *J. Am. Chem. Soc.* **2001**, *123*, 183.
- [8] W. W. Yu, X. Peng, *Angew. Chemie Int. Ed.* **2002**, *41*, 2368.
- [9] V. K. LaMer, R. H. Dinegar, *J. Am. Chem. Soc.* **1950**, *72*, 4847.
- [10] J. Park, J. Joo, S. G. Kwon, Y. Jang, T. Hyeon, *Angew. Chemie Int. Ed.* **2007**, *46*, 4630.
- [11] R. Comparelli, F. Zezza, M. Striccoli, M. L. Curri, R. Tommasi, A. Agostiano, *Mater. Sci. Eng. C* **2003**, *23*, 1083.
- [12] I. L. Medintz, H. T. Uyeda, E. R. Goldman, H. Mattoussi, *Nat. Mater.* **2005**, *4*, 435.
- [13] R. A. Sperling, W. J. Parak, *Philos. Trans. R. Soc. London A Math. Phys. Eng. Sci.* **2010**, *368*, 1333.
- [14] N. Gaponik, D. V Talapin, A. L. Rogach, A. Eychmüller, H. Weller, *Nano Lett.* **2002**, *2*, 803.
- [15] D. Dorokhin, N. Tomczak, M. Han, D. N. Reinhoudt, A. H. Velders, G. J. Vancso, *ACS Nano* **2009**, *3*, 661.

- [16] Y. Wei, J. Yang, J. Y. Ying, *Chem. Commun.* **2010**, 46, 3179.
- [17] X. Michalet, F. F. Pinaud, L. A. Bentolila, J. M. Tsay, S. Doose, J. J. Li, G. Sundaresan, A. M. Wu, S. S. Gambhir, S. Weiss, *Science*. **2005**, 307, 538.
- [18] M. Green, *J. Mater. Chem.* **2010**, 20, 5797.
- [19] B. O. Dabbousi, J. Rodriguez-Viejo, F. V Mikulec, J. R. Heine, H. Mattoussi, R. Ober, K. F. Jensen, M. G. Bawendi, *J. Phys. Chem. B* **1997**, 101, 9463.
- [20] X. Peng, M. C. Schlamp, A. V Kadavanich, A. P. Alivisatos, *J. Am. Chem. Soc.* **1997**, 119, 7019.
- [21] I. Mekis, D. V Talapin, A. Kornowski, M. Haase, H. Weller, *J. Phys. Chem. B* **2003**, 107, 7454.
- [22] J. J. Li, Y. A. Wang, W. Guo, J. C. Keay, T. D. Mishima, M. B. Johnson, X. Peng, *J. Am. Chem. Soc.* **2003**, 125, 12567.
- [23] O. Chen, J. Zhao, V. P. Chauhan, J. Cui, C. Wong, D. K. Harris, H. Wei, H. Han, D. Fukumura, R. K. Jain, *Nat. Mater.* **2013**, 12, 445.
- [24] D. Chen, F. Zhao, H. Qi, M. Rutherford, X. Peng, *Chem. Mater.* **2010**, 22, 1437.
- [25] J. S. Steckel, J. P. Zimmer, S. Coe-Sullivan, N. E. Stott, V. Bulović, M. G. Bawendi, *Angew. Chemie Int. Ed.* **2004**, 43, 2154.
- [26] K. Bourzac, *Nature* **2013**, 493, 283.
- [27] A. P. Alivisatos, W. Gu, C. Larabell, *Annu. Rev. Biomed. Eng.* **2005**, 7, 55.
- [28] P. Alivisatos, *Nat. Biotechnol.* **2004**, 22, 47.
- [29] A. J. Nozik, M. C. Beard, J. M. Luther, M. Law, R. J. Ellingson, J. C. Johnson, *Chem. Rev.* **2010**, 110, 6873.
- [30] Y. Shirasaki, G. J. Supran, M. G. Bawendi, V. Bulović, *Nat. Photonics* **2013**, 7, 13.

- [31] E. Jang, S. Jun, H. Jang, J. Lim, B. Kim, Y. Kim, *Adv. Mater.* **2010**, *22*, 3076.
- [32] T. Kim, K. Cho, E. K. Lee, S. J. Lee, J. Chae, J. W. Kim, D. H. Kim, J. Kwon, G. Amaratunga, S. Y. Lee, *Nat. Photonics* **2011**, *5*, 176.
- [33] J. Du, Z. Du, J. Hu, Z. Pan, Q. Shen, J. Sun, D. Long, H. Dong, L. Sun, X. Zhong, *J. Am. Chem. Soc.* **2016**, *138*, 4201.
- [34] K. K. Sakimoto, A. B. Wong, P. Yang, *Science*. **2016**, *351*, 74.
- [35] K. A. Brown, D. F. Harris, M. B. Wilker, A. Rasmussen, N. Khadka, H. Hamby, S. Keable, G. Dukovic, J. W. Peters, L. C. Seefeldt, *Science*. **2016**, *352*, 448.
- [36] J. Zhou, Y. Yang, C. Zhang, *Chem. Rev.* **2015**, *115*, 11669.
- [37] G. Zan, Q. Wu, *Adv. Mater.* **2016**.
- [38] C. T. Dameron, R. N. Reese, R. K. Mehra, A. R. Kortan, P. J. Carroll, M. L. Steigerwald, L. E. Brus, D. R. Winge, *Nature* **1989**, *338*, 596.
- [39] J. W. Moreau, P. K. Weber, M. C. Martin, B. Gilbert, I. D. Hutcheon, J. F. Banfield, *Science*. **2007**, *316*, 1600.
- [40] R. Y. Sweeney, C. Mao, X. Gao, J. L. Burt, A. M. Belcher, G. Georgiou, B. L. Iverson, *Chem. Biol.* **2004**, *11*, 1553.
- [41] R. K. Mehra, D. R. Winge, *J. Cell. Biochem.* **1991**, *45*, 30.
- [42] S. H. Kang, K. N. Bozhilov, N. V Myung, A. Mulchandani, W. Chen, *Angew. Chemie Int. Ed.* **2008**, *47*, 5186.
- [43] E. D. Spoerke, J. A. Voigt, *Adv. Funct. Mater.* **2007**, *17*, 2031.
- [44] C. Mao, C. E. Flynn, A. Hayhurst, R. Sweeney, J. Qi, G. Georgiou, B. Iverson, A. M. Belcher, *Proc. Natl. Acad. Sci.* **2003**, *100*, 6946.
- [45] C. E. Flynn, C. Mao, A. Hayhurst, J. L. Williams, G. Georgiou, B. Iverson, A. M.



- Belcher, *J. Mater. Chem.* **2003**, *13*, 2414.
- [46] R. Cui, H. Liu, H. Xie, Z. Zhang, Y. Yang, D. Pang, Z. Xie, B. Chen, B. Hu, P. Shen, *Adv. Funct. Mater.* **2009**, *19*, 2359.
- [47] J. W. Fellowes, R. A. D. Patrick, J. R. Lloyd, J. M. Charnock, V. S. Coker, J. F. W. Mosselmans, T. Weng, C. I. Pearce, *Nanotechnology* **2013**, *24*, 145603.
- [48] S. A. Kumar, A. A. Ansary, A. Ahmad, M. I. Khan, *J. Biomed. Nanotechnol.* **2007**, *3*, 190.
- [49] A. K. Suresh, *Spectrochim. Acta Part A Mol. Biomol. Spectrosc.* **2014**, *130*, 344.
- [50] T. J. Park, S. Y. Lee, N. S. Heo, T. S. Seo, *Angew. Chemie Int. Ed.* **2010**, *49*, 7019.
- [51] A. Ahmad, P. Mukherjee, D. Mandal, S. Senapati, M. I. Khan, R. Kumar, M. Sastry, *J. Am. Chem. Soc.* **2002**, *124*, 12108.
- [52] C. Mi, Y. Wang, J. Zhang, H. Huang, L. Xu, S. Wang, X. Fang, J. Fang, C. Mao, S. Xu, *J. Biotechnol.* **2011**, *153*, 125.
- [53] H. Bai, Z. Zhang, Y. Guo, W. Jia, *Nanoscale Res. Lett.* **2009**, *4*, 717.
- [54] H. J. Bai, Z. M. Zhang, Y. Guo, G. E. Yang, *Colloids surfaces B Biointerfaces* **2009**, *70*, 142.
- [55] Y. Li, R. Cui, P. Zhang, B. Chen, Z. Tian, L. Li, B. Hu, D. Pang, Z. Xie, *ACS Nano* **2013**, *7*, 2240.
- [56] L. Xiong, R. Cui, Z. Zhang, X. Yu, Z. Xie, Y. Shi, D. Pang, *ACS Nano* **2014**, *8*, 5116.
- [57] C. I. Pearce, V. S. Coker, J. M. Charnock, R. A. D. Patrick, J. F. W. Mosselmans, N. Law, T. J. Beveridge, J. R. Lloyd, *Nanotechnology* **2008**, *19*, 155603.
- [58] C. Chien, C. Hung, C. Han, *Environ. Toxicol. Chem.* **2007**, *26*, 664.

- [59] R. P. Ryan, S. Monchy, M. Cardinale, S. Taghavi, L. Crossman, M. B. Avison, G. Berg, D. van der Lelie, J. M. Dow, *Nat. Rev. Microbiol.* **2009**, *7*, 514.
- [60] D. Pages, J. Rose, S. Conrod, S. Cuine, P. Carrier, T. Heulin, W. Achouak, *PLoS One* **2008**, *3*, e1539.
- [61] H. Bai, Z. Zhang, Y. Guo, W. Jia, *Nanoscale Res. Lett.* **2009**, *4*, 717.
- [62] M. N. Borovaya, A. P. Naumenko, N. A. Matvieieva, Y. B. Blume, A. I. Yemets, *Nanoscale Res. Lett.* **2014**, *9*, 1.
- [63] L. Tan, A. Wan, H. Li, *ACS Appl. Mater. Interfaces* **2013**, *6*, 18.
- [64] Z. Yan, J. Qian, Y. Gu, Y. Su, X. Ai, S. Wu, *Mater. Res. Express* **2014**, *1*, 15401.
- [65] C. Gallardo, J. P. Monrás, D. O. Plaza, B. Collao, L. A. Saona, V. Durán-Toro, F. A. Venegas, C. Soto, G. Ulloa, C. C. Vásquez, *J. Biotechnol.* **2014**, *187*, 108.
- [66] C. L. Wang, P. C. Michels, S. C. Dawson, S. Kitisakkul, J. A. Baross, J. D. Keasling, D. S. Clark, *Appl. Environ. Microbiol.* **1997**, *63*, 4075.
- [67] G. Chen, B. Yi, G. Zeng, Q. Niu, M. Yan, A. Chen, J. Du, J. Huang, Q. Zhang, *Colloids Surfaces B Biointerfaces* **2014**, *117*, 199.
- [68] E. V Krupko, G. Y. Grodzyuk, Y. B. Khalavka, G. M. Okrepka, L. P. Shcherbak, *Theor. Exp. Chem.* **2011**, *47*, 101.
- [69] A. Chatterjee, A. Priyam, S. K. Das, A. Saha, *J. Colloid Interface Sci.* **2006**, *294*, 334.
- [70] S. Tamang, G. Beaune, I. Texier, P. Reiss, *ACS Nano* **2011**, *5*, 9392.
- [71] D. P. S. Negi, T. I. Chanu, *Nanotechnology* **2008**, *19*, 465503.
- [72] C. Dong, J. Ren, *Analyst* **2010**, *135*, 1395.
- [73] J. Zhang, X. Wang, M. Xiao, L. Qu, X. Peng, *Appl. Phys. Lett.* **2002**, *81*, 2076.

- [74] M. L. Mastronardi, F. Maier-Flaig, D. Faulkner, E. J. Henderson, C. Kübel, U. Lemmer, G. A. Ozin, *Nano Lett.* **2011**, *12*, 337.
- [75] J. J. Beato-López, C. Fernández-Ponce, E. Blanco, C. Barrera-Solano, M. Ramírez-del-Solar, M. Domínguez, F. García-Cozar, R. Litrán, *Nanomater. Nanotechnol.* **2012**, *2*, 2.
- [76] A. E. Ennos, *Br. J. Appl. Phys.* **1953**, *4*, 101.
- [77] R. F. Egerton, P. Li, M. Malac, *Micron* **2004**, *35*, 399.
- [78] K. M. Mullaugh, G. W. Luther III, *J. Nanoparticle Res.* **2011**, *13*, 393.
- [79] A. Chemseddine, H. Weller, *Berichte der Bunsengesellschaft für Phys. Chemie* **1993**, *97*, 636.
- [80] Y. Shen, M. Y. Gee, R. Tan, P. J. Pellechia, A. B. Greytak, *Chem. Mater.* **2013**, *25*, 2838.
- [81] W. W. Yu, L. Qu, W. Guo, X. Peng, *Chem. Mater.* **2003**, *15*, 2854.
- [82] T. Gladysheva, J. Liu, B. P. Rosen, *J. Biol. Chem.* **1996**, *271*, 33256.
- [83] W. Liu, H. S. Choi, J. P. Zimmer, E. Tanaka, J. V Frangioni, M. Bawendi, *J. Am. Chem. Soc.* **2007**, *129*, 14530.
- [84] C. Steegborn, T. Clausen, P. Sondermann, U. Jacob, M. Worbs, S. Marinkovic, R. Huber, M. C. Wahl, *J. Biol. Chem.* **1999**, *274*, 12675.
- [85] H. Shinbo, *Insect Biochem.* **1982**, *12*, 571.
- [86] F. C. Brown, P. H. Gordon, *Can. J. Biochem.* **1971**, *49*, 484.
- [87] M. Gao, S. Kirstein, H. Möhwald, A. L. Rogach, A. Kornowski, A. Eychmüller, H. Weller, *J. Phys. Chem. B* **1998**, *102*, 8360.
- [88] A. Priyam, A. Chatterjee, S. K. Das, A. Saha, *Res. Chem. Intermed.* **2005**, *31*, 691.

- [89] Z. Cai, H. Yang, Y. Zhang, X. Yan, *Anal. Chim. Acta* **2006**, 559, 234.
- [90] H. Li, W. Y. Shih, W. Shih, *Ind. Eng. Chem. Res.* **2007**, 46, 2013.
- [91] Y. Nosaka, K. Yamaguchi, H. Miyama, H. Hayashi, *Chem. Lett.* **1988**, 605.
- [92] J. Chen, A. Zheng, Y. Gao, C. He, G. Wu, Y. Chen, X. Kai, C. Zhu, *Spectrochim. Acta Part A Mol. Biomol. Spectrosc.* **2008**, 69, 1044.
- [93] J. O. Winter, N. Gomez, S. Gatzert, C. E. Schmidt, B. A. Korgel, *Colloids Surfaces A Physicochem. Eng. Asp.* **2005**, 254, 147.
- [94] Y. Wang, R. Hu, G. Lin, W. Law, K. Yong, *RSC Adv.* **2013**, 3, 8899.
- [95] L. Nguyen, R. Kho, W. Bae, R. K. Mehra, *Chemosphere* **1999**, 38, 155.
- [96] R. Dunleavy, L. Lu, C. J. Kiely, S. McIntosh, B. W. Berger, *Proc. Natl. Acad. Sci.* **2016**, 201523633.
- [97] H. Kimura, *Amino Acids* **2011**, 41, 113.
- [98] L. E. Shea-Rohwer, J. E. Martin, *J. Lumin.* **2007**, 127, 499.
- [99] S. F. Wuister, C. de Mello Donega, A. Meijerink, *J. Phys. Chem. B* **2004**, 108, 17393.
- [100] L. Huang, X. Wang, J. Yang, G. Liu, J. Han, C. Li, *J. Phys. Chem. C* **2013**, 117, 11584.
- [101] M. Protiere, P. Reiss, *Nanoscale Res. Lett.* **2006**, 1, 62.
- [102] G. Zhu, L. Pan, H. Sun, X. Liu, T. Lv, T. Lu, J. Yang, Z. Sun, *ChemPhysChem* **2012**, 13, 769.
- [103] G. Zhu, Z. Cheng, T. Lv, L. Pan, Q. Zhao, Z. Sun, *Nanoscale* **2010**, 2, 1229.
- [104] C. Chang, Y. Lee, *Appl. Phys. Lett.* **2007**, 91, 5350.
- [105] D. C. Marcano, D. V Kosynkin, J. M. Berlin, A. Sinitskii, Z. Sun, A. Slesarev, L. B. Alemany, W. Lu, J. M. Tour, *ACS Nano* **2010**, 4, 4806.

- [106] P. F. Erickson, I. H. Maxwell, L. J. Su, M. Baumann, L. M. Glode, *Biochem. J.* **1990**, 269, 335.
- [107] M. H. Stipanuk, P. W. Beck, *Biochem. J.* **1982**, 206, 267.
- [108] G. Yang, L. Wu, B. Jiang, W. Yang, J. Qi, K. Cao, Q. Meng, A. K. Mustafa, W. Mu, S. Zhang, *Science*. **2008**, 322, 587.
- [109] L. C. Spangler, L. Lu, C. J. Kiely, B. W. Berger, S. McIntosh, *J. Mater. Chem. A* **2016**, 4, 6107.
- [110] G. P. Mitchell, C. A. Mirkin, R. L. Letsinger, *J. Am. Chem. Soc.* **1999**, 121, 8122.
- [111] D. R. Baker, P. V Kamat, *Langmuir* **2010**, 26, 11272.
- [112] V. Swayambunathan, D. Hayes, K. H. Schmidt, Y. X. Liao, D. Meisel, *J. Am. Chem. Soc.* **1990**, 112, 3831.
- [113] X. Peng, L. Manna, W. Yang, J. Wickham, E. Scher, A. Kadavanich, A. P. Alivisatos, *Nature* **2000**, 404, 59.
- [114] S. Singh, K. Bozhilov, A. Mulchandani, N. Myung, W. Chen, *Chem. Commun.* **2010**, 46, 1473.
- [115] H. Qian, L. Li, J. Ren, *Mater. Res. Bull.* **2005**, 40, 1726.
- [116] W. K. Bae, L. A. Padilha, Y.-S. Park, H. McDaniel, I. Robel, J. M. Pietryga, V. I. Klimov, *ACS Nano* **2013**, 7, 3411.
- [117] F. García-Santamaría, S. Brovelli, R. Viswanatha, J. A. Hollingsworth, H. Htoon, S. A. Crooker, V. I. Klimov, *Nano Lett.* **2011**, 11, 687.
- [118] L. A. Swafford, L. A. Weigand, M. J. Bowers, J. R. McBride, J. L. Rapaport, T. L. Watt, S. K. Dixit, L. C. Feldman, S. J. Rosenthal, *J. Am. Chem. Soc.* **2006**, 128, 12299.

- [119] S. R. Cordero, P. J. Carson, R. A. Estabrook, G. F. Strouse, S. K. Buratto, *J. Phys. Chem. B* **2000**, *104*, 12137.
- [120] M. Jones, J. Nedeljkovic, R. J. Ellingson, A. J. Nozik, G. Rumbles, *J. Phys. Chem. B* **2003**, *107*, 11346.
- [121] T. Ida, T. Sawa, H. Ihara, Y. Tsuchiya, Y. Watanabe, Y. Kumagai, M. Suematsu, H. Motohashi, S. Fujii, T. Matsunaga, *Proc. Natl. Acad. Sci.* **2014**, *111*, 7606.
- [122] T. Yamanishi, S. Tuboi, *J. Biochem.* **1981**, *89*, 1913.
- [123] J. I. Toohey, A. J. L. Cooper, *Molecules* **2014**, *19*, 12789.
- [124] M. Flavin, *J. Biol. Chem.* **1962**, *237*, 768.
- [125] D. Cavallini, B. Mondovi, C. De Marco, A. Sciosciasantoro, *Arch. Biochem. Biophys.* **1962**, *96*, 456.
- [126] D. Cavallini, B. Mondovi, C. De Marco, A. Sciosciasantoro, *Enzymologia* **1962**, *24*, 253.
- [127] N. Esaki, T. Nakamura, H. Tanaka, T. Suzuki, Y. Morino, K. Soda, *Biochemistry* **1981**, *20*, 4492.
- [128] N. Esaki, T. Nakamura, H. Tanaka, K. Soda, *J. Biol. Chem.* **1982**, *257*, 4386.
- [129] C. Wang, A. Lum, S. Ozuna, D. Clark, J. Keasling, *Appl. Microbiol. Biotechnol.* **2001**, *56*, 425.
- [130] E. C. Kendall, F. F. Nord, *J. Biol. Chem.* **1926**, *69*, 295.
- [131] R. C. Dickson, A. L. Tappel, *Arch. Biochem. Biophys.* **1969**, *130*, 547.
- [132] V. V. Nikesh, A. D. Lad, S. Kimura, S. Nozaki, S. Mahamuni, *J. Appl. Phys.* **2006**, *100*, 113520.
- [133] G. Jones, W. R. Jackson, C. Y. Choi, W. R. Bergmark, *J. Phys. Chem.* **1985**, *89*,

294.

[134] K. Rurack, M. Spieles, *Anal. Chem.* **2011**, *83*, 1232.

[135] C. Bollet, A. Davin-Regli, P. De Micco, *Appl. Environ. Microbiol.* **1995**, *61*, 1653.

# Appendix

## Experimental Section

### A1. Apparatus and characterizations.

The luminescence of purified QD suspensions was analyzed using a UV Bio-Rad Gel Doc 2000 system. Absorption spectra of QD suspensions were collected using an Ultrospec 3300 Pro (Amersham Biosciences) or UV-2600 Spectrophotometers (Shimadzu). Fluorescence excitation and emission spectra for QD suspensions were collected using a Cary Eclipse Fluorescence Spectrophotometer (Varian). Room temperature photoluminescence quantum yields (PL QYs) were calculated using coumarin 1 in ethanol as a standard with a PL QY of 73 %<sup>[133]</sup> for CdS test and coumarin 153 in ethanol with PL QY of 54 %<sup>[134]</sup> for CdSe test. Powder XRD measurements (Rigaku Miniflex II) were performed at room temperature by using Cu K $\alpha$  (1.5418 Å) radiation. For enzyme identification, a standard SDS-PAGE technique was used to study the associated enzyme and the dry sample after lyophilisation was analysed via electrospray ionization mass spectrometry (ESI-MS). For QD solar cell test, the photocurrent density-voltage (J-V) performance characteristic was measured using an electrochemical workstation (Reference 600, Gamry Instruments) under irradiation (AM 1.5 G solar simulator, Model No. 10500, ABET Technologies) with an incident light intensity of 100 mW cm<sup>-2</sup>.

For scanning transmission electron microscopy (STEM), selected area electron diffraction (SAED) and X-ray energy dispersive spectroscopy (XEDS) analysis, purified samples were prepared by drop casting the aqueous QD suspension onto a holey carbon-coated copper grid and allowing the liquid component to fully evaporate. The specimen



was then analyzed in either (i) a 200kV aberration corrected JEOL ARM 200CF analytical electron microscope equipped with a Centurio XEDS system or (ii) a 200kV JEOL 2000FX conventional TEM equipped with an Oxford Instruments XEDS system.

## **A2. *Stenotrophomonas maltophilia* and cystathionine $\gamma$ -lyase production.**

SMCD1 was isolated from soil collected from the mountaintop campus of Lehigh University in Pennsylvania using previously described methods.<sup>[135]</sup> Strain identification was confirmed using 16S rRNA sequencing (SeqWright). Standard microbiology techniques were used for the growth and cultivation of SMCD1 using Luria-Bertani (LB) broth and M9 minimal media. Selection of cadmium resistant strains was performed iteratively in three steps by increasing the concentration of cadmium acetate: (1) Cultures were grown for 8 - 12 h at 37 °C in an orbital shaker in LB broth containing increasing concentrations of cadmium acetate (0.1 ~ 5 mM); (2) serial dilutions of cultures were plated onto LB-agar plates containing equivalent concentrations of cadmium acetate; and (3) individual colonies were isolated from plates. Cell growth rate in culture was measured by monitoring the change in optical density at 600 nm (OD<sub>600</sub>). Colonies tolerant to cadmium acetate at concentrations in excess of 1 mM were selected from cadmium-containing plates. Using this selection procedure, we isolated a specific strain (SMCD1) that exhibits continuous formation of luminescent particles. Expression and purification of recombinant cystathionine  $\gamma$ -lyase was achieved according to the protocol reported by our group.<sup>[96]</sup> In short, an *E. coli* codon-optimized form of the putative *S. maltophilia* CSE (Smal\_0489; Genscript) was subcloned into pET28a (+) and transformed in BL21 cells with expression and purification.

### **A3. CdS quantum dot biosynthesis.**

In a typical experiment, the selected SMCD1 were sub-cultured into LB broth (100 mL) and grown for 12 h at 37 °C with shaking. Cells were isolated by centrifugation and re-suspended in M9 minimal media (100 mL, OD<sub>600</sub>=0.5). Then, cadmium acetate (1 mM) and L-cysteine (8 mM) were added and the mixture was placed in a 37 °C incubator with shaking. Sample aliquots were collected every 30 min, and CdS QDs separated from intact cells by centrifugation (5000 rpm), dialysis (Snakeskin 3500 MWCO; Thermo Pierce) with ultrapure, deionized water as the buffer and gravity-feed size exclusion chromatography (PD-10; Amersham). In order to investigate the mechanism of particle growth, the same growth procedure was followed for 30 min growth time. At this point, the cell solution was centrifuged at 8000 rpm for ten minutes, reducing the optical density at 600 nm to 2 % of the original value. The centrifuge supernatant was then returned to the incubator at 37 °C and sample aliquots were collected every 30 min.

### **A4. CdSe quantum dot biosynthesis.**

In a typical procedure, 1 mM cadmium acetate (99.999%, Alfa Aesar), 8 mM seleno-L-cystine (95%, Sigma Aldrich), 20 mM 3-Mercaptopropionic acid (99%, Sigma Aldrich) and 0.05 mg/mL cystathionine  $\gamma$ -lyase enzyme in 0.05 M Tris-HCl buffer (pH = 9.0) were prepared in a N<sub>2</sub> controlled glovebox and sealed properly. The mixture was then transferred and placed in the incubator with shaking at 37 °C. After synthesis, CdSe nanocrystals solution was purified by centrifugation at 8000 rpm, followed by syringe filtration (0.2  $\mu$ m). After that, CdSe QDs were either precipitated/resuspended in 0.05 M Tris-HCl buffer (pH = 9.0) by introducing ethanol or dialyzed (Snakeskin 3500 MWCO;

Thermo Pierce) against ultrapure water to remove residual salts depending on the particle size. For small particle size, both techniques work well; for large particle size, the precipitation by ethanol resulted in aggregates which cannot be resuspended, thus dialysis was used.

#### **A5. Phase transfer and capping exchange of quantum dots.**

Phase transfer protocol is applicable to both CdS and CdSe or related core/shell QDs from aqueous to organic phase. In a typical procedure, taking CdS as the example, the biosynthesized aqueous soluble CdS QDs was transferred into 1-octadecene (ODE, 90%, Alfa Aesar) in the presence of oleylamine (98%, sigma Aldrich) capping agent. 15 ml of the purified aqueous CdS QD sample was shaken with 5 ml oleylamine and 10 ml ODE. The solution was degassed for 10 min and then stirred vigorously under argon for 1h at 60 °C. A centrifuge (5000 rpm) and decantation procedure was applied for separation of the organic and aqueous phases. A hexane and methanol (volume ratio of 1:3) solution was contacted with the organic phase as an extraction solvent to purify the organic phase and this was repeated several times to wash excess capping agents. The nanocrystals can be further precipitated by introducing acetone or ethanol and resuspended in solvents, such as chloroform and toluene.

Phase transfer with 1-dodecanethiol (DDT, 98%, Alfa Aesar) was carried out according to the report by Gaponik et al.<sup>[14]</sup> In a typical experiment, 2 mL CdS QDs solution was mixed with 2 mL DDT and 4 mL acetone; the mixture was then heated up to ~ 60 °C with vigorous stirring under inert. After about 20 min, the solution was cooled down and phase separation was obtained; the top organic phase was collected and an equal amount

of toluene was added; The nanocrystals were precipitated by methanol and resuspended in chloroform.

Capping ligand exchange from oleylamine to oleic acid (90%, Alfa Aesar) was accomplished through addition of oleic acid to the purified oleylamine capped CdS QDs. Typically, 20 ml of the oleylamine capped CdS QDs in ODE was mixed with 10 ml oleic acid. The solution was degassed for 10 min and placed under argon for 3 h at room temperature. The same hexane/methanol extraction procedure as previously described was utilized prior to precipitation of the QDs by methanol addition. The isolated precipitate is readily soluble in chloroform to yield an optically clear solution.

#### **A6. Core/shell structure synthesis.**

Growth of a ZnS shell on CdS QDs was carried out following the procedure described by Chen et al.<sup>[24]</sup> using oleic acid capped CdS QDs as the core material. A 2 ml quantity of CdS QDs in chloroform was mixed with 10 ml ODE. The solution was degassed in argon for 30 min and then heated to 50 °C prior to dropwise addition of 0.5 mL 0.01 M zinc diethyldithiocarbamate ( $\text{Zn(DDTC)}_2$ , >99%, TCI America) under argon flow. The solution was then immediately heated to 170 °C. After 20 min, the solution was cooled down to 120 °C and a second injection of  $\text{Zn(DDTC)}_2$  carried out before once again heating to 170 °C. This procedure was repeated for a third time. Finally, the temperature of the solution was increased to 240 °C and maintained for 20 min. The final solution was washed and purified by the same hexane/methanol extraction procedure. The CdS/ZnS QDs so generated were precipitated by acetone addition and then re-suspended in chloroform.

Biosynthesis of a CdS shell on CdSe QDs was also carried out. The purified CdSe QDs solution was used as the core seeds. In a typical procedure, CdSe QDs (absorbance peak intensity around 0.3), 1 mM cadmium acetate (99.999%, Alfa Aesar), 8 mM L-cysteine (98%, Alfa Aesar) and 0.05 mg/mL smCSE enzyme in 0.05 M Tris-HCl buffer (pH = 9.0) were prepared inert and sealed properly. The mixture was then placed in the incubator with shaking at 37 °C for 12 h. After synthesis, CdSe/CdS nanocrystals solution was purified by centrifugation at 8000 rpm, followed by syringe filtration (0.2 µm). The solution was further dialyzed (Snakeskin 3500 MWCO; Thermo Pierce) against ultrapure water to remove residual salts.

#### **A7. Quantum dot sensitized solar cell assembly.**

QD sensitized solar cells were fabricated using commercially available glass slides coated with F-doped tin oxide (FTO,  $\sim 7\Omega/\text{sq}$ , Sigma Aldrich), that were covered with a TiO<sub>2</sub> blocking layer by dipping it into a 40 mM TiCl<sub>4</sub> (>99.0%, Sigma Aldrich) solution, followed by sintering in air at 500 °C for 3 h. A second mesoporous TiO<sub>2</sub> film (TiO<sub>2</sub> paste, 27.0 wt-%, Sigma Aldrich) was deposited on top of the blocking layer with a doctor blade followed by sintering at 500 °C for 1 h in air. The CdS QDs capped by oleic acid in chloroform were loaded into the mesoporous TiO<sub>2</sub> by drop casting. The completed photo-electrode was dried under ambient conditions. The counter electrode was prepared by painting a conductive gold paste (Electron Microscopy Sciences) onto FTO glass. The working and counter electrodes were assembled into a sandwich structure. The electrolyte was prepared by dissolving 0.5 M Na<sub>2</sub>S (98%, Alfa Aesar), 0.5 M S (99.5%, Alfa Aesar) and 0.055 M NaOH (99.99%, Alfa Aesar) in water.

#### **A8. Quantum dot/reduced graphene oxide composite.**

Graphene oxide was synthesized according to a improved method by Marcano et al.<sup>[105]</sup> The graphene oxide (0.5 g/L) was then reduced by sodium borohydride (150 mM for 2 h) and the precipitated product was washed by precipitation/resuspension multiple times with deionized water. The purified reduced graphene oxide was then mixed with equal volume of purified CdS QDs solution and the mixture was sonicated by a tip sonicator for 2 h. Finally, the product was collected after centrifugation and ready for test.

# Curriculum Vitae

## Zhou Yang

Email: yangzhou06@gmail.com

Place of Birth: Xiantao City, P.R. China

Date of Birth: February 23, 1986

Parents: Luocheng Yang (father) and Wangying Zhou (mother)

### Education and Work Experience

- Ph.D., Chemical Engineering, Aug. 2011 – Sep. 2016, Lehigh University, USA. Advisor: Prof. Steven McIntosh and Bryan Berger.
- M.S., Chemical Engineering, Aug. 2006 – Jul. 2009, Tsinghua University, P.R. China. Advisors: Prof. Guohua Luo and Fei Wei.
- B.S., Chemical Engineering, Aug. 2002 – Jul. 2006, Tsinghua University, P.R. China.
- Senior engineer, R&D department, Jul. 2009 – Jul. 2010, Beijing Easpring Material Technology Co., Ltd., Beijing, P.R. China.

### Research Experience

#### (1) Doctoral Dissertation: Biosynthesis of Cadmium Chalcogenide Quantum Dots and Enhancement of their Functional Properties via Surface Modification.

- Conducted research on synthesis of cadmium and lead based colloidal materials via a facile bio-process: protocol optimization, purification and characterization.
- Carried out research on cadmium sulfide quantum dot sensitized solar cell.
- Improved the properties of the as-grown cadmium sulfide particles by surface modifications, such as capping ligand exchange, core/shell structure synthesis.
- Achieved synthesis of two dimensional nanomaterial composite of reduced graphene oxide and metal/semiconductor nanoparticles for photocatalysis.
- Participated in research on support catalyst (barium zirconium oxide) decorated by precious metal nanoparticles (cobalt and platinum) for methanation of carbon dioxide.
- Synthesized multiple phases of bismuth molybdate via sol-gel method and characterized their crystal structures using *Spallation Neutron Source* in Oak Ridge National Laboratory.

#### (2) Master Thesis: Process Study on Synthesis of Carbon Nanotube from Polymers.

- Conducted research on synthesis of carbon nanotubes from different types of polymers, such as polypropylene, polyethylene and polyvinyl chloride.
- Provided fundamental study of polymers for carbon nanotube synthesis in

large scale.

- Achieved ultra-long carbon nanotube arrays (~5 mm) synthesis.
- Accomplished the substrate design by photolithography technique for reaction kinetics study.

### Work Experience

Jul. 2009 – Jul. 2010, Beijing Easpring Material Technology Co., Ltd., *R&D Senior Engineer*

- Improved the properties of Li(Ni/Co/Mn)O<sub>2</sub> battery cathode material to an advanced level with better high-temperature cycling performance and higher specific capacity.
- Modified the humidity control system of the production line for better product quality.
- Accomplished an analysis report for technical and economic feasibility of LiFePO<sub>4</sub> cathode material.

Jul. 2008 – Aug. 2008, PetroChina, *Process engineer & Team Leader*

- Involved in solving technical problems and monitoring product quality on the production line.
- Participated in *Health, Safety and Environment* project and submitted 2 reports.
- Initiated contacts with company and organized seminars for 15 student participants.

Aug. 2005 – Sep. 2005, Duoshengduo Co., Ltd., Jiaozuo City, *Summer Intern*

- Participated in the project of improving the biosynthesis efficiency of acrylamide.

Aug. 2004 – Sep. 2004, Sinopec., *Summer Intern*

- On site study of the phenol-acetone plant and drew entire flow chart.

### Journal Publications

- **Z Yang**, et al. Biomanufacturing of CdS quantum dots. *Green Chemistry*, 2015, 17(7):3775-3782. (*Featured cover article*)
- **Z Yang**, et al. Biomineralized CdS Quantum Dot Nanocrystals: Insights into the Biomineralization Mechanism and Enhancing their Functional Properties. 2016 submitted.
- H Shin, L Lu, **Z Yang** et al. Atomic Pt decorated Co Catalysts on Barium Zirconate Supports Provide Enhanced Activity and Selectivity for CO<sub>2</sub> Methanation. *ACS Catalysis*, 2016, 6:2811-2818.
- A Chakrabarti, M. E. Ford, D Gregory, R Hu, C. J. Keturakis, S Lwin, Y Tang, **Z Yang**, M Zhou, and I. E. Wachs. A Decade of Operando Spectroscopy Studies, in preparation.
- **Z Yang**, et al. Biomanufacturing of CdSe quantum dots from *cystathionine γ-lyase* enzyme. 2016, in preparation.



- **Z Yang**, et al. Coupled process of plastics pyrolysis and chemical vapor deposition for controllable synthesis of vertically aligned carbon nanotube arrays. *Applied Physics A*, 2010, 100(2):533-540.
- **Z Yang**, et al. Growth of super long vertically aligned carbon nanotube arrays from cyclohexane via floating catalyst method. *New Carbon Materials*, 2010, 3(25):168-174.
- R Xiang, G Luo, **Z Yang** et al. Large area growth of aligned CNT arrays on spheres: cost performance and product control. *Materials Letters*, 2009, 63(1):84–87.
- R Xiang, **Z Yang** et al. Growth deceleration of vertically aligned carbon nanotube arrays: Catalyst deactivation or feedstock diffusion controlled? *The Journal of Physical Chemistry C*, 2008, 112(13):4892–4896.
- Q Zhang, W Qian, R Xiang, **Z Yang** et al. In situ growth of carbon nanotubes on inorganic fibers with different surface properties. *Materials Chemistry and Physics*, 2008, 107(2–3):317–321
- R Xiang, G Luo, **Z Yang** et al. Temperature effect on the substrate selectivity of carbon nanotube growth in floating chemical vapor deposition. *Nanotechnology*, 2007, 18(41):415703

#### **Patent**

- F Wei, Q Zhang, W Zhou, G Xu, **Z Yang**, W Qian, G Luo. Synthesis method of carbon nanotube aerogel and its applications. CN1884058A, WO2008000163 A1.

#### **Honors and Awards**

- Leonard A. Wenzel Award for Ph.D. qualifying examination, Lehigh University, 2012.
- Graduate Fellowship, Lehigh University, 2011.
- Outstanding Undergraduate Thesis Reward, Tsinghua University, 2006.
- Third Prize of Excellent General Performance, Tsinghua University, 2005.